# From the regulatory role of PDPN in mTOR/PI3K/Akt signaling to clinical trials

**Inauguraldissertation**

zur

Erlangung der Würde eines Doktors der Philosophie

vorgelegt der

Philosophisch-Naturwissenschaftlichen Fakultät

der Universität Basel

von

**Vincent Prêtre**

aus

Boncourt (JU), Schweiz

Basel, 2019

Genehmigt von der Philosophisch-Naturwissenschaftlichen Fakultät
auf Antrag von

Prof. Michael N. Hall, PD Dr. Andreas Wicki, Prof. Gerhard Christofori

Basel, den 17. Oktober 2017

Prof. Dr. Martin Spiess

# I. Table of content

# II. List of Tables

# III. List of Figures

# IV. Abbreviations

| | |
|---|---|
| 4E-BP1 | Eukaryotic translation initiation factor 4E-binding protein 1 |
| ALP | Alkaline phosphatase |
| ALP | Alkylphosphocholine |
| ALT | Alanine transaminase |
| AMPKa | 5' adenosine monophosphate-activated protein kinase alpha |
| ANC | Absolute neutrophil count |
| ANOVA | Analysis of Variance |
| AST | Aspartate aminotransferase |
| AST | adenocarcinoma transition to squamous cell carcinoma |
| AUC | Area under the curve |
| Bad | Bcl-2-associated death promoter protein |
| BAD | Bcl-2-associated death promoter |
| Braf | v-Raf murine sarcoma viral oncogene homolog B |
| cAMP | Cyclic adenosine monophosphate |
| CDx | Cluster of differentiation |
| cGMP | Cyclic guanosine monophosphate |
| CT | Computer tomography |
| CTCAE | Common Toxicity Criteria for Adverse Events |
| CYP17 | Cytochrome P450 17 |
| DAPI | 4',6-Diamidino-2-phenylindole |
| DEPTOR | DEP domain containing mTOR interacting protein |
| DLBCL | Diffuse large B cell lymphoma |
| DLT | Dose limiting toxicity |
| DMEM | Dulbecco's Modifies Eagle's Medium |
| DNA | Desoxyribonucleic Acid |
| DOTA | 1,4,7,10-tetraazacyclododecane-1,4,7,10-tetraacetic acid |
| DOTATATE | DOTA-($Tyr^3$)-octreotate |
| DOTATOC | ($DOTA^0$-$Phe^1$-$Tyr^3$)octreotide |
| DOX | Doxycyline |
| ECM | Extracellular matrix |
| ECOG | Eastern Cooperative Oncology Group |
| EGF | Epidermal growth factor |
| EGF | Epidermal growth factor |
| EGFR | Epidermal growth factor receptor |

| | |
|---|---|
| EMA | European Medicines Agency |
| Erb-B2/3 | Avian erythroblastosis oncogene B 2/3 |
| ERK 1/2 | Extracellular-signal-regulated Kinase 1/2 |
| ERM | ezrin, radixin and moesin |
| FBDD | Fragment-based drug discovery |
| FCS | Fetal Calf Serum |
| FDA | Federal Drug Agency |
| FOXP3 | Forkhead box P3 |
| GCP | Good Clinical Practice |
| GFP | Green Fluorescent Protein |
| GLP-1 | glucose-like peptide 1 |
| GLP-1R | glucose-like peptide 1 receptor |
| Glu | Glutamic acid |
| GPCRs | G protein coupled receptors |
| GSK3a/b | Glycogen synthase kinase 3 alpha/beta |
| Gx | Grade |
| H&E | Hematoxylin and eosin |
| HbA1c | Hemoglobin A1c |
| HER2 | Human Epidermal Growth Factor Receptor-2, Erb-b2 |
| HIV | Human immunodeficiency virus |
| HNSCC | Head & neck squamous cell carcinoma |
| HPV | Human papilloma virus |
| i.v. | Intravenous |
| IDSMB | Independent data safety monitoring board |
| IGF | Insulin-like growth factor |
| IGFR | Insulin-like growth factor receptor |
| INFy | Interferon gamma |
| JNK | c-Jun N-terminal kinase |
| ko | knockout |
| Kras | V-Ki-ras2 Kirsten rat sarcoma viral oncogene homolog |
| LECs | Lymphatic Endothelial Cells |
| Lu-177 | Lutetium 177 |
| Lys | Lysine |
| MAPK | Mitogen-activated protein kinases |
| MDM2 | Mouse double minute 2 homolog |
| MEK | Mitogen-activated protein kinase kinase |

| | |
|---|---|
| mLST8 | mammalian lethal with Sec13 protein 8 |
| MRI | Magnetic resonance imaging |
| mRNA | Messenger RNA |
| MTD | Maximum tolerated dose |
| mTOR | Mammalian target of rapamycin |
| mTORC1/2 | Mammalian target of rapamycin complex 1/2 |
| NETs | Neuroendocrine tumors |
| NFkB | Nuclear factor kappa-light-chain-enhancer of activated B cells |
| NOAEL | No-Observed-Adverse-Effect-Level |
| NSCLC | Non small cell lung cancer |
| OCT | Optimal cutting temperature |
| OCT | Ocular coherence tomography |
| p.o. | Per os |
| p53 | Tumor protein *p53* |
| PBS | Phosphate Buffered Saline |
| PCR | Polymerase Chain Reaction |
| PD | Pharmacodynamics |
| PDGFRA | Platelet-derived growth factor receptor A |
| PDK1 | 3-phosphoinositide dependent protein kinase-1 |
| PDPN | Podoplanin |
| PFA | Paraformaldehyde |
| PI3K | Phosphatidylinositol-3-kinase |
| PIK3CA | Phosphatidylinositol-4,5-bisphosphate 3-kinase, catalytic subunit alpha |
| PK | Pharmacokinetics |
| PKA | cAMP-dependent protein kinase 1 |
| PKB | Protein kinase B or akt |
| PKC | Protein Kinase C |
| PKG | cGMP-dependent protein kinase 1 |
| pMARCKS | Phosphorylated myristoylated alanine-rich C kinase substrate |
| PRAS40 | proline-rich Akt substrate of 40 kDa |
| PRRT | Peptide receptor radiotherapy |
| PTEN | Phosphatase and tensin homolog |
| qRT-PCR | Quantitative Real Rime Polymerase Chain Reaction |
| RECIST | Response Evaluation Criteria in Solid Tumors |
| RFP | Red Fluorescent Protein |
| Rho | Rho family of GTPases |

| | |
|---|---|
| RICTOR1 | Rapamycin-insensitive companion of mammalian target of rapamycin 1 |
| RNA | Ribonucleic Acid |
| ROCK | Rho-associated protein kinase |
| RP2D | Recommanded phase 2 dose |
| RP-HPLC | Reverse phase high liquid chromatography |
| RSK1 | Ribosomal Protein S6 Kinase 1 |
| RTKs | Receptor tyrosine kinases |
| RT-PCR | Real Time Polymerase Chain Reaction |
| S6 | Ribosomal protein S6 |
| S6K | S6 Kinase |
| SCC | Squamous cell carcinoma |
| SD | Standard Deviation |
| Ser | Serine |
| SGK2 | Serine/Threonine Kinase 2 |
| SGLT-2 | Sodium/glucose cotransporter 2 |
| shPDPN | Short hairpin podoplanin |
| SMARCB1 | SWI/SNF-related matrix-associated actin-dependent regulator of chromatin subfamily B member 1 |
| SPF | Specific Pathogen-Free |
| STAT3 | Signal transducer and activator of transcription 3 |
| STE | Homologues of yeast sterile 7 |
| TGFb | Transforming growth factor b |
| Thr | Threonine |
| TK | Tyrosine kinase |
| TLK | Tyrosine-like kinase |
| TNFa | Tumor necrosis factor alpha |
| TSC1/2 | Tuberous sclerosis proteins 1/2 |
| wt | Wild-type |

# V. General introduction

## Targeted inhibition of mTOR/PI3K/Akt in clinical cancer therapies

Cancer deaths in U.S. have fallen dramatically since the early 90's but the new cancer cases is expected to jump from 1.7 million in 2017 to 2.3 million in 2030 ("AACR Cancer Progress Report 2017", 2017). The mTOR/PI3K/Akt pathway is the most frequently altered network in human neoplasms. Mutations leading to the activation of this pathway is associated with cancer initiation, progression, metastasis and drug resistance. Since many years, multiple molecular targets were identified for therapy and the signaling pathway has been thoroughly reviewed (Engelman 2009; Laplante et al. 2012; Yuan & Cantley 2008; Courtney et al. 2010; Guri & Hall 2016; Thorpe et al. 2015). There are plenty of redundancy and feedback between the RAS–RAF–MEK–ERK and PI3K–AKT–mTOR signaling networks (Fruman & Rommel 2014). Almost all key components along these two signaling axes, such as BRAF, MEK, PI3K, Akt, and mTOR, have been therapeutically targeted to allow for serial and parallel blockade of these two pathways (Wicki et al. 2016).

**mTORC1/2.** mTOR is a serine-threonine kinase in the PI3K-related kinase (PIKK) family, involved in several central role for the cell such as mRNA translation, metabolism or autophagy (Hall 2016). It is part of two distinct protein complexes know as mTOR Complex 1 (mTORC1) and mTOR Complex 2 (mTORC2). mTORC1 is defined by his three major components, mTOR, Raptor and mLST8. In addition, two other component are part of the mTORC1, PRAS40 and DEPTOR (Peterson et al. 2009) and the rapamycin-FKBP12 complex binds to the FRB domain of mTOR and inhibits it (Yang et al., 2013). mTORC1 functions as a downstream effector for many frequently mutated oncogenic pathways, including the PI3K/Akt pathway as well as the Ras/Raf/Mek/Erk (MAPK) pathway, resulting in mTORC1 hyperactivation in a high percentage of human cancers (Saxton & Sabatini 2017). mTORC2 is characterized by its insensitivity to acute rapamycin treatment and like mTORC1, mTORC2 contains mTOR and mLST8 which are rapamycin derivatives (Saxton & Sabatini 2017). mTORC2 also contains DEPTOR, Rictor, mSin1 and Protor1/2 (Jacinto et al. 2006; Pearce et al. 2007).

Historically two classes of mTOR inhibitor were developed: One class is rapalogues, like everolimus and temsirolimus, that inhibit allosterically mTOR in mTORC1. Most patients tend to develop resistance from allosteric inhibitors and combinations with other compounds has revealed to be challenging regarding the toxicity. The second class is ATP competitive inhibitors inhibit mTOR in both mTORC1 and mTORC2. By inhibiting both mTOR complexes, the ATP-competitive inhibitors are theoretically more bioactive, and could decrease the TORC2-mediated feedback loop, although no comparisons with

rapalogues have yet been reported (Turner et al. 2017a). No drug from the second category is yet approved for treatment. This subject is further developed in the introduction of the chapter VIII.

**PI3K.** Phosphorylation of membrane phospholipids is key to signal transduction and has a major role in driving cancer initiation and progression (Whitman et al. 1988). PI3K are heterodimers comprising a 110 kDa catalytic isoform encoded by one of the four genes (PIK3CA, PIK3CB, PIK3CD and PIK3CG) and a 85kDa regulatory subunit encoded by three genes (PIK3R1, PIK3R2 and PIK3R3). The catalytic isoforms share considerable sequence homology, produce the same lipid product (PtdIns(3,4,5)P3) and can be activated by GTPases and RTK (Fritsch et al. 2013). PI3K activation initiates a signal transduction cascade that promotes cancer cell growth, survival and metabolism. The PI3K/Akt pathway is mainly negatively regulated by PTEN, a major tumor suppressor (Maehama & Dixon 1998). In human cancer, only PIK3CA (encoding p110α) is frequently mutated (Zardavas et al. 2014; Samuels et al. 2004).

Three strategies are currently used to inhibit PI3K: pan-isoform PI3K, isoform-specific PI3K and dual PI3K/mTOR inhibition. Pan-isoform PI3K inhibitor such as buparlisib and pictilisib inhibit all four isoforms and have therefore been associated with many side effects. Alpha-selective inhibitors like tselisib and alpelisib inhibit the driver oncogene and thus should reduce toxicities. Most of the dual non-selective inhibitors trials ceased due to poor PK properties or extended toxicities. This subject is further developed in the introduction of the chapter IX.

## A special case: the AGC kinases

AGC kinases are part of the mTOR/PI3K/Akt pathway or closely related in many ways. The rest of this general introduction and part of the general discussion has been published under the title “Inhibition of Akt and other AGC kinases: A target for clinical cancer therapy?” in Seminar Cancer Biology in February 2018 (Prêtre & Wicki 2018).

ELSEVIER

Seminars in Cancer Biology
Volume 48, February 2018, Pages 70-77

Review

# Inhibition of Akt and other AGC kinases: A target for clinical cancer therapy?

Vincent Prêtre [a], Andreas Wicki [a, b]

[a] Department of Biomedicine, University of Basel, 4031 Basel, Switzerland
[b] Department of Medical Oncology, University Hospital Basel, 4031 Basel, Switzerland

Received 29 November 2016, Revised 4 April 2017, Accepted 25 April 2017, Available online 1 May 2017.

## The rationale for AGC kinase-directed therapy in clinical cancer care

AGC kinases are a subgroup of Ser/Thr protein kinases. Based on the structure of their catalytic kinase domain, kinases are related to cAMP-dependent protein kinase 1 (PKA), cGMP-dependent protein kinase (PKG) and protein kinase C (PKC), building the acronym AGC (Hanks & Hunter 1995). The AGC family contains 60 of the 518 human protein kinases and 42 possess functional domains other than the kinase core, which are mostly involved in regulating kinase activity and localization (Manning et al. 2002).

Recent studies have identified around 1100 cancer drivers, both oncogenes and tumor suppressor genes. Roughly 10% of those cancer drivers correspond to protein kinases, making this group of enzymes a prime target for cancer therapy. Although some of these kinases are mutated at high frequency (>10% in a given cancer entity), the mutation rate of most cancer drivers is low. The most common genetic aberration of protein kinases are somatic mutations, followed by copy number aberrations and gene fusions. Of the eight main classes of kinases, by far the most frequent genomic aberrations have been identified in tyrosine kinases (TK), followed by tyrosine-like kinases (TLK) and homologues of yeast sterile 7 (STE).

Cancer driving genomic alterations of AGC kinases are less frequent. However, a number of AGC kinases have been identified to contribute to cancer development and progression, including Akt 1, Akt 3, PRKCI, PRKCZ, RPS6KB1, and SGK1 (Fleuren et al. 2016). The role of those kinases in tumorigenesis and cancer progression depends on the context in which a mutation occurs. In cervical cancer for example, tumor cells only become dependent from SGK2 upon loss of p53 (Baldwin et al. 2010). This has implications for the development of clinical biomarkers.

## Predictive biomarkers in oncology

True predictive markers are able to estimate the likelihood of clinical benefit of a specific therapy in an individual. Predictive markers can be genetic by nature but markers based on RNA arrays or protein expression have been validated in the clinic as well. Examples for predictive markers in oncology include Her2 amplification as well as the expression of the oestrogen and progesterone receptor in breast cancer, the Braf V600 mutation in melanoma, EGFR mutation and Alk translocation in non-small cell lung cancer (NSCLC), and Ras mutation in colorectal cancer. For genomic markers, it is not enough to understand the (activating, inactivating or neutral) effect of a sequence variation in order to predict clinical response to a targeted agent. First, the predictive value of a biomarker must be assessed in a way that takes into account the biological context, e.g., the tissue of origin, the co-occurrence of other mutations or the influence of the tumor stroma. Second, the source of the biomarker may impact on the

predictive value. In the BELLE-2 trial (Forte et al. 2016), activating PI3K mutations found in cell-free tumor DNA predicted response to PI3K-mTOR inhibition, while PI3K mutations in solid tumor biopsies did not. Finally, the predictive value of a genomic alteration also depends on the threshold of detection. The best-known example for this is Ras. Ras mutations predict resistance against anti-EGFR antibodies. Sequencing Ras with a method sensitive enough to detect Ras mutations in 10-15% or more of the tumor cells (i.e., by Sanger sequencing) results in an inferior predictive value of Ras compared to sequencing with a method that allows for a detection of the mutation in as few as 1-5% of the tumor cells (e.g., by ion torrent based next-generation sequencing). However, if Ras is found mutated by very sensitive sequencing techniques (e.g., droplet digital PCR) in less than 0.1-1% of the tumor cells, the predictive value of the marker starts to drop again (Tougeron et al. 2013; Laurent-Puig et al. 2015).

In summary, the predictive value of a (genetic) marker depends on the biological context, the source of the biomarker (e.g., liquid versus solid tissue biopsy) and the sensitivity of the detection method. Biomarkers of response must be integrated into the development of a pharmaceutical compound, and they need to be tested in a prospective, randomized, and double-blinded trial. For most cancer therapies, predictive markers are not available. No robust biomarker for prediction of response to AGC kinase inhibitors has been identified so far.

## Approved AGC kinase inhibitors in clinical use

Apart from the gold-compound aurothiomalate, the only approved structural AGC kinase inhibitor is miltefosine (hexadecylphosphocholine). Miltefosine is an oral synthetic alkylphosphocholine (ALP), structurally similar to endogenous phospholipids. It can be incorporated into cell membranes and inhibits the membrane-linked protein kinase C (PKC) as well as Akt signalling (Uberall et al. 1991; Ruiter et al. 2003). Miltefosine was evaluated in patients with soft tissue sarcomas (Verweij, Krzemieniecki, et al. 1993), colorectal cancer (Planting et al. 1993) and squamous cell carcinoma of the head and neck (Verweij, Gandia, et al. 1993). Unfortunately, the dose required for an anti-tumor effect was above the maximum tolerated dose (MTD) and thus this drug was not developed as a systemic anti-cancer drug. Some preclinical studies tried to reduce the toxicity by encapsulating miltefosine in pegylated liposomes. This was not successful (Papagiannaros et al. 2006; Teymouri et al. 2015; Laplante et al. 2012). Applied locally, it has a limited effect against cutaneous breast cancer (Clive et al. 1999; Leonard et al. 2001) and cutaneous lymphoma (Sindermann et al. 1993). At a low systemic dose, miltefosine (Impavido®) is approved by the FDA against visceral, mucosal and cutaneous leishmaniasis.

Its derivative perifosine is better tolerated (Hilgard et al. 1997), inhibits AKT, and activates JNK (Hideshima 2006; Fu et al. 2010; Chiarini et al. 2008). Alkylphosphocholines may increase the effect of radiotherapy when given concomitantly or before the radiation (Principe et al. 1992). Thus, perifosine

showed a radiosensitizing effect in prostate cancer (Gao et al. 2011), gliomablastoma (Rübel et al. 2006), lymphoma (Ruiter et al. 1999) and squamous cell carcinoma (Vink et al. 2006). It was tested as single agent in solid tumors but with limited antitumor activity: in a phase 3 trial in patients with advanced colorectal cancer it was found to be ineffective in an otherwise unselected population (Bendell 2012). A phase 3 trial of perifosine in combination with bortezomib (a proteasome inhibitor) and dexamethasone was stopped based on a futility analysis. Perifosine is the most extensively studied ALP in combination with other anti-cancer treatments, such as radiation, mTOR inhibition, and conventional chemotherapy (van Blitterswijk & Verheij 2013). For example, based on a synergistic cytotoxic activity against lymphoma cell lines in vitro and in vivo (Locatelli et al. 2013), perifosine was tested in a phase 2 trial in combination with sorafenib in patients with Hodgkin's lymphoma (Guidetti et al. 2014). So far, there are no positive clinical data for perifosine-based combination therapies.

## Development of AGC kinase inhibitors for cancer therapy

A range of AGC kinase inhibitors have entered clinical development. Table V-1 offers an overview on the most recent trials with a series of AGC kinase-directed inhibitors while Figure V-1 gives a simplified graphical overview of the pathways affected by these inhibitors.

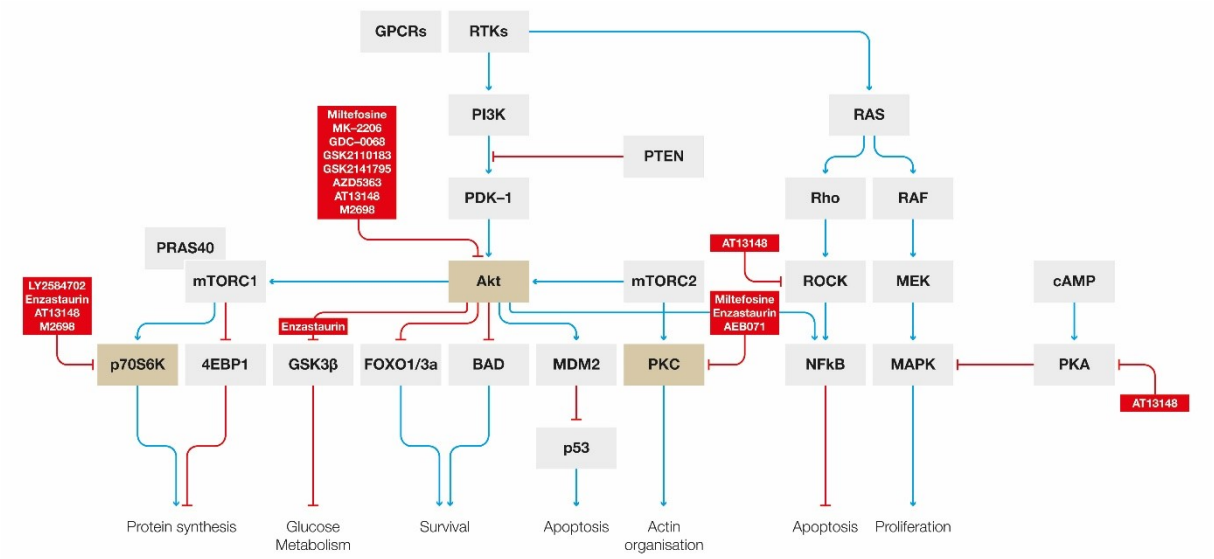


Figure V-1 A simplified overview of the AKT, p70S6K and PKC signaling networks.

Clinical trials with AGC inhibitors are mostly running in this pathway. Red bars represent inhibition, bluearrows represent activation and red boxes indicate the inhibitors and their targets. Part of the crosstalk between the different pathways has been omitted for simplification.

**Akt.** Most Akt inhibitors in clinical development are pan-Akt inhibitors. MK-2206 is an allosteric oral Akt1 & 2 inhibitor with an additional but low potency against Akt3 (Yan 2014; Hirai et al. 2010). Allosteric Akt inhibitors do not result in hyperphosphorylation of Akt Serine 473 and threonine 308,

unlike ATP-competitive inhibitors (Okuzumi et al. 2009). Studies combining MK-2206 with cisplatin showed additive or synergistic activity in vitro and in vivo in gastric (Li et al. 2013) and lung cancer (Galvez-Peralta et al. 2014). Sensitivity to carboplatin and paclitaxel was also increased in breast cancer (Sangai et al. 2012), gastric cancer (Almhanna et al. 2013), and melanoma cell lines (Rebecca et al. 2014). The half-life of MK-2206 is more than 40 hours, arguing in favour of an alternate-day dosing schedule (Yap et al. 2014). The first-in-man dose escalation trial investigated tolerability, safety, and maximal tolerated dose (MTD) of the compound in 33 patients with advanced solid tumors (Yap et al. 2011). Paired biopsies were mandatory. Phosphorylated serine 473 declined in all assessed tumor biopsies, indicating that the target was hit. Drug-related adverse events included skin rash (52%), nausea (36%), pruritus (24%), hyperglycemia (21%), and diarrhea (21%). Skin rash, pruritus and hyperglycemia are typical side-effects occurring upon inhibition of the PI3K-mTOR axis. The rate of hyperglycemia was lower than in trials investigating pan-PI3K or PI3K-alpha inhibitors (with hyperglycemia rates above 50%), but higher than observed in patients on oral mTOR inhibitors (the rate of hyperglycemia of Everolimus for example is roughly 10%). Thus, the side-effect profile is within the expected range for this class of compounds, and adverse events are at least in part related to the downstream blockade of insulin signalling. The MTD was 60mg on alternate days. Three minor responses were observed. One of the responding patients suffered from a PTEN-deficient and Kras G12D mutant pancreatic adenocarcinoma. The two others had metastatic neuroendocrine cancers of the pancreas. This is in line with the fact that mTOR inhibitors such as everolimus are clinically effective and have been approved for therapy of neuroendocrine tumors of the digestive and the respiratory system.

| Target | Subunit | Compound | Name | Company | Mechanism | Phase | Indication | Combination | Comparator | NCT | Start | Status |
|---|---|---|---|---|---|---|---|---|---|---|---|---|
| **AKT** | **pan-AKT** | **MK-2206** | - | Merck | allosteric | Phase 2 | Platinum-Resistant Ovarian, Fallopian Tube, or Peritoneal Cancer | - | - | NCT01283035 | 2011 | Completed |
| | | | | | | Phase 2 | Metastatic Neuroendocrine Tumors | - | - | NCT01169649 | 2010 | Completed |
| | | | | | | Phase 2 | Relapsed Acute Myelogenous Leukemia | - | - | NCT01253447 | 2010 | Completed |
| | | | | | | Phase 2 | Relapsed Lymphoma | - | - | NCT01258998 | 2010 | Completed |
| | | | | | | Phase 2 | Relapsed Diffuse Large-B Cell Lymphoma | - | - | NCT01481129 | 2011 | Completed |
| | | | | | | Phase 2 | Advanced Gastric and Gastroesophageal Junction Cancer | - | - | NCT01260701 | 2011 | Completed |
| | | | | | | Phase 2 | Refractory Biliary Cancers | - | - | NCT01425879 | 2011 | Completed |
| | | | | | | Phase 2 | Non-small Cell Lung Cancer Progredient After Erlotinib Therapy | Erlotinib | - | NCT01294306 | 2011 | Completed |
| | | | | | | Phase 2 | Metastatic Pancreatic Cancer After Prior Chemotherapy | AZD6244 | mFOLFOX | NCT01658943 | 2012 | Completed |
| | | | | | | Phase 2 | Recurrent and Metastatic Nasopharyngeal Carcinoma | - | - | NCT01370070 | 2011 | Ongoing |
| | | | | | | Phase 2 | Progressive, Recurrent/Metastatic Adenoid Cystic Carcinoma | - | - | NCT01604772 | 2012 | Ongoing |
| | | | | | | Phase 2 | Recurrent or Advanced Endometrial Cancer | - | PIK3CA Mutation Stratified | NCT01307631 | 2011 | Ongoing |
| | | | | | | Phase 2 | Previously Treated Metastatic Colorectal Cancer Patients Enriched for PTEN Loss and PIK3CA Mutation | - | - | NCT01802320 | 2013 | Ongoing |
| | | | | | | Phase 2 | Patients With Advanced Breast Cancer Who Have Tumors With a PIK3CA Mutation, or an AKT Mutation, and/or PTEN Loss/PTEN Mutation | - | - | NCT01277757 | 2011 | Ongoing |
| | | | | | | Phase 2 | Refractory Renal Cell Carcinoma | - | Everolimus | NCT01239342 | 2011 | Ongoing |
| | | | | | | Phase 2 | Clinical Stage 2 or 3 PIK3CA Mutant Estrogen Receptor Positive and HER2 Negative Invasive Breast Cancer | Anastrozole if Postmenopausal, Anastrozole and Goserelin if Premenopausal | - | NCT01776008 | 2013 | Ongoing |
| | | | | | | Phase 2 | Prostate with Rising PSA at High-Risk of Progression After Primary Therapy | Bicalutamide | - | NCT01251861 | 2010 | Ongoing |
| | | **GDC-0068** | Ipatasertib | Genentec | allosteric | Phase 2 | Locally Advanced or Metastatic Gastric or Gastroesophageal Junction Adenocarcinoma | Fluoropyrimidine Plus Oxaliplatin | - | NCT01896531 | 2013 | Ongoing |
| | | | | | | Phase 2 | Paclitaxel | Metastatic Triple-Negative Breast Cancer | - | NCT02162719 | 2014 | Ongoing |
| | | | | | | Phase 2b | Glioblastoma / Gliosarcoma | - | MK-3475 (Pembrolizumab) | NCT02430363 | 2015 | Recruiting |
| | | | | | | Phase 2 | Early Stage Triple Negative Breast Cancer | Paclitaxel | - | NCT02301988 | 2015 | Recruiting |
| | | **GSK2110183** | Afuretesib | GSK | ATP-competitive | Phase 2 | Relapsed and Refractory Chronic Lymphocytic Leukemia (CLL) | GSK2110183 (Afuresertib) | - | NCT01532700 | 2012 | Ongoing |
| | | **GSK2141795** | Uprosertib | GSK | ATP-competitive | Phase 2 | BRAF Wild-type Melanoma | GSK1120212 (Trametinib) | - | NCT01941927 | 2013 | Ongoing |
| | | **AZD5363** | - | AstraZeneca | n.k. | Phase 2 | Metastatic Breast Cancer | - | AZD2014, AZD4547, AZD8931, Selumetinib, Vandetanib, Bicalutamide, Olaparib, Anthracyclines, Taxanes, cyclophosphamide, DNA intercalators, Methotrexate, vinca alkaloids, Platinum based chemotherapies, Bevacizumab, Mitomycine C, Eribuline, MEDI4736. | NCT02299999 | 2014 | Recruiting |
| | | | | | | Phase 2 | Metastatic Non-small Cell Lung Cancer | - | AZD2014, AZD4547, AZD8931, Selumetinib, Vandetanib, Erlotinib, Pemetrexed, MEDI4736 | NCT02117167 | 2014 | Recruiting |
| | | | | | | Phase 2 | Triple-Negative Advanced or Metastatic Breast Cancer | Paclitaxel | - | NCT02423603 | 2014 | Recruiting |
| | | | | | | Phase 2 | Metastatic Castration-Resistant Prostate Cancer | Enzalutamide (MDV3100) | - | NCT02525068 | 2015 | Recruiting |
| | | | | | | Phase 2 | Advanced Gastric Adenocarcinoma Patients Harboring PIK3CA Mutation and/or PIK3CA Amplification | Paclitaxel | - | NCT02451956 | 2015 | Recruiting |
| | | | | | | Phase 2 | Biomarker Negative (PIK3CA/MEK/RAS/TP53/MET) Gastric Adenocarcinoma | Paclitaxel | AZD2014 Plus Paclitaxel | NCT02449655 | 2015 | Recruiting |
| | | | | | | Phase 2 | NSCLC | - | AZD4547, AZD2014, Palbociclib, Crizotinib, Selumetinib, Docetaxel, AZD9291, MEDI4736 | NCT02664935 | 2015 | Recruiting |
| | | | | | | Phase 2 | Solid Tumors or Lymphomas | - | Afatinib, Binimetinib, Crizotinib, Dabrafenib, Dasatinib, Defactinib, AZD4547, Nivolumab, Osimertinib, Palbociclib, GSK2636771, Sunitinib Malate, Taselisib, Trametinib, Trastuzumab Emtansine, Vismodegib | NCT02465060 | 2015 | Recruiting |
| | | | | | | Phase 2 | Advanced Solid Tumors | Olaparib (AZD2281) | AZD1775, AZD2014 | NCT02576444 | 2015 | Recruiting |
| **PKC** | **pan-PKC** | **AEB-071** | Sotrastaurin | Novartis | n.k. | Phase 1b/ | CD79-mutant or ABC Subtype Diffuse Large B-Cell Lymphoma | Everolimus | | NCT01854606 | 2013 | Ongoing |
| | | | | | | Phase 1b | Metastatic Uveal Melanoma | BYL719 | | NCT02273219 | 2014 | Recruiting |
| | **PKCβ** | **LY317615** | Enzastaurin | Eli Lilly | n.k. | Phase 3 | Prevention of Relapse in Lymphoma | | Placebo | NCT00332202 | 2006 | Completed |
| | | | | | | Phase 3 | Glioblastoma | Lomustine | | NCT00295815 | 2006 | Completed |
| **Multi-AGC** | **Akt1/2/3, p70S6K, PKA, ROCKI/II** | **AT13148** | - | Cancer Research UK | ATP-competitive | Phase 1 | Advanced Solid Tumours | - | | NCT01585701 | 2012 | Recruiting |

Table V-1 : Recent clinical trials with AGC kinase inhibitors. The most advanced clinical studies were selected.

A second phase 1 trial with the same compound in 50 children with refractory or recurrent malignancies failed to show objective responses (Fouladi et al. 2014). Prolonged stable disease (3 or more months) was observed in 7 patients. The safety profile was comparable to the first-in-man trial.

A phase 2 trial investigated the combination of MK-2206 together with selumetinib, a MEK 1/2 inhibitor (Do et al. 2015). 21 patients with advanced colorectal cancer were enrolled. Akt and Erk phosphorylation were assessed in sequential biopsies. Significant dual target inhibition, defined by downregulation of pAkt and pErk by ≥70%, was not achieved. Since there was no correlation between the PK level and the degree of pAkt/pErk downregulation, it is difficult to decide whether this was due to a suboptimal dose and schedule or rather to an AKT/MEK independent activation of Erk. Gastrointestinal, hepatic, dermatologic and hematologic adverse events were observed, including 3 patients with subretinal fluid accumulation as assessed by ocular coherence tomography (OCT). Overall the toxicity profile was again in line with previous data from AKT and MEK inhibitors, including the mentioned reversible subretinal oedema caused by MEK inhibition.

GDC-0068 (Ipatasertib) is a competitive pan-Akt inhibitor (Lin Kui 2011). It showed efficacy in vitro and in a broad spectrum of human cancer xenograft models. Consistent with findings in other Akt

inhibitors, GDC-0068 enhanced the antitumor activity of chemotherapeutic agents (Lin et al. 2013). In preclinical and clinical settings, compensatory feedback activation of ERK and HER3 was observed (Yan et al. 2013; Tao et al. 2014). The phase 1 trial included 21 patients with advanced solid tumors (Tabernero et al. 2011). Platelet-rich plasma (as a surrogate) and tumor tissue were used to assess pharmacodynamics. Akt inhibition was dose-dependent. As a consequence of Akt inhibition, insulin levels increased up to 1000 fold. The major adverse events included hyperglycemia, asthenia, nausea, and loss of appetite. No objective responses were observed. A recent phase 2 trial has assessed GDC-0068 in 253 patients with castration-resistant prostate cancer after chemotherapy with docetaxel, a taxane derivative. This was a randomized trial with three arms: two different doses of GDC-0068 or placebo in combination with the CYP17 inhibitor abiraterone. There was a trend towards better overall survival in the GDC-0068 arm. Patients with loss of PTEN seemed to benefit more. This may be of importance since more than 20% of prostate cancers have biallelic loss of PTEN (Phin et al. 2013).

GSK2110183 (Afuresertib) is an oral ATP-competitive pan-Akt inhibitor. 73 patients with advanced solid tumors were treated in the phase 1 trial (Spencer et al. 2015). Common adverse events were nausea (20%), diarrhea (16%), dyspepsia (15%), fatigue (15%), anorexia (12%) and gastroesophageal reflux disease (11%). One patient suffered from loss of short-term memory. This is particularly interesting since the symptom is rare but it has been described in patients under therapy with PI3K inhibitors as well. However, no other neurological or neuropsychiatric disorders were observed with this compound. The expansion cohort of this trial focused on multiple myeloma. In a group of 32 heavily pre-treated patients, the response rate was 19% (6/32). A preclinical study showed enhanced anti-tumor efficacy of GSK2110183 in mouse models of KRAS driven pancreatic cancer when combined with trametinib, a MEK1/2 inhibitor (Dumble et al. 2014). However, a phase I study reported high toxicity when both compounds were continuously dosed. Intermittent dosing schedules may be warranted. A phase 2 trial with GSK2110183 in combination with the monoclonal anti-CD20 antibody Ofatumumab is ongoing in refractory chronic lymphocytic leukemia (CLL).

The pan-AKT inhibitor GSK2141795 (Uprosertib) in ovarian cancer enhanced cisplatin-induced apoptosis in vitro and decreased phospho-PRAS40 also in vivo (Pachl et al. 2013; Cheraghchi-Bashi et al. 2015). Based on these results, it was tested with or without platinum in 12 patients with ovary cancer (Gungor et al. 2011). The $^{18}$F-deoxy-glucose (FDG) uptake decreased in >70% of tumors that were visible on the CT scan. No objective responses were observed. The same compound was tested in combination with the MEK1/2 inhibitor trametinib (Algazi et al. 2015). This phase 2 trial accrued 48 patients with advanced melanoma. Although the combination had an acceptable toxicity profile, no responses were observed, neither in the NRAS wildtype nor in the NRAS mutant group of patients. Efforts have been made to identify biomarkers of response to AKT inhibitors. At least for GSK2141795, there may be a correlation between the activity of the mTORC1 phospho-protein network and the

susceptibility of cells to AKT inhibition (Cheraghchi-Bashi et al. 2015). However, no clinical trial with stratification of patients according to the level of mTORC1 activation has been conducted so far.
AZD5363 is an oral pan-Akt inhibitor that was identified through fragment-based drug discovery (FBDD) and shows a favourable PK and toxicity profile (Erlanson et al. 2016; Coleman et al. 2011). Assessment of pharmacodynamics in tumor and surrogate tissue demonstrated effective downregulation of phospho-Akt in a range of tumors (Elvin et al. 2014). AZD5363 is currently being investigated in a series of phase 2 trials (table 1).

Taken together, AKT inhibitors have a clear impact on cancer cell proliferation and survival. They make cancer cells more sensitive to DNA damage by radiotherapy or conventional chemotherapy in vitro and in vivo. They have demonstrated efficacy in early trials for metastatic cancer. Yet, the level of efficacy in the single-agent setting is low and therefore (i) combination therapies and (ii) a selection of patients according to their level of AKT activation must be envisaged (Jansen et al. 2016). Nevertheless, the first Akt inhibitors are moving into phase 3 trials and hopefully there will be some positive data in the near future.

**p70S6K inhibition.** LY2584702 tosylate is selective competitive inhibitor of p70S6K and demonstrated efficacy in glioblastoma and colon carcinoma xenograft models (Tolcher et al. 2014). 34 patients with advanced solid tumors were enrolled in a phase 1 trial (Tolcher et al. 2014). Repetitive skin biopsies were taken as a surrogate tissue for the assessment of phospho-S6 suppression. More than half of the patients had decreased expression of phospho-S6 by immunohistochemistry, indicating that the drug was able to downregulate p70S6K activity. Dose-limiting toxicities included vomiting, increased lipase, nausea, hypophosphatemia, fatigue and pancreatitis. Although the compound suppressed p70S6 activity, no objective response was observed. A phase 1b trial investigated the same compound in combination with erlotinib or everolimus (Hollebecque et al. 2014). The LY2584702/erlotinib combination was not well tolerated. Dose-limiting toxicities included vomiting, hypophosphatemia, pulmonary embolism and decreased clotting factor V. The observed coagulation disorder was surprising since all three compounds did not show signs of coagulopathies when used as single agents. No formal DLTs were observed in the LY2584702/everolimus combination arm. However, no objective response was observed in either arm.

Due to toxicity concerns and an apparent lack of activity, it is unclear whether p70S6 inhibitors in combination with MAPK or mTOR targeting agents will be developed further. Some more recent trials have focused on the inhibition of p70S6 in the setting of multi-AGC kinase blockade (see below).

**PKC.** Enzastaurin (LY317615) is an inhibitor of PKCβ, a component of the B cell receptor signalling pathway. It was initially developed as an antiangiogenic agent. It blocks the phosphorylation of PKCβ,

Akt, GSK3β and p70S6K (Graff et al. 2005). It decreases tumor proliferation (Moreau et al. 2007; Song et al. n.d.) and increases apoptosis in a 4E-BP1-dependent manner in glioma and colon cancer cells (Dumstorf et al. 2010). It showed preliminary efficacy in a range of phase 1 and 2 trials in the setting of haematological malignancies (Morschhauser et al. 2008; Hainsworth et al. 2016; Schwartzberg et al. 2014; Ghobrial et al. 2012; Querfeld et al. 2011; Robertson et al. 2007). The phase 3 PRELUDE trial has investigated enzastaurin as a maintenance therapy following R-CHOP (rituximab, cyclophosphamide, doxorubicine, vincristine, prednisone) therapy of diffuse large B cell lymphoma (DLBCL). The primary endpoint was disease-free survival (DFS). The hazard ratio (HR) of the primary endpoint was 0.92. This was not significant. A phase 3 trial in high-risk DLBCL patients yielded the same (negative) result (Crump et al. 2016). Another phase 3 trial investigated enzastaurin in recurrent glioblastoma in comparison to lomustine, an alkylating agent. The primary endpoint of this trial was progression-free survival (PFS). No benefit of enzastaurin was noted.

PRKCI gene amplification is a frequent reason for the overexpression of PKCι in squamous cell cancer of the lung (Regala et al. 2005), serous ovarian cancer (Eder et al. 2005; Kojima et al. 2008; Zhang et al. 2006) and oesophageal (Yang et al. 2008) cancer. The gold compound aurothiomalate, which is an FDA-approved treatment for rheumatoid arthritis, inhibits PKCι signalling and suppresses cell growth in the four major subtypes of lung cancer in vitro (Stallings-Mann et al. 2006; Regala et al. 2008). A phase 1 trial evaluated aurothiomalate in 15 patients with non-small cell lung cancer (NSCLC) as well as in ovarian and pancreatic cancer (Mansfield et al. 2013). Adverse events included rather mild cytopenia and electrolyte disturbances (hypokalemia). No objective response was detected. Since the level of PKCι suppression was not monitored in this trial, we do not know whether this lack of efficacy is due to subtherapeutic dosing or the biological irrelevance of targeting PKCι in this population.

AEB071 (sotrastaurin) is a selective oral PKC inhibitor. It blocks both classical (α, β) and novel (δ, ε, η, θ) PKC isoforms (Evenou et al. 2009; Naylor et al. 2011). In a phase 1 trial, 118 patients with uveal melanoma were treated. Adverse events included nausea (68%), dysgeusia (58%), constipation (48%), vomiting (42%), diarrhea (36%), abnormal coloration of the urine (35%) and asthenia (26%). The in vivo activity was monitored by assessment of the PKC substrate phosphorylated myristoylated alanine-rich C kinase substrate (pMARCKS). pMARCKS was reduced by 40-90% after two weeks of therapy. However, pMARCKS downregulation did not correlate with response. Out of 118 patients, there was only one objective response. In a recent study, AEB071 was combined with either CGM097 (a p53-MDM2 inhibitor) or RAD001 (a mTORC1 inhibitor) and inhibited the growth of a large panel of patient-derived xenografts of uveal melanoma (Carita et al. 2016). AEB071 is being assessed in the same patient population in combination with binimetinib (a MEK inhibitor) or BYL719 (a PI3K inhibitor) (Carvajal et al. 2016). While the MEK combo was halted early, the trial with BYL719 is still ongoing. Results are pending.

In summary, convincing data that PKC inhibitors are effective clinical anti-cancer agents is still missing despite frequent alterations of the corresponding gene in various cancers. It remains to be determined whether there is a molecularly defined population of cancer patients that draw meaningful benefit from the blockade of PKC isoforms.

**Multi-AGC inhibitors.** The inhibition of PI3K-mTOR signalling through clinically approved, mTOR directed drugs, leads to the activation of a feedback loop that upregulates AKT and upstream (receptor) tyrosine kinases (Rodrik-Outmezguine et al. 2011; Carita et al. 2016; Soares et al. 2015; O'Brien et al. 2014; Britschgi et al. 2012). This may be avoided by a dual blockade of p70S6K and AKT or multiple blockade of AGC kinases.

AT13148 is a first-in-class oral multi-AGC kinase inhibitor. It targets Akt, p70S6K, PKA and ROCK1/2 (Yap et al. 2012). Preclinical data showed antitumor activity gastric cancer cells (Xi et al. 2016) and reduction of metastasis in vitro and in vivo in melanoma cells (Sadok et al. 2015). The first-in-man trial enrolled 14 patients with advanced solid tumors (Kumar et al. 2014). Tumor tissue as well as platelet-rich plasma and hair follicles were used to assess pharmacodynamic endpoints. Only the data for the low dose levels up to 20mg have been published. No downregulation of Akt and no adverse events were observed so far. The trial is ongoing.

M2698 (previously MSC2363318A) is a potent p70S6K, Akt1 and Akt3 inhibitor that crosses the blood-brain barriers in rodents (Machl et al. 2016). 15 patients with advanced solid tumors have been treated so far in a phase 1 trial. One dose-limiting toxicity (a grade 3 lipase increase) was observed (Janku et al. 2014). There is no full publication of this trial yet and further toxicity and efficacy data are expected.
Taken together, there is yet insufficient data to draw conclusions on the potential of multi-AGC kinase inhibitors in the field of clinical cancer therapy. The ongoing trials will hopefully shed a light on the potential of these compounds in clinical cancer care.

# VI. Aims of the thesis

The aims of my thesis were threefold.

Firstly, we aimed to decipher the role, the inter-connections and the mechanisms of regulation of Podoplanin with any druggable targets from patients biopsies and in vitro.

Secondly, we aimed to evaluate the efficacy of a combined treatment with an clinical mTOR inhibitor and a targeted radionuclide in a pancreatic neuroendocrine tumor mouse model.

Thirdly, we intended to investigate a novel combined PI3K-mTOR inhibitor pharmacodynamic properties using serial needle biopsies from advanced cancer patients.

# VII. Podoplanin regulates EGFR-driven Akt activation and resistance to treatment in squamous cell carcinoma.

## Abstract

### Introduction

Collective invasion is one way for cancer cells to disseminate effectively to distant organs and is essential for tumor progression. Podoplanin (PDPN), a highly O-glycosylated cell membrane protein, is a marker for collective invasion at the invasive front in several malignancies. PDPN is known to interact with some ECM proteins and have multiple roles in the immune compartment but how PDPN is regulated is poorly understood.

### Material and methods

Using patient fresh biopsies from head & neck, lung and cervix squamous cell carcinoma (SCC) cohorts, we isolated by laser capture microdissection the invasive margin of the tumor for further analysis. In addition we compared them with three corresponding SCC established cell lines, A431, H226 and Cal 27, to test PDPN-mediated invasiveness in different 3D in vitro experiments.

### Results

PDPN and EGFR are overexpressed in our tumor cohorts and in vitro system and correlate inversely with overall survival. PDPN is responsible for EGFR-induced cell protrusions and cell invasion in 3D environment. Moreover, PDPN regulates the activation of two of the downstream key element of EGFR pathway, Akt and STAT3 but independently of EGFR. Additionally, Erk 1/2 is not regulated by PDPN. Finally, PDPN downregulation sensitizes to EGFRi-induced apoptosis and acquired resistance in the three different squamous carcinoma cell lines.

### Conclusion

The EGFR-dependent activation of Akt and STAT3 is regulated by PDPN. Our results support a role for PDPN as a potential biomarker of resistance to EGFR tyrosine kinase inhibitors (TKIs) already approved in the clinic in malignancies such as non-small cell lung cancer (NSCLC).

## Introduction

Squamous cell carcinoma (SCC) is a malignancy arising within the stratified epithelium of the upper aerodigestive tract, skin, lung, esophagus, pancreas as well as anus and cervix. It is the most common malignancy of head and neck mucosa and the second most common skin cancer (Ferlay et al. 2010). The malignancies are characterized by phenotypic, biological, etiological and clinical heterogeneity. With exception of HPV status, there are no clinically relevant risk factors or biomarkers. Over the last three decades, the 5-year survival rates remain low due to treatment-induced resistance and distant metastasis (Hedberg et al. 2016; Leemans et al. 2011). Therefore, it is important to understand the resistance and metastasis mechanisms of SSC.

EGFR is overexpressed in more than 90% of head & neck squamous cell carcinoma (HNSCCs)(Sacco & Cohen 2015) and present in more than 60% of lung SCC (da Cunha Santos et al. 2005). Beside the FDA approved monoclonal antibody cetuximab, several tyrosine kinase inhibitors (TKI) have been investigated. As monotherapy, Gefitinib has limited activity compared with standard chemotherapy in head and neck (Argiris et al. 2013) but is already approved by the FDA for non-small cell lung cancer. Another TKI, Afatinib, became the first oral TKI to demonstrate efficacy and improvement in patient-reported outcomes in a phase III trial (Machiels et al. 2015). De novo or acquired resistance to EGFR-targeted therapy is a major hurdle for cancer treatment. For instance, secondary somatic mutation of EGFR, T790M, was reported in relapsed NSCLC (Kobayashi et al. 2005; Pao et al. 2005). The EGFR pathway has several downstream element like Akt, Pi3K, RAS, MAPK or the member of the JAK/STAT family (Tebbutt et al. 2013). In addition, the pair EGFR – STAT3 has been shown to be extremely active in malignancies (Lee et al. 2014).

The phosphatidylinositol 3-kinase (PI3K)/AKT/mammalian target of rapamycin (mTOR) signaling pathway is one of the main growth regulatory pathways in both normal cells and cancer (Mayer & Arteaga 2016; Laplante et al. 2012). Multiple genetic events have been described that lead to activation of the PI3K/AKT/mTOR pathway in cancer (Thorpe et al. 2015; Guri & Hall 2016). In different integrated genomic and molecular characterization, the Cancer Genome Atlas Research Network showed that the HPV-negative SSC malignancies were highly mutated for this pathway, either with activating mutation of PIK3CA or inactivating mutations of PTEN (Cancer Genome Atlas Research Network et al. 2017; Hammerman et al. 2012).

Podoplanin (PDPN), also known as T1α, aggrus and gp36, is a type-I transmembrane protein composed of 162 amino acids, whose expression is widely distributed in different tissues including kidney, lung, heart and skeletal muscle (Breiteneder-Geleff et al. 1997; Wicki & Christofori 2007). PDPN emerged to be selectively expressed in lymphatic endothelia and many other types of human tissues but absent

from blood vessel endothelium (Breiteneder-Geleff et al. 1999). Podoplanin (PDPN) is expressed at the invasive front of several malignancies like squamous cell carcinomas (Wicki & Christofori 2007), tumors of the central nervous systems, germ cell tumors (Sonne et al. 2006), mesotheliomas (Kimura & Kimura 2005), vascular tumors (Naqvi et al. 2008) and bone tumors (Ariizumi et al. 2010).

How PDPN actually promotes tumorigenesis is poorly understood. Three of basic amino acids of its nine amino acid intracellular tail has been shown to interact with proteins of the ERM family (ezrin, radixin and moesin) (Yonemura et al. 1998; Martin-Villar et al. 2006; Wicki et al. 2006). Other interactions or direct binding have been shown with Tetraspanin CD9 (Nakazawa et al. 2008), Galectin 8 (Cueni & Detmar 2009), Heat Shock Protein A9 (Tsuneki et al. 2013) and CD44 (Martin-Villar et al. 2010). The interaction between the third platelet aggregator domain (PLAG3) of the extracellular domain of PDPN and platelet CLEC-2 (Nagae et al. 2014; Kato et al. 2003; Herzog et al. 2013) is critical for the separation of the lymphatic compartment from the blood vascular system. It can also protect PDPN positive cancer cell in the blood stream from the immune surveillance by covering them with platelets (Erpenbeck & Schön 2010).

We previously showed that PDPN is expressed in the leading cells at the collective front bypassing EMT in vitro and in vivo. Recently, we showed that PDPN can be induced by single or combined treatment with interferon interferon γ (IFN ), transforming growth factor β (TGFβ) and/or tumor necrosis factor α (TNFα) (Kunital et al, in preparation). Here we report that EGFR resistance to EGFR inhibitor is mediated by PDPN *in vivo*, using 3 cell lines from skin, lung and head & neck SCCs. In this setting, EGFR-dependant Akt activation is also effective only in presence of PDPN, These findings are further confirmed by patient biopsies from lung, head & neck and cervical tumors. Together, PDPN could be a new EGFR-treated resistance biomarker.

## Material & Methods

*Cell lines*

H226 and Cal 27 were purchased from the ATCC collection. A431 was grown in Dulbecco's modified Eagle medium (DMEM; Sigma), and H226 was cultured in RPMI 1640 (Sigma) with 10% fetal bovine serum (FBS), 100 U/mL penicillin and 100 mg/mL streptomycin (Sigma), at 37°C saturated with 5% $CO_2$ in a humid atmosphere.

*Lentivirus production, infection and selection.*

Lentivirus were produced, infected and selected using shPDPN pTRIPZ-based vectors (V3THS_401024, Dharmacon GE, USA) and trans-lentiviral packaging shRNA packaging kit (Dharmacon GE, USA) according to manufacturer's instruction. The cells were then sorted by an Aria (BD, USA) according to their RFP fluorescence in single clones in a 96 well plate with 20% FCS and 20% of conditioned medium. PDPN knockdown was confirmed subsequently by qRT-PCR and FACS. Knockdown is activated by adding 2ug/ml of doxicyclin (Sigma Aldrich, USA) to the medium every 2 days.

*Reagents*

PQR309, GDC-0980 were a generous gift from Piqur Therapeutics AG (Basel, Switzerland). MK2206 was provided by Brian Hemmings. Erlotinib and Afatinib were purchased from Selleck Chemical (USA). Phosphate buffered saline (PBS) and Bovine Serum Albumin (BSA) were purchased at Sigma Aldrich (USA).

*Immunoblotting*

Whole cell lysates from cultured cells were prepared, separated using SDS-PAGE and immunoblotted. The membranes were incubated with antibodies against PDPN, phospho-Akt, Akt and GAPDH, all purchased from Cell Signaling Technology (USA) and diluted according to recommended manufacturer's recommendations.

*Cell migration and matrigel assays*

A wound healing assay was performed by use of the Ibidi chambers (Ibidi GmbH, Switzerland). After serum starvation overnight, the cell migration was visualized and recorded (Olympus IX61) for 30 hours at 37°C.

Grow Factor Reduced (GFR) Matrigel (Corning, USA) was melted at 4°C and applied on the bottom of a 12-well plate. 500 Cells were filtered through a cell strainer and seeded on Matrigel for 24h. Then

fresh medium was added with or without EGF (100ng/ml, generous gift from Brian Hemmings lab) for 16 hours. Pictures were taken by an Olympus IX61 (Olympus, Japan).

*Histological analysis of primary human tumor sections*

Tumor biopsies were freshly frozen in isopentan at -80°C, fixed 60 min in 4% paraformaldehyde, embedded in OCT, and cut into 8 µm sections on a cryostat. The plates were blocked for 1 hour at RT in PBS + 4% BSA and incubated O.N. at +4°C with primary antibody. The plates were washed 3x5min with PBS and incubated for 30 min at RT in a dark room with the secondary antibodies coupled with Alexa Fluor 488 or 555 (Invitrogen) and diluted 1:200 in PBS + 4% BSA. After washing, the fluorescent nuclear stain 4',6'-diamidino-2-phenylindole dihydrochloride (DAPI, Sigma Aldrich) was added and the plates incubated for 2 min at RT. Immunofluorescence microscopy was performed on a Olympus BX63.
Primary antibodies were Podoplanin (Angobio, clone NZ-1), pSTAT3 (Cell Signaling Technology, #9145).

*Laser capture microdissection*

Tumor biopsies were freshly frozen in isopentan at -80°C, embedded in OCT, and cut into 8 µm sections on a cryostat onto a LCM-specific MembraneSlide 1.0 PEN NF (Zeiss). Tumor slides were stained with Arcturus HistoGene LCM Frozen Section Staining Kit (Applied Biosystems) according to manufacturer's instruction. Laser capture microdissection was performed on LSM Palm and tumor tissue was lifted up onto RNAse-free AdhesiveCap 500 opaque (Zeiss). RNA was then extracted using Arcturus PicoPure RNA Isolation Kit (Applied Biosystems).

*Quantitative RT-PCR and PCR arrays*

Whole slide total RNA was prepared using Trizol (Invitrogen), reverse transcribed with Maxima Reverse Transcriptase (Thermoscientific, USA), and quantified by PCR using SYBR green PCR MasterMix (Applied Biosystems, Rotkreuz, Switzerland) and the following primers' pairs: human PDPN, 5'-AAA TGT CGG GAA GGT ACT CG-3' (F) and 5'-AGG GCA CAG AGT CAG AAA CG-3' (R); human HPRT1, 5'-TGA CCT TGA TTT ATT TTG CAT ACC-3' (F) and 5'-CGA GCA AGA CGT TCA GTC CT-3' (R). Human HPRT1 primers were used for normalization. PCR assays were performed in triplicate, and fold induction was calculated against control-treated cell lines using the comparative *C*t method ($\Delta\Delta C$t).
After microdissection, RNA was first preamplified using RT² PreAMP cDNA Synthesis Kit and analyzed on RT² Profiler PCR Array according to manufacturer's instruction (Sabioscience, Qiagen,

USA). Quantitative RT-PCR was performed on ABI ViiA 7 real time PCR-System (Applied Biosystems, USA).

*Protein arrays*

Whole slide were lysed with Pathscan sandwich elisa lysis buffer (Cell Signaling Technology, USA) freshly added with Protease Inhibitor Cocktail (Cell Signaling Technology, USA). Protein lysates were loaded onto PathScan Akt Signaling Antibody Array Kit (Cell Signaling Technology, USA). Protein array near infrared detection were done on Odissey CLx (Li-cor, USA).

*Establishment of the resistant cell line*

A431 cells were treated with an EGFR inhibitor during at least 1 month with 0.1µM the first week, 0.5µM the second and 1µM for the subsequent weeks.

*Long-term proliferation assay*

A431, Cal 27 or H226 cells were seeded into 6-well plates at 500 cells per well in the presence/absence of inhibitor (0.5 or 1 µM) for 21 days or until 100% confluency of the controls. Fresh medium was added 3 times per week. The colonies were fixed with PFA and stained with crystal violet for 30min, followed by 3 times of rinsing with PBS, air-drying and photography of the entire plates. Samples were prepared in triplicates.
In another experiment, 10'000 cells for A431 and Cal 27 and 15'000 cells for H226 per well were seeded into a 6-well plate 16 hours prior to treatment. Then cells were treated with fresh medium 3x per week during 2 to 14 days. At each time point, the cells were rinsed, dissociated using trypsin, diluted according to their confluence (range 1:20 to 1:800) and counted by a cell counter. Samples were prepared in triplicates.

*Flow cytometry*

Cells were trypsinized, washed with FACS buffer and incubated with Ki67, AnnexinV (BD Bioscience) and/or the indicated primary and secondary antibodies for 30 minutes on ice. Dead cells were excluded by staining with UV Live/Dead (ThermoFisher Scientific) and gating on the negative population. After fixation with IC Fixation Buffer (eBioscience), cells were acquired on a LSR II Fortessa and analyzed using FlowJo 10.

*CRISPR-mediated gene editing*

Guide RNAs were designed using E-CRISPR(Heigwer et al. 2014) and respective oligos cloned into the pX458 vector according to protocol (pSpCas9(BB)-2A-GFP (PX458). This vector was a gift from Feng Zhang, Addgene plasmid # 48138)(Arowolo et al. 2011).
Target cells were transiently transfected and GFP+ cells single cell sorted 48h later. Growing clones were analyzed for Podoplanin expression by flow cytometry and negative clones pooled.

*Spheroid assay*

A431 RFP-negative cells were first pre-stained with DII (Molecular Probes, USA) according to manufacturer's instructions .Cells were filtered through a cell strainer and then 1250 cells in 40 µL in an GravityPLUS spheroids plate (Insphero Sàrl, Switzerland) according to manufacturer's instructions.

*Statistical analysis*

Data were analyzed using Graphpad Prism v.6 (Graphpad Software Inc., San Diego, CA) and presented as means ± SEM. Mann-Whitney U-test or one-way ANOVA followed by Tukey-Kramer multiple comparisons were performed.

## Results

*PDPN is upregulated in squamous cell carcinoma tumors.*

First, we wanted to confirm that the patient biopsies from our cohort were expressing Podoplanin. We stained tumors from head & neck, lung and cervical biopsies and compared them to a positive control, an adjacent lymphatic vessel (Figure VII-1A). We also controlled that the staining was at the membrane area by co-staining with cytokeratin 14, a membrane and invasion marker (Suppl. Figure VII-1A). The podoplanin expressing tumors were in majority only in head & neck cohort (21/26, 84%) whereas its content was only 41% in lung and 27% in cervix (Figure VII-1B).

When we checked on a bigger cohort freely available, the Atlas Genome Cohort, the overall survival was better in the top 20% of high PDPN expression compared to the low 20% ($p=0.017$) in head & neck (Figure VII-1D), whereas only a non-significant trend in lung SSC (Suppl. Figure VII-1C). To validate our observation from the clinic in an *in vitro* experimental model, we checked by FACS the amount of PDPN of three SSC cell lines, their inducible knockdown clones (Figure VII-1D) and their knockout clones using the CRISPR-Cas9 method (Suppl. Figure VII-1B). The knockout had no measurable expression of PDPN whereas the shPDPN clones of A431, H226 and Cal 27 had 77%, 45% and 16% of reduction respectively.

*PDPN is responsible for EGFR-induced cell motility.*

We tested then the invasiveness of PDPN expressing cell lines. When A431 cells are cultured in growth factor-reduced matrigel, the membrane protrusion is dramatically delayed but rapidly rescued by EGF (Figure VII- 2A). Interestingly, when A431 cells are cultured in hanging drop, the size of spheroid-like mass is ~3.5-fold smaller in PDPN-depleted cells after 72h ($p<0.001$, Figure VII-2B). This PDPN-dependent phenotypic change in 3D could also be replicated by growing on matrigel. In the control sphere expressing PDPN after 5 days, the daughter cells (Suppl. Figure VII-2A, black arrow) start to disseminate from the sphere. However, the PDPN-depleted sphere shows smooth edge and proliferative pattern. Both spheres are maintained up to 21 days with gradually enhanced distinction of phenotypes, which the disseminated cells are capable of clustering to form new sphere and re-disseminate in a PDPN-dependent manner ((Suppl. Figure VII-2A, blue arrow). In fact, although we could occasionally observe a migratory potential in PDPN-depleted sphere, the outgrowing clusters often undergo apoptosis in spheroids (Suppl. Figure VII-2B) or in vessel-like structures (Suppl. Figure VII-2C).

In a wound healing assay, A431 cell migration stimulated by EGF is decreased when PDPN is knocked down, and incubation with Akt1/2 inhibitor MK-2206 also suppresses cell motility in presence of EGF (Figure VII-2C). PDPN-depleted A431 cells grown on matrigel form similar luminal structures as treated with inhibitors targeting PI3K/Akt/mTOR pathway (Suppl. Figure VII-2D). The invasive potential of A431 cells is regulated through PDPN, at least in part, through active degradation of

extracellular matrix, because PDPN-depleted A431 cells dramatically lose the capacity of degrading gelatin within 72h (Suppl. Figure VII-2E).

*Cellular localization of EGFR-activated Akt is regulated by PDPN*

We then wanted to assess whether downstream element of EGFR were activated. The whole slice lysis of patient tumors showed an increased phosphorylation of PDPN positive SSC tumors of the lung and head and neck ($p<0.01$, Figure VII-3A). RNA is more stable compared to phospho-protein so we performed a laser capture microdissection of the region of interests (ROI) in the same patient biopsies and EGFR was upregulated by 2.3 fold in the tumors expressing PDPN ($p=0.015$, Figure VII-3B).
Moreover, in response to EGF, the cells expressing PDPN showed membrane protrusions, while in absence of PDPN, the filopodia-like structures are significantly diminished (Figure VII-3C). The localization of phosphorylated Akt is remarkably different upon PDPN depletion; there is massive accumulation of phosphorylated Akt specifically located at membrane protrusions where the actin polymerization is greatly enhanced (Figure VII-3D). When PDPN is depleted, upon stimulation with either insulin or IGF, induced Akt phosphorylation could also be observed but restricted to intercellular junctions (Figure VII-3D). We blotted the phospho-Akt expression when activated with EGF for 16 hour upon serum starvation and it can re-activate p-Akt in presence of PDPN but less in absence of PDPN.
In addition, the erlotinib resistant clones showed an increased activation of Akt when starved or activated with EGF (Figure VII-3E). Lastly, we observed that PDPN can be rapidly cleaved upon serum starvation, which could be inhibited in presence of EGF stimulation (Suppl. Figure VII-3A). This data showed that EGFR signaling may functionally regulate PDPN through supporting its correct folding and/or stability.

*EGFR-dependent activation of STAT3 is regulated by PDPN*

To further confirm the activation of the EGFR pathway, we looked at another canonical downstream element, STAT3. In our head & neck und lung cohort, 63% of the PDPN expressing tumors were co-expressing phospho-STAT3 whereas only 11% of the non-PDPN expressing tumors were positive (Figure VII-4A). The co-expression of phosphor-STAT3 was within the invasive strand, a finger-like structure invading its surrounding like in Figure VII-4B. These features could be recapitulated when A431 cell were grown on Matrigel but only in presence of EGF in PDPN-expressing cells. (Figure VII-4C). These data further confirmed the PDPN-driven EGFR activation with phospho-STAT3 in complement of Akt.

*PDPN upregulation is associated with EGFRi-induced acquired resistance and apoptosis in squamous carcinoma cell lines*

Interestingly, we observed that PDPN-positive cells were less sensitive to EGFR inhibition than their respective knockout or knockdown clones. Our three cell lines are negative for the EGFR T790M mutation. We assessed these properties in a resistance assay. The shPDPN clones were significantly more resistant to Erlotinib and Afatinib for A431 and H226 compared to the untreated cells, whereas Cal27 was very sensitive with or without PDPN (Figure VII-5A). The knockdown clones showed a similar or slightly increased effect for Cal-27 on day 14 (Figure VII-5B). We analyzed the PDPN protein expression in these wild type resistant clones and PDPN was increased by 1.65, 1.45 and 1.88 fold for A431, H226 and Cal 27 respectively (Figure VII-5C). When analyzed with FACS, these cells show that PDPN downregulation sensitizes to EGFRi-induced apoptosis by elevating cleaved caspase 3 (Figure VII-6A) and consistently elevated amount of cells in early (Figure VII-6C) as well in late apoptosis (Figure VII-6D). Finally, we also observed similar reaction to other classes of inhibitors such as a combined PI3K inhibitor PQR-309 and the PI3Ka/d inhibitor GDC-0941 in a different resistance assay (Supplementary Figure VII-4A). Together these data indicate a PDPN-dependent resistance mechanism.

## Discussion

These data potentially indicates that PDPN-dependent cell proliferation, migration and invasion are substantially promoted by a 3D environment; secondly, PDPN potentially regulates cell fitness in stressed conditions such as nutrient restriction and lastly, PDPN may potentially contribute to resistance to unfavorable environments during cell proliferation. It has been noticed that the cancer cells in the core of spheroid are capable of continuous proliferation in a PI3K/Akt-dependent manner, although the nutrient supply is restricted.

Consistent with those findings, treating these spheroids with PI3K/Akt/mTOR inhibitors induces notable apoptosis in the center of the spheroid, while the cancer cells at the edge that access the environmental nutrients and associate with reactivated PI3K/Akt signaling will still survive (Muranen et al. 2012), indicating that this signaling axis contributes to unresponsiveness to drugs potentially targeting the PI3K/Akt signalosomes.

Our results show that PDPN expressing cancer cells have a survival advantage toward EGFR inhibition. A similar phenomenon was observed in the clinic, especially in the lung malignancies where upon EGFR inhibition by TKI or antibody, adenocarcinoma transition to squamous cell carcinoma (AST, reviewed in (Hou et al. 2016)). This mechanism may be responsible for drug resistance and it would be interesting to check the PDPN status of these evolving tumors.

The quite low level of PDPN-expressing lung and cervix tumor may be partially caused by the tumor heterogeneity, as we resect only a small fraction of the tumor that may not include the invasive front. Another explanation for the lung cohort is the difficulty of assessing precisely the SSC subtype and the transition from SSC to adenocarcinoma in these malignancies.

Using the K14-HPV16 mouse model of invasive uterine cervical SCC (Giraudo et al. 2004), Kunita and colleague had similar findings in a recent paper (Kunita et al. 2018). They showed that inflammatory cytokines, including phospho-STAT3, co-localized with PDPN-expressing cells in the invasive areas of cervix of mice and of cervix SCC in patients. In our study, we did not investigate the other related cytokines.

Interestingly, the efficiency of shPDPN in its reduction of PDPN was correlated with the resistance assay. A431 had the better PDPN reduction and the bigger difference in proliferation compared to Cal 27 that has exactly the opposite. This may be a gradient effect in the PDPN depletion and should be further investigated.

Together, these data indicate that PDPN is interfering with a druggable target and a well-known signaling pathway. It would be interesting to discover the real underlying mechanism of these interactions. Hence, a screening of resistant SSC patient prior to their treatment with EGFR inhibitors should be conducted and could provide some predictive insights.

## Acknowledgements

We would like to thank Bruno Grilli from the Department of Pathology of the University Hospital Basel for the support concerning all the Laser Capture Microdissection experiments. We also would like to thank the DBM Sorting and DBM microscopy facilities of the Department of Biomedicine of the University Hospital Basel.

## Figures

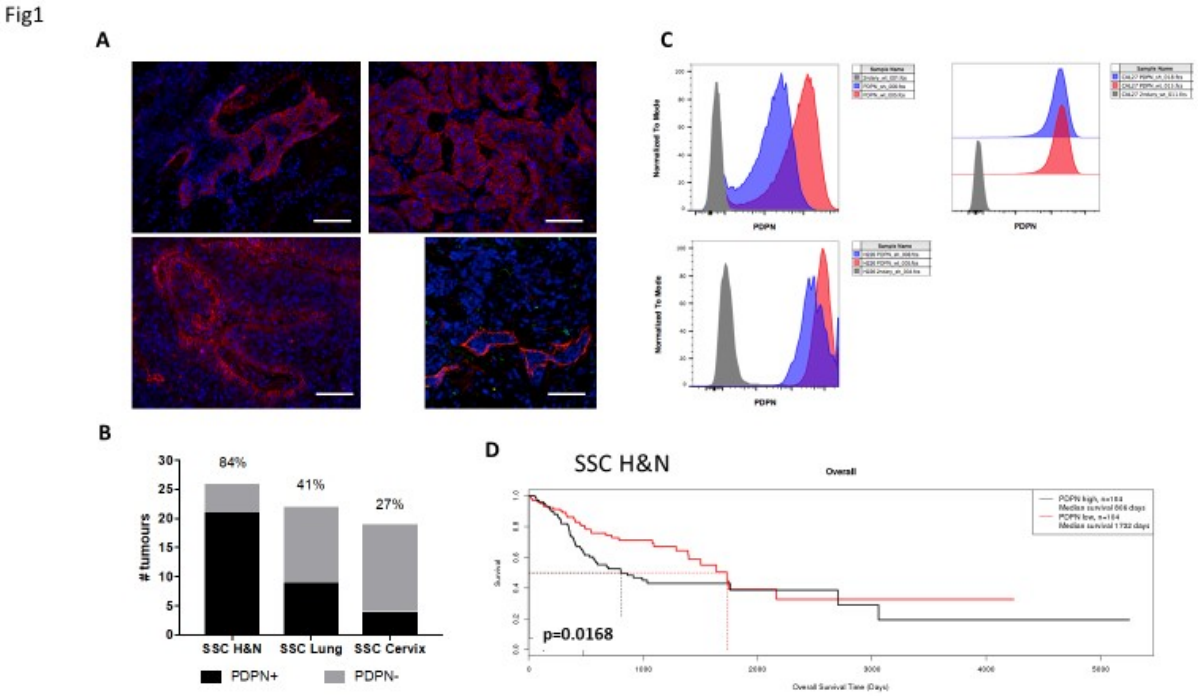


Figure VII-1 : Podoplanin is expressed at the invasive front of SSC.

**A**, Immunoflurescence staining of H&N (upper left), lung (upper right), cervix (lower left) and a positive control, a lymphatic vessel (lower right). Red is PDPN, blue is DAPI. Scale bar is 60um. **B**, Proportion of Podoplanin positive tumors from each cohort with percentage on top of each bar. **C**, Histograms of FACS staining of A431, H226 and Cal27 and their respective shPDPN conditional knockdown clones. Logarithmic scale on the x-axis. **D**, Overall survival of the head & neck SCC TCGA cohort in days. Red is low PDPN expressing patients, black is high PDPN expression patients.

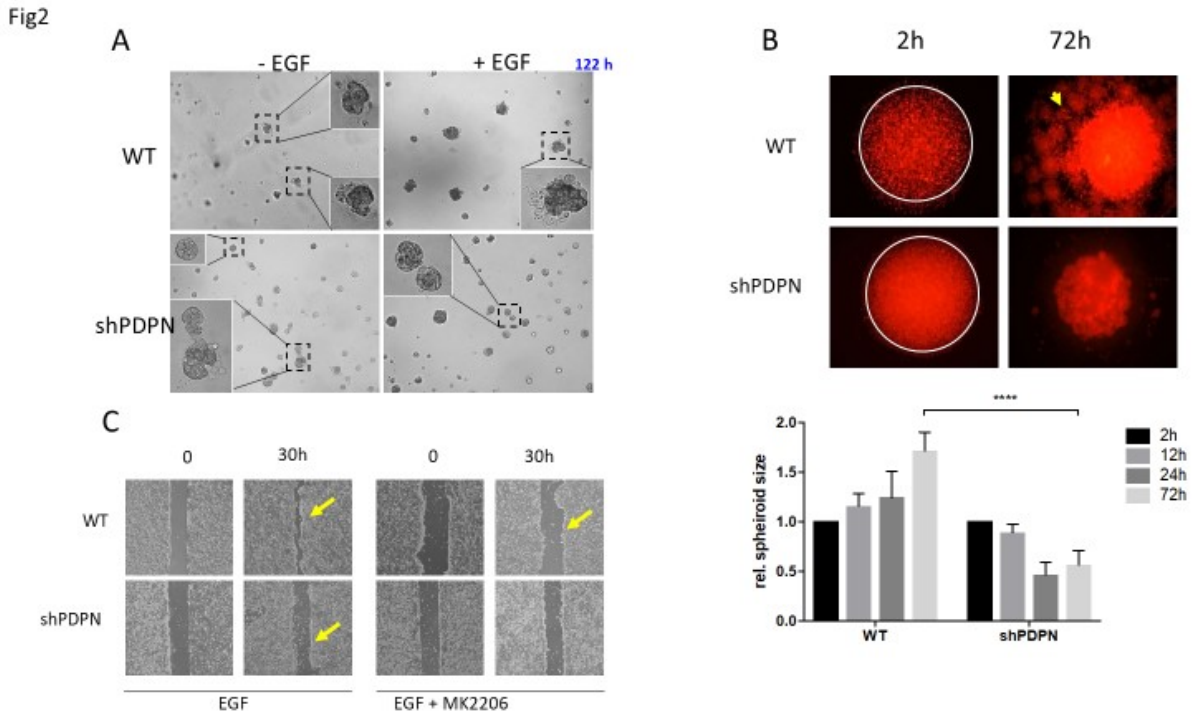


Figure VII-2 : PDPN is responsible for EGFR-induced motility

**A**, Single A431 cells forming spheroids after 5 days on growth factor reduced Matrigel with or without EGF in medium (left or right) for WT (upper) or shPDPN cells (lower). **B,** Spheroids in hanging drops after 2 and 72 hours. Lower graph is relative spheroid size to 2h time point. Mean + SEM, ****p<0.0001. **C,** Wound healing assay with A431 cells with EGF and EGF + MK2206 Akt inhibitor before and after 30h of treatment. The yellow arrow indicates the invasive front.

Fig3

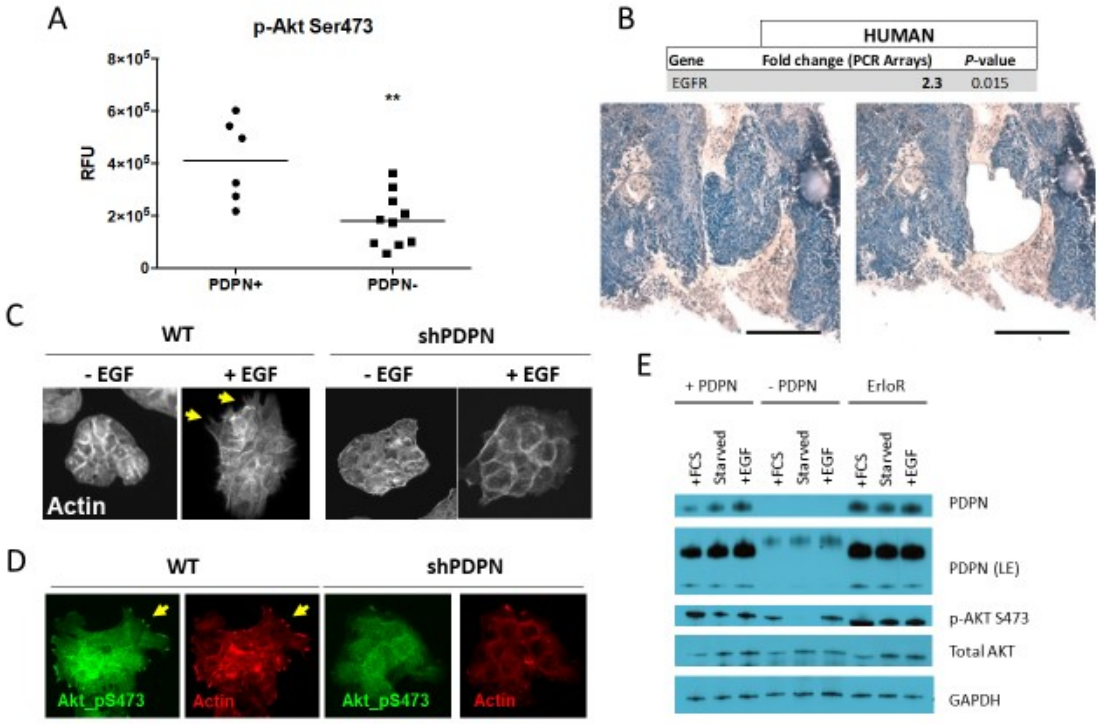


Figure VII-3 : EGFR-dependent activation of Akt is regulated by PDPN

**A**, Graph of the phospho-protein level of Akt at the serine 473 site for PDPN+ (n=6) and PDPN- (n=10) tumor biopsies. RFU= relative fluorescent units, **P<0.01. **B,** Table with the EGFR fold change in PDPN+ tumors compared to PDPN- (upper). The ROI stained before laser capture microdissection (left) and after (right). Scale bar = 60um. **C,** A431 cells grown on Matrigel in absence or presence of Matrigel after 14 days. Slides are stained for actin. Yellow arrows indicate the philopodia-like structures. **D,** Immunofluorescence pictures of phospho-Akt Serine 473 site (green, left) and actin (red, right). Yellow arrows indicate the membrane protrusion. **E,** Immunoblotting for control (FCS), starved and EGF treated cells. Proteins are PDPN, total Akt, phosphor-Akt Serine 473 and GAPDH. ErloR mean erlotinib resistant clone. PDPN (LE) means long exposure.

Fig4

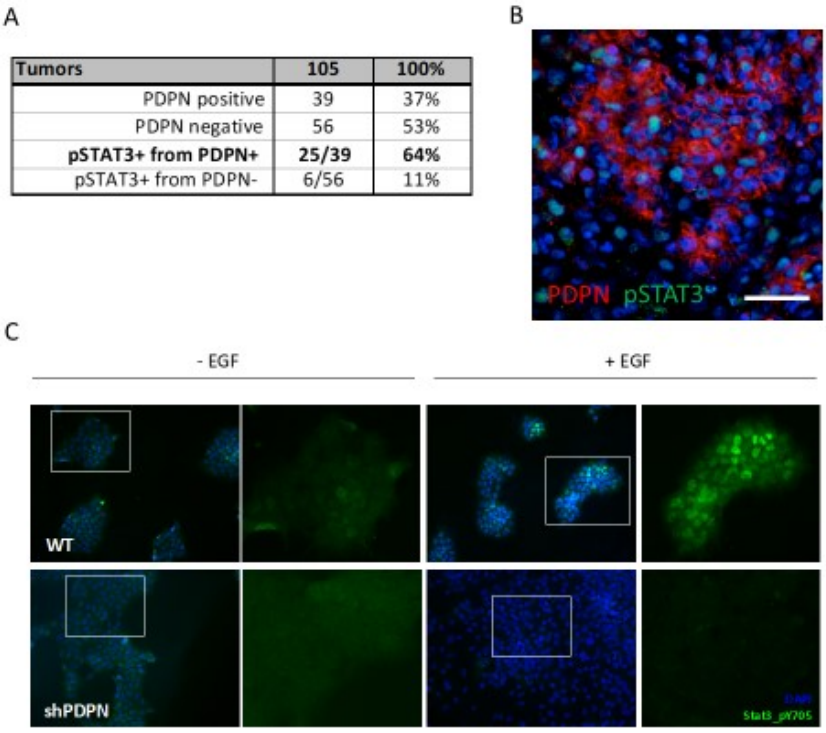


| Tumors | 105 | 100% |
|---|---|---|
| PDPN positive | 39 | 37% |
| PDPN negative | 56 | 53% |
| **pSTAT3+ from PDPN+** | **25/39** | **64%** |
| pSTAT3+ from PDPN- | 6/56 | 11% |

Figure VII-4 : EGFR-dependent activation of STAT3 is regulated by PDPN

**A,** Table with total number and percentage of tumors in each category: PDPN positive, negative, proportion of phospho-STAT3 positive in PDPN positive and negative tumors. **B,** Immunofluorescent cross-section of an invasive strand in a human biopsy. Red, PDPN; Green, phospho-STAT3; blue, DAPI. Scale bar = 60um. **C,** Immunofluorescent pictures of A431 cells on Matrigel with or without EGF in presence or absence of PDPN. Square are magnified areas. Green, phospho-STAT3; blue, DAPI.

Fig5

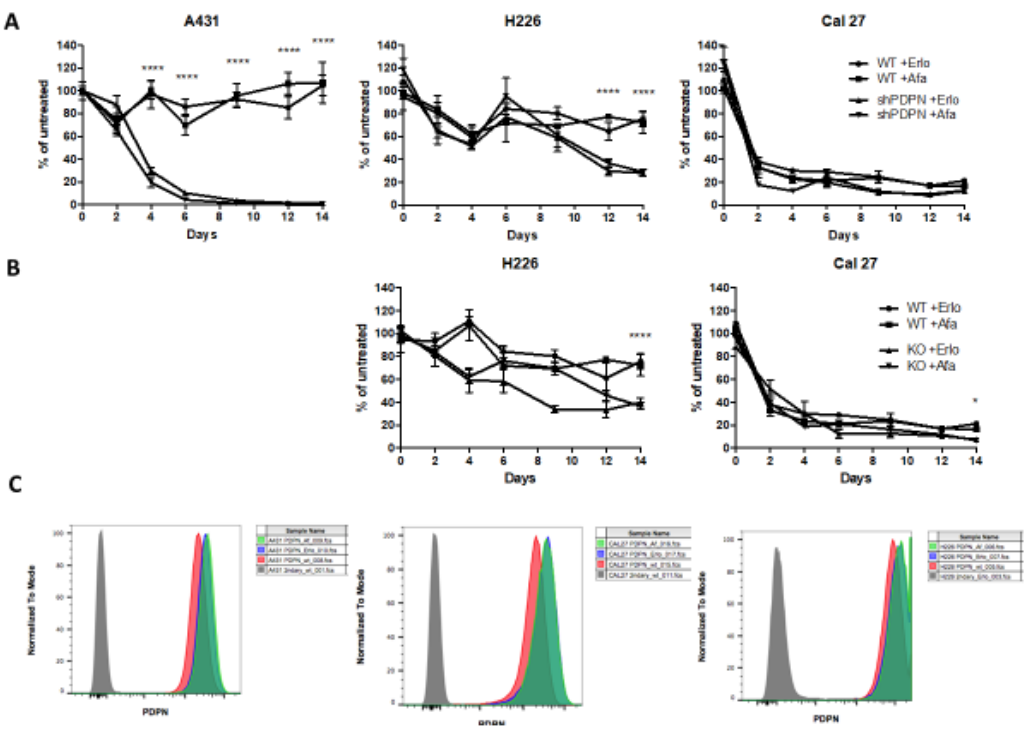


Figure VII-5 : PDPN upregulation is associated with EGFR-induced acquired resistance

Graphs of A431, H226 and Cal 27 cell lines as a percentage of the untreated controls comparing wild type cells with **A,** shPDPN clones and **B,** CRISPR/Cas9 knockout. In each graph, the two upper lines are WT. **C,** Histograms of FACS staining for WT, erlotinib and afatinib resistant clones. Logarithmic scale on the x-axis.

Fig6

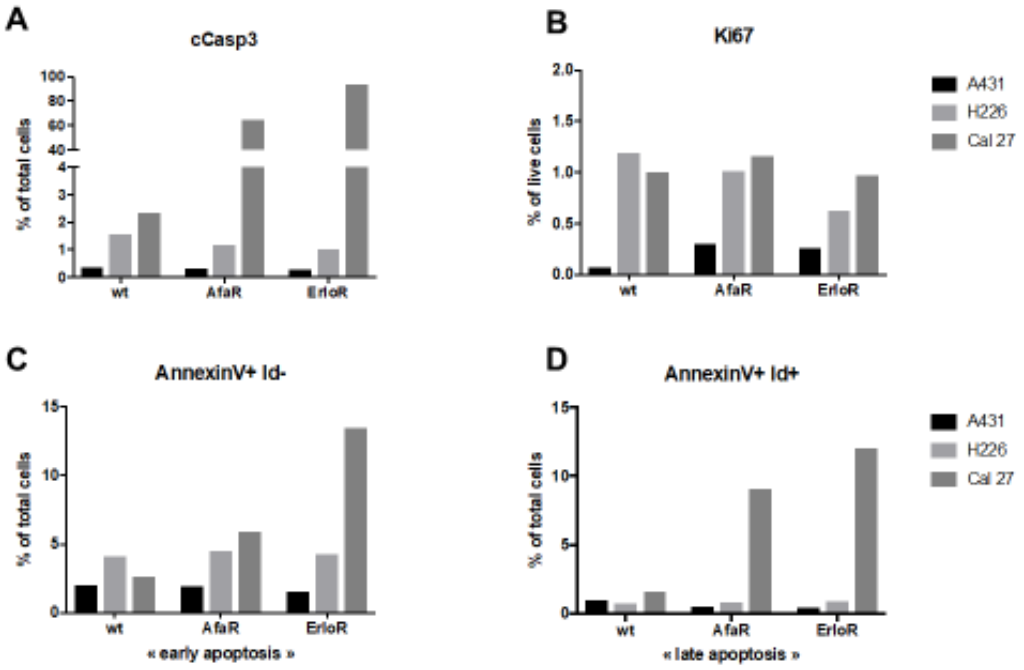


Figure VII-6 : PDPN upregulation is associated with EGFR-induced apoptosis

FACS staining of resistant cell from figure VII-5. Percentage of cells positive for **A**, cleaved caspase 3, **B**, Ki67, **C,** AnnexinV+ LiveDead- and **D**, AnnexinV+ LiveDead-. Scale in percent of total viable cells.

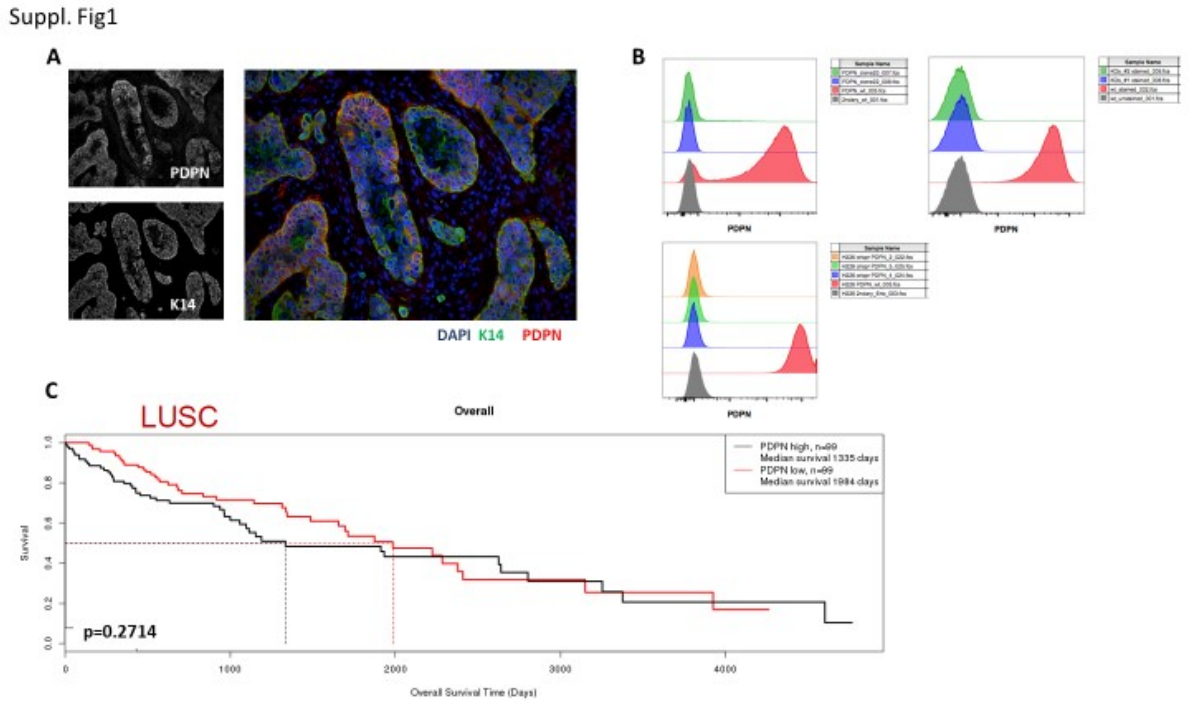


Suppl. Figure VII-1

**A**, Immunoflurescence co-staining of H&N tumors (right) with PDPN (upper left) and membrane marker K14 (lower left). Red is PDPN, green is K14 and blue is DAPI. **B**, Histograms of FACS staining for A431, H226 and Cal27 and their respective CRISPR/Cas9 knockout clones (n=2 or 3). **C**, Overall survival of the lung SCC TCGA cohort in days. Red is low PDPN expressing patients, black is high PDPN expression patients.

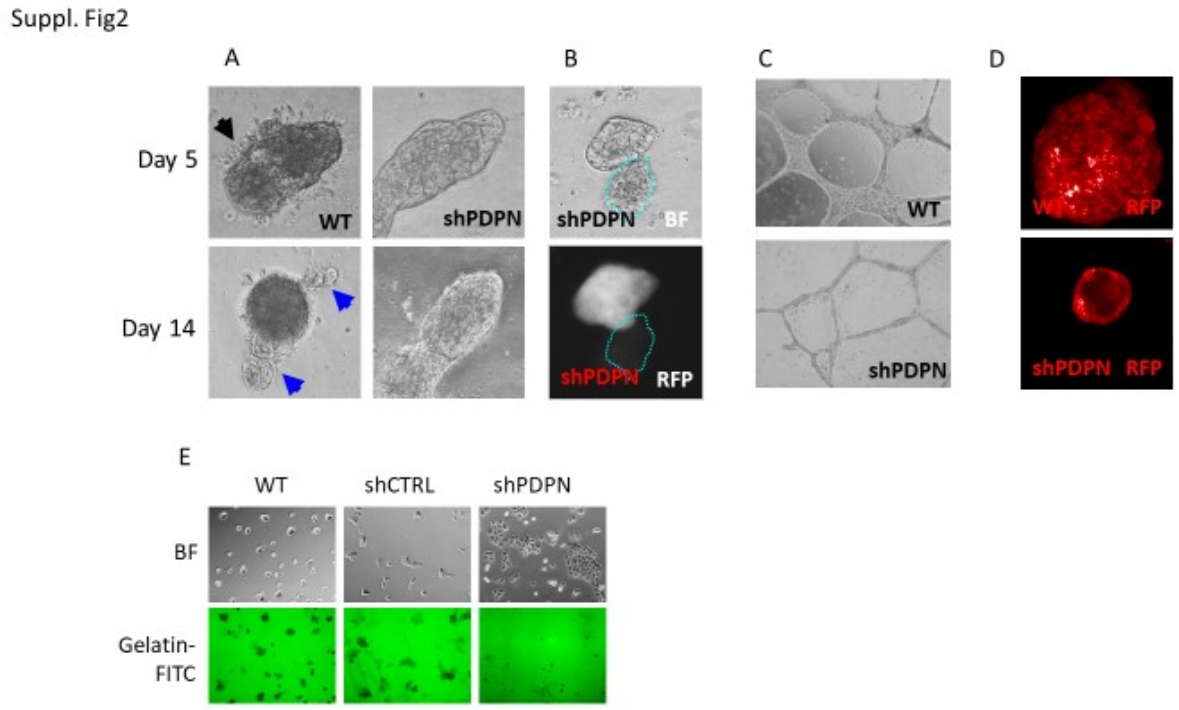


Suppl. Figure VII-2

**A,** Bright-field microscopy of A431 cells protrusion on Matrigel in presence or absence of PDPN after 5 and 14 days. Blue arrow and black arrows indicate new spheres. **B,** Bright-field microscopy of A431 cells undergoing apoptosis in bright field (BF) and corresponding red fluorescence with DII die (RFP). **C,** A31 cells forming stabilized tubule-like structures after 21 days on Matrigel with PDPN and apoptotic without PDPN. **D,** luminar-like structure in absence of PDPN in A431 cells on Matrigel stained with DII. **E,** zymography of cells with bright field (upper) and fluorescent picture of GFP-labeled gelatin (lower). Black staining shows the degradation of the matrix by the cells.

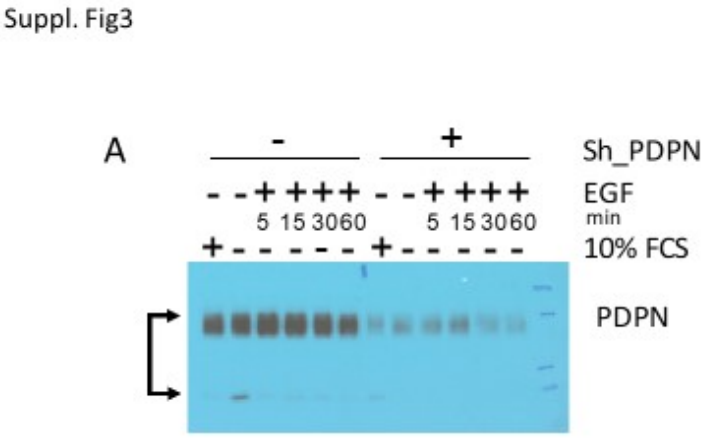


Suppl. Figure VII-3

**A,** Immunoblotting of shPDPN with or without doxycycline (knockdown). The second line represents the time of treatment with EGF without serum. The third line, the starvation status. The arrows indicate 40kDa and 15kDa respectively.

Suppl. Fig4

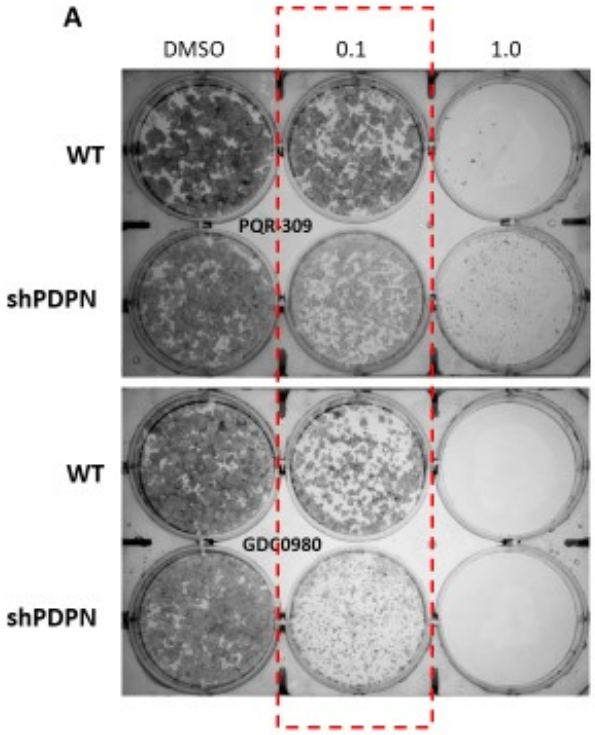


Suppl. Figure VII-4

**A,** Bright field picture of a 6-well plate with wt and shPDPN clone. The doses are 0.1 and 1.0 uM, DMSO is the negative control. The points represent the colonies stained with crystal violet.

# VIII. Combined treatment of neuroendocrine tumors with Lu-177-Exendin-4 and mTOR Inhibitor: a long-term preclinical study

## Abstract

**Purpose**: The aim of this study is to evaluate the combined treatment of neuroendocrine tumors with PRRT and mTOR inhibitor Everolimus in a preclinical setting. Rip1Tag2 mice develop insulin producing neuroendocrine tumors in the pancreas that are known to express GLP-1-receptor and to be dependent on mTOR. This makes Rip1Tag2 mice an ideal model to study PRRT with 177Lu-DOTA-exendin-4 ([Lys40(Ahx-DOTA-177Lu)NH2]-exendin-4) and Everolimus. We investigated the long-term survival as well as histology and phospho-proteins of the pNET tumors.

**Methods and Materials**: Rip1Tag2 mice were treated with 177Lu-DOTA-exendin-4 (2MBq day1, 1MBq day36), Everolimus 5mg/kg daily or every third day and combination of both. n=10 planned. One series is carried out over 20 days, a second series over a maximum of 9 months. Besides tumor size and survival, AKT/mTOR-pathway, proliferation, apoptosis activity was analyzed.

**Results**: Preliminary long-term results (5-7 mice/group) showed minor prolonged survival for PRRT alone (37.8+/-11.9 days) over control (27.3+/-5.9 days). Everolimus (77.1+/-24.3 days, ) as well as the combined treatment (73.0+/-17.1 days) clearly extended survival.

While daily treatment over 20 days with Everolimus lead to reduced tumor weight (41.8+/-40mg; control 73.4+/-26mg), Everolimus given every third day didn’t alter tumor weight (81.5+/-44mg). Combination of Everolimus daily and PRRT showed high synergistic potential (7.8+/-10mg).

Histology showed no alteration in mTOR/AKT-pathway activity through PRRT but reduced activity in combination with Everolimus daily. Everolimus given every third day had a paradox effect with a tendency to activate mTOR/AKT-pathway.

**Conclusion**: These results demonstrate efficacy of both treatments alone and the potential of combined treatment. Everolimus is only effective when given daily. Intermittent administration of Everolimus isn't effective, which explains previous contrary results published by Pool SE, CancerRes2013.

## Introduction

Neuroendocrine tumors (NETs) are a rare malignancy with increasing incidence (Modlin et al. 2003). NETs arise predominantly from the gastrointestinal tract or the pancreas, belong to the less aggressive malignancies and may develop no or only mild clinical symptoms over years. Most of the patients are diagnosed in an already metastasized stage and only complete surgical removal can cure.
Well differentiated NETs overexpress the somatostatin receptors at high density (Reubi & Waser 2003) as well as glucacon-like peptide 1 receptor (GLP-1R) (Wild et al. 2006) among other specific receptors. Peptide receptor radiotherapy (PRRT) with radiolabelled somatostatin analogues, such as $^{90}$Y-/$^{177}$Lu-DOTATOC or $^{177}$Lu-DOTATATE, can be used for the specific targeting of these tumors (Imhof et al. 2011; Kwekkeboom et al. 2008). According to the last ENETS guidelines, PRRT is recommended as a the second line treatment option of metastasized intestinal neuroendocrine tumors with other targeted therapies (Pavel et al. 2016). Though PRRT can cause kidney insufficiency and has hematotoxic potential, the balance of side effects to treatment effect is favorable (Villard et al. 2012; Kwekkeboom et al. 2008). Therefore there is a rational for combined treatment demonstrating? lower side effects due to reduced doses and an additive or synergetic potential effect. Only palliative systemic therapy are used in the clinic. Combination therapy, such as $^{177}$Lu-DOTATATE and CAPTEM (Claringbold & Turner 2016), have the potential to ameliorate these palliative therapies. Previously, we applied successfully combined treatment with Vatalanib, an antiangiogenic drug (Wicki et al. 2014).

mTOR inhibitor RAD-001 (Everolimus®) is approved by FDA and EMA for the treatment of metastasized NET since the RADIANT trials approved efficacy of Everolimus® (Pavel et al. 2011; Yao et al. 2008; Yao et al. 2011). For many NETs, it has been shown that proliferation is dependent on mTOR (Johannessen et al. 2005). RAD-001 interferes with the mTOR complex after it bound to the intracellular receptor FKBP12 (O'Donnell et al. 2008; Laplante et al. 2012) and possibly has some anti-angiogenic properties (Lane et al. 2009). Moreover, in vitro data show the radio-sensitizing effect of Everolimus (Mauceri et al. 2012; Shinohara et al. 2005), where the PI3K pathway seems to play a pivotal role (Manegold et al. 2008; Prevo et al. 2008).

In 2013 and 2014, two papers proposed that Everolimus does not have an additive or synergistic effect in combination with PRRT and even promotes metastases in a rat xenograft model of neuroendocrine tumor (Pool et al. 2013; Bison et al. 2014). Up to now, such an effect has not been found in clinical studies. In the setting of controversial preclinical and clinical data many centers ask patients to stop mTOR inhibition before PRRT. The fear of additive side effects, such as low blood count pronounced by both PRRT and Everolimus, may contribute to the retentiveness.

The aim of this study was to evaluate any additive or synergistic effect of combined PRRT and mTOR inhibitor treatment and clarify the existing controversies in the literature. Using transgenic Rip1Tag2 mice, this study was carried out in an immune competent, more physiological and potentially better suited neuroendocrine tumor model than a xenograft model.

## Methods

*Mice*

Rip1Tag2 transgenic mice develop insulin producing neuroendocrine tumors in the pancreas in a well characterized multistep tumorigenesis (Hanahan 1985). Mice were kept in a C57Bl/6 genetic background and breeded as previously described (Wicki et al. 2007). All mice were tested with PCR for the Rip1Tag2 defect. Mice were included in the experiment at the age of 11 weeks. All animal experiments were performed according to the guidelines and legislation of the Swiss Federal Veterinary Office (SFVO) and the Cantonal Veterinary Office, Basel-Stadt, Switzerland, under license number 2597.

*Radionuclide labelling*

$^{177}$Lu-DOTA-exendin-4 was prepared after incubation of 7.5 µg DOTA-exendin-4 (1 mg/mL in water) with 80-170 MBq $^{177}LuCl_3$, at 95°C for 30 min in ammonium acetate buffer (0.4 M, pH 5.0). Quality control was performed by reverse phase high performance liquid chromatography (RP-HPLC). The radiolabeled peptide solutions were prepared by dilution with 0.9% NaCl containing 0.05% HSA at specific activities of 50 MBq/nmol and 100 MBq/nmol, for biodistribution and therapy studies, respectively.

*Biodistribution studies*

Biodistribution studies of $^{177}$Lu-DOTA-exendin-4 (1.1 MBq, 20 pmol) were done in untreated groups (n >= 5) of Rip1Tap2 mice, serving as control and Rip1Tag2 mice after pre-treatment with Everolimus at 1, 5 or 10 mg/ kg bodyweight. Pre-treatment consisted of oral drug administration over 3, 7 and 10 days daily. Furthermore biodistribution of 1 MBq $^{177}$Lu-DOTA-Exendin-4 were performed after treating mice with 5 mg Everolimus daily (E cont) over 10 days and a period of withdraw of 10 days. Another group (E pulse) had been analysed after pre-treatment with 5 mg/kg bodyweight Everolimus every third day. 4 hours after the injection of 1 MBq $^{177}$Lu-DOTA-Exendin-4 in the tail vein, the mice were euthanized. Then blood and the following organs were resected : stomach, both kidneys, bowel, pancreas, spleen, liver, leg muscle, lung heart, adrenals, bone, pituitary and the tumors. The organs were weighed in a precision balance and activity was measured by a beta-counter.

*Therapy studies*

Different therapy regimen have been analysed for the efficacy after 10 or 20 days as well. Groups of Rip1Tag2 mice included untreated control, Everolimus 5 mg / Kg bodyweight daily (E cont), Everolimus 5 mg / Kg bodyweight every third day (E pulse), PRRT with 2.2 MBq $^{177}$Lu-DOTA-Exendin-4 (PRRT) at start of treatment. Treatment of Everolimus 5 mg / Kg bodyweight daily was

combined with the PRRT of 2.2 MBq $^{177}$Lu-DOTA-Exendin-4 (Combined). Mice were euthanized, total tumor burden (weight) assessed and tumors were analysed for proliferation, apoptosis, microvessel density.

Mice were injected 1.1 MBq or 2.2 mBq of Lu-177-Exendin-4 at a peptide mass of 10 pmol each via tail vein injection.

Everolimus (also known as RAD001) was administered orally after dissolving in 5% glucose at a dose of 1 mg/ KG bodyweight, 5 mg/ KG bodyweight or 10 mg/ KG bodyweight. Volumes administered were bodyweight adapted (1 ml / 100 g bodyweight). Stock solution of Everolimus was provided by Novartis Pharma, Switzerland.

Furthermore long term survival was examined in groups of 10, including untreated control, Everolimus 5 mg / Kg bodyweight daily (E cont), 5 mg / KG bodyweight every third day (E pulse), PRRT with 2.2 MBq $^{177}$Lu-DOTA-Exendin-4 at start of treatment and a second injection 1.1 MBq at day 36 (PRRT) as well as the combination of Everolimus 5 mg / Kg bodyweight daily and PRRT with the regimen mentioned above (Combined). This series was carried out over a maximum of 9 month or until predefined endpoints (loss of bodyweight, behavioural impairment, low blood glucose levels) were reached as previously described (Bill & Christofori 2016). The termination criteria were based on a weight score (+/- 2g = 0, +/- 4g = 2, >= 4g = 3), an activity score (normal activity = score 0; wiggling/reduced activity = 2; still/hunchback/poor general condition = 3) and blood glucose levels (>2.1 mmol/L = score 0; 1.1–2.0 mmol/L = 1; 0.7–1.0 mmol/L = 2; <0.7 mmol/L = 3) measured using the blood glucose meter Contour Next (Bayer). Mice were euthanized when reaching a total score of 6 or if presenting with score 3 in one of the three criteria.

*GPL1-R density*

Untreated control mice and mice treated over 10 days with Everolimus 10 mg / Kg Bodyweight (groups of 4 each, with 2 or 3 tumors per mice) were freshly frozen on dry ice for GLP-1-receptor density. Then GPL1-R quantification was performed by in vitro receptor autoradiography as previously described (Reubi et al. 2010).

*Tissue preparation for histology*

For immunofluorescence (IF) staining, organs (pancreas, kidney, adrenal gland, lung, colon, liver, heart and spleen) were isolated, fixed during 2 hours in PBS/4%PFA and cryopreserved in PBS/20% sucrose overnight, both at 4°C. Pancreas were embedded, snap frozen in optimal cutting temperature (OCT) freezing solution (Thermo Scientific), and stored at −80°C.

*Immunofluorescence and TUNEL assay*

Pre-fixed tumors were cut with the cryotome in 7µm sections and air dried overnight. They were permealized with 0.1% Triton X-100 in PBS for 5min then blocked with a 5% BSA in PBS solution for one hour. Primary antibody were diluted in 1% BSA, 0.3% Triton X-100 in PBS. The following primary antibodies were used : rat anti-CD31 (BD, 550274, 1:40), rabbit anti-cleaved Caspase-3 (Cell Signaling, 9664, 1:50) and rabbit anti-phospho Histone H3 (Millipore, 06-570, 1:200). After over night incubation at 4°C, the samples were stained with species corresponding 2$^{nd}$ antibodies with either Alexa Fluor 488 or 568 (Molecular Probes, 1:250) for one hour at room temperature and nuclei were stained with DAPI (Sigma).

Double strand DNA breaks associated with apoptotic and non-apoptotic cell death were visualized using a fluorescent TUNEL assay (In Situ Cell Death Detection Kit, Fluorescin; Roche) according to the manufacturer`s recommendations, using Proteinase K pretreatment. Slides were then mounted with Dako Mounting Medium (DAKO) and stored at 4° until imaging. Fluorescence images were acquired with a microscope Olympus BX63. Images analysis and quantification was performed using Fiji distribution of ImageJ.

*Phosphoprotein analysis*

The PathScan® Akt Signaling Antibody Array Kit (Fluorescent Readout, #9700, Cell Signaling Technology, USA), Protease Inhibitor Cocktail 100x and the Pierce™ BCA Protein Assay Kit (Thermo Fischer Scientific, USA) were used for the biodistribution studies.

For lysate preparation, the centrifuge was pre-cooled at +4°C and the aluminum blocks were put on ice. The lysis buffer (LB) was prepared by adding the Proteinase Inhibitor Cocktail, diluted 1:100 and used within 1 hour. 150µl of LB were needed for 1 tumor before physical crushing in a pre-cooled glass mortar. BCA assay was used to determine the total protein quantity.

To perform the assay, PathScan® Akt Signaling Antibody Array Kit protocol was followed according to the manufacturer's instructions.

The image was captured and analyzed by LiCOR Image Studio (Ver4.0 or later), analyzed with a grid array composed of 8x2 arrays, each consisting of 6 rows and 6 columns. The size of each case is 1005 pixels and the background was adjusted.

For the survival studies, we use a MSD Akt Signaling Panel II Base Kit (K15177A) and 4-EBP1 kit (K151OLD, MesoScale Discovery, USA). The protocol was followed according to the manufacturer's instructions. After lysate preparation like for the Pathscan protocol, the plate was read in a Sector Imaging 6000 (MesoScale Discovery, USA).

*Statistical methods*

Data were analyzed and graphs were generated with using IBM SPSS Statistics Ver. 22 or GraphPad Prism 6 (GraphPad Prism Software Inc.).

## Results

*High dose Everolimus pre-treatment reduces $^{177}$Lu-DOTA-exendin-4 tumor uptake*

Treatment for 3 days (Figure VIII-1A), 7 days (Figure VIII-1B) and 10 days (Figure VIII-1C) all show a significant decrease in $^{177}$Lu-DOTA-exendin-4 uptake at the higher dosis of 10 mg/kg bodyweight. The sub-therapeutic dose of 1mg/kg shows no reduction at all and 5mg/kg uptake is decreased significantly only after 7 days ($p=0.01$, Kruskal-Wallis). The pancreas (suppl. Figure VIII-1A), both kidneys (suppl. Figure VIII-1B) and all the other resected organs show no significant uptake (data not shown). Moreover, the receptor density is not affected after 10 days of Everolimus treatment at the highest dose (Figure VIII-1D). The inhibition of mTOR on its serine 2448 phosphorylation site (Ser2448) was confirmed by phophoprotein analysis for the 10mg/kg bodyweight compared to the control group and the 1 mg/kg bodyweight group (Figure VIII-1E).

*PRRT alone is sufficient to promote tumor shrinkage but acts synergistically with Everolimus*

The mean tumor weight is significantly reduced with PRRT as a single therapy and synergistically in combination with continuous Everolimus (Figure VIII-2A) but not if Everolimus is pulsed, i.e given every 3 days. Everolimus monotherapy does not significantly reduce tumor weight. Moreover, the average tumor number is statistically reduced in every treatment groups compared to control (figure VIII-2B) but the combined treatment acts synergistically in reducing average tumor number. Macroscopically we could observe a decrease of the average size and the color with less red-ish tumors (Supplementary Figure VIII-2). 177Lu-DOTA-exendin-4 SPECT/CT at day 0 and 30 days after beginning of combination treatment shows good tumor response to combined treatment (Figure VIII-2C).

*Everolimus alone and in combination inhibits mTOR pathway and microvessel formation*

The microvasculature of the tumor was decreased by each treatment and each dose of Everolimus. The most significant decrease was reached by Everolimus continuously given at 5 mg/kg bodyweight (Figure VIII-3A) and represented microscopically by the Figure VIII-3B. In addition, the phosphor riboprotein S6, an essential downstream element of the mTOR pathway, was decreased in all the groups that received Everolimus in a daily manner (E cont, Figure VIII-3C). It is significantly higher when given every 3 days (E pulse). Other targets more downstream like Akt (Suppl. Figure VIII-3A), S6K (Suppl. Figure VIII-3B) and 4E-BP1 (Suppl. Figure VIII-3C) are not significantly inhibited. Only for 4E-BP1 did intermittent Everolimus induce an up-regulation compared to control.

*Combined treatment tends to reduce proliferation and enhance apoptosis*

A TUNEL assay shows no significant differences between the control and the treated groups (Figure VIII-4A). In PRRT and combination treatment group, only a small proportion has a high apoptosis

pattern. The proliferation is reduced for all the groups treated with $^{177}$Lu-Exendin-4, alone or in combination (Figure VIII-4B). They are significantly increased when the mice are treated with Everolimus alone and even more with Everolimus given intermittently.

*Combined treatment doesn't significantly improve survival over Everolimus as single treatment*

The group treated with PRRT or Everolimus every 3 days show no improvement over the control mice (Figure VIII-5). Combination of PRRT and Everolimus alone at 5 mg/kg bodyweight doesn't improve survival compared to Everolimus given daily. In addition, to our knowledge, the 151 days of survival after onset of the disease is a record for the Rip1Tag2 mice model.

## Discussion

Objective response after 20 days of daily oral Everolimus administration as well as long term survival show a significant effect of Everolimus (5mg / kg bodyweight daily) compared to untreated control. At first glance these results seem to be contradictory to the study by Pool et al. that suspected promotion of metastases by Everolimus in a neuroendocrine tumor model (Pool et al. 2013; Bison et al. 2014). Using a protocol of Everolimus dosage similar to that of Pool et al. with intermittent administration of Everolimus in the Rip1Tag2 mice, the stable anti-tumor effect of (daily) Everolimus was lost or gave some sign of possible resistance. In fact the S6 and S6K phosphorylation was increased, as well as the proliferation marker pH3. We hypothesize that low or inconsistent levels of Everolimus may activate feed-back loop regulations that could lead to upregulation of mTOR pathway. This matches to results of the Rotterdam group that noticed promotion of metastases in a model of implanted tumors.

Furthermore, our data suggest a dose dependent effect of Everolimus. While 1 mg/kg body weight/day did show only minor effect compared to 5 mg/kg bodyweight/day, 10 mg/kg bodyweight/day dramatically reduced tumor load after 20 days. The dose dependency of Everolimus in the treatment of Rip1Tag2 mice is in concordance to other previous studies in different animal models (Yao et al. 2011). With increased treatment length and increased dose of Everolimus we observed a reduced tumor uptake of $^{177}$Lu-Exendin-4. Since the receptor density is not changed, we interpret the biodistribution results as expression of treatment effect.

As mentioned above, Everolimus daily at 5 mg / kg body weight significantly reduced tumor size and prolonged survival compared to control in Rip1Tag2 mice. PRRT with Lu-177-Exendin-4 showed tendency of tumor size reduction. Nevertheless, Everolimus significantly outperformed PRRT with Lu-177-Exendin-4 ($p<0.000$). Combining both treatments resulted in a statistically significant objective response by tumor volume reduction of xxx and prolonged survival of 73 +/- 17.1 days. Interestingly, tumor volume reduction by combined treatment was significantly reduced compared to mono-therapy with daily Everolimus ($p=0.001$), survival of the combination treatment group was not prolonged when compared to mono Everolimus therapy. Rip1Tag2 is continuously creating new tumors under the impulse of the rat insulin promotor. Thus this animal model may not be the best to assess this question.

One major drawback of our study is the lack of toxicity analysis. In our opinion, analyses of renal toxicity or bone marrow toxicity in Rip1Tag2 mice is unreliable and of limited value for clinical translation of our results. Since untreated Rip1Tag2 mice have a short life expectancy and kidney toxicity of PRRT occurs later in the course of treatment, any analyses of xxx would lack a sufficient control group. Second, Rip1Tag2 mice request PRRT with GLP-1 receptor analogue Exendin-4. Exendin-4 is known to accumulate to a significant amount in the kidneys, more intense than DOTATOC

or DOTATATE do. Results of kidneys toxicity analyses in Rip1Tag2 mice after exposure to Exendin-4 aren't comparable to DOTATOC-treatment in humans.

Everolimus when administered properly has a very stable and high anti-tumor potential in the NET model of RIP1Tag2 mice. We hypothesize that as soon as the amount of Everolimus is reduced beyond a critical level, a significant number of individuals do not benefit or are even exposed to a risk of mTOR upregulation. Combing PRRT and mTOR inhibition additive treatment effect is preferable. In the mouse model, we demonstrated additive effects on tumor volume compared to single treatments of mTOR inhibition of PRRT. Simulation of combined treatment in Rip1Tag2 mice is not suited to predict long term outcomes.

## Acknowledgements

We would like to thank the DBM animal facility for their support throughout the whole study as well as the lab of Gerhard Christofori for the supply of the Rip1Tag2 mice.

**Figures**

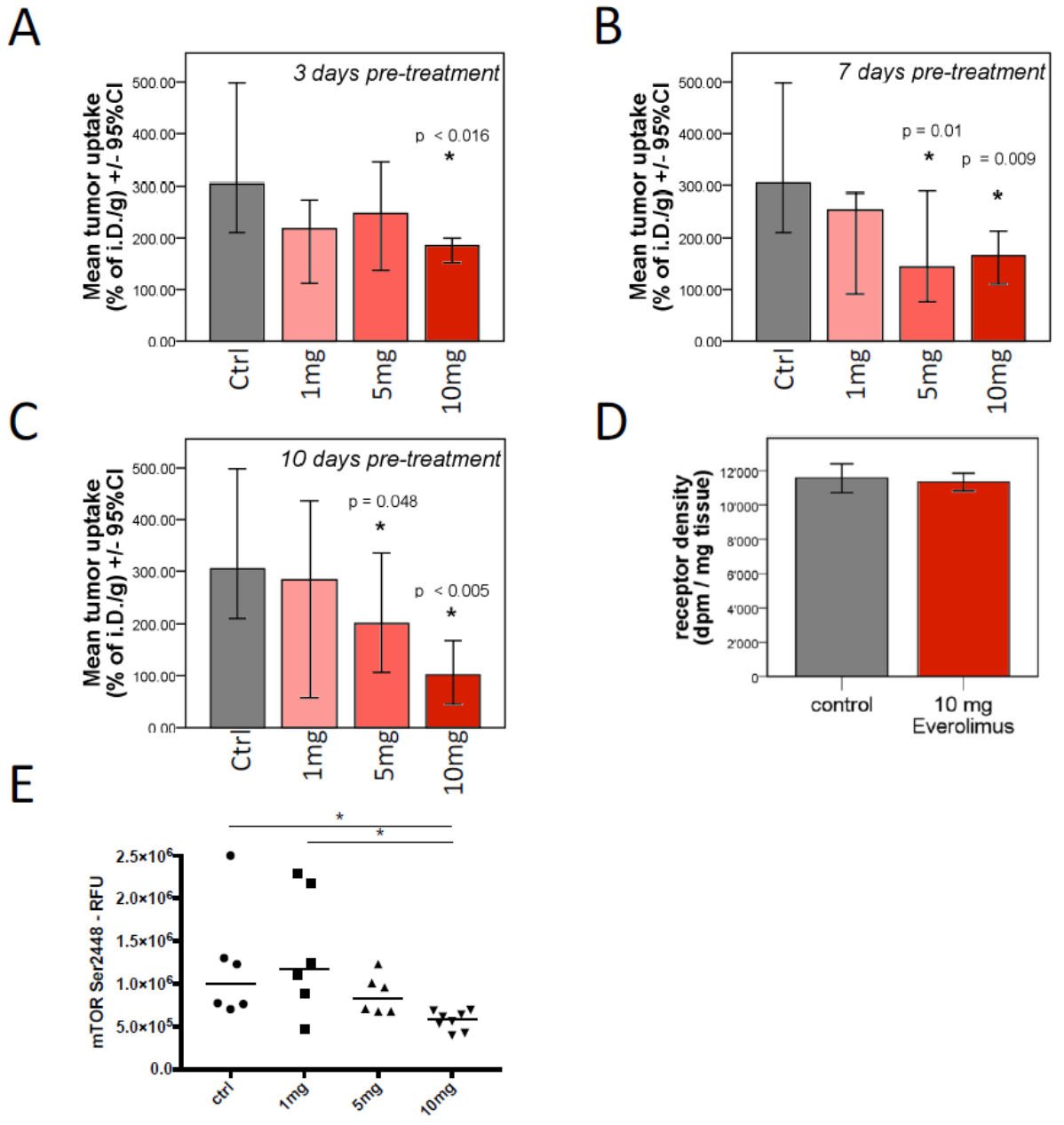


Figure VIII-1 : Reduced uptake of radionuclide but same receptor density upon Everolimus pre-treatment.

**A**, **B** and **C**, Mean tumor uptake +/- 95% confidence interval for 3, 7 and resp. 10 day of pre-treatmin with Everolimus. From left to right: control, 1 mg/kg body weight, 5 mg/kg body weight and 10 mg/kg body weight. *n*= 5-6 mice per group; *, *P*<0.05. **D**, Receptor density after assay in dpm/mg tissue. Statistical analysis by Kruskal-Wallis test. N.S. means not significant. **E**, Relative Fluorescence Unit of Pathscan analysis for control, 1, 5 and 10 , 5 mg/kg body weight group. *p<0.05.

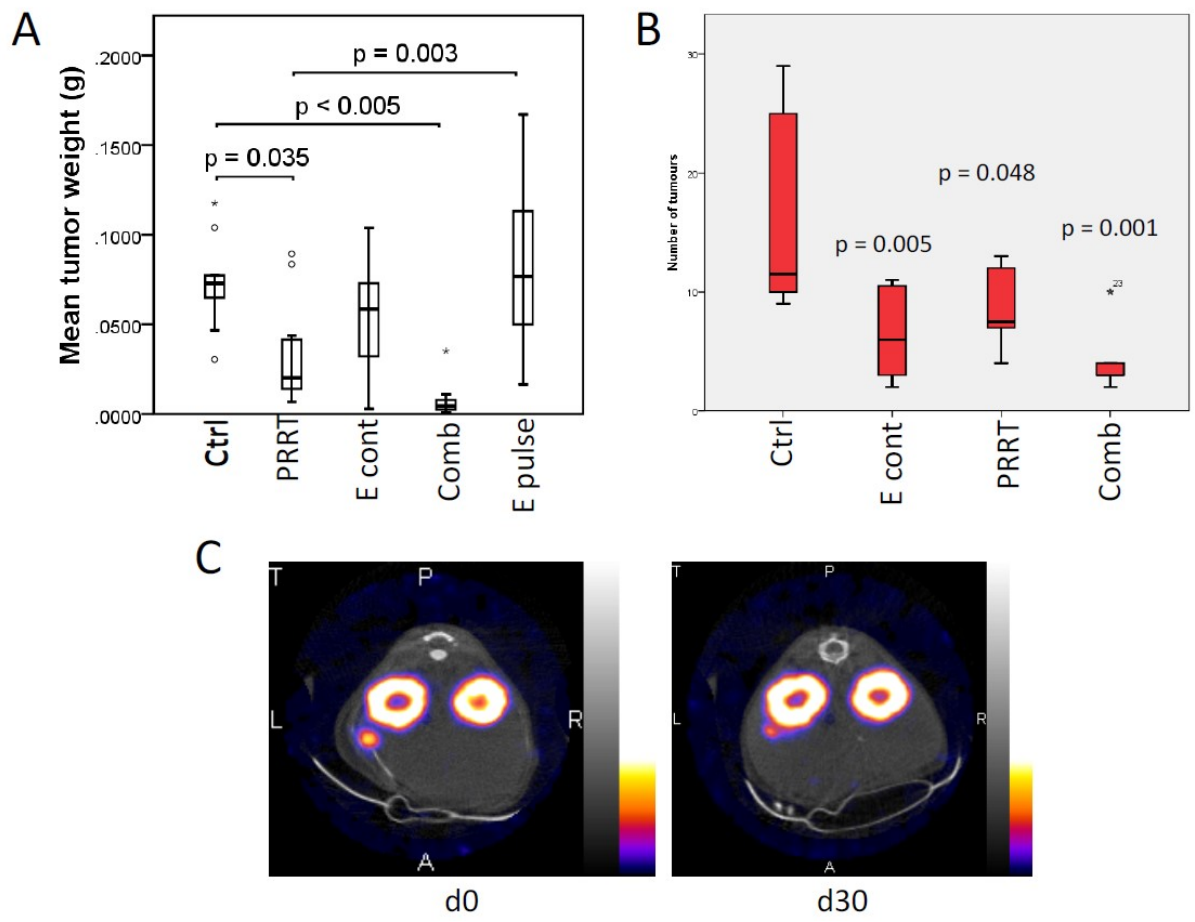


Figure VIII-2 : Combination of Lu-177-Exendin4 and Everolimus dramatically reduces tumor formation.

**A**, Mean tumor weight +/- 95% confidence interval for control (ctrl, n=9), Lu-177-Exendin4 (PRRT, n=9), Everolimus continuous (E cont, n=9), combination (Comb, n=10) and Everolimus pulse (E pulse, n=12) groups. Statistical analysis by Kruskal-Wallis test. **B**, Number of tumors per pancreas for control, Everolimus continuous, PRRT and combination treatment. Statistics are shown directly on the graph. **C**, PET-CT cross-sectional scans of a combination group mice. Left is baseline, right is after 30 days of treatment. A, anterior, P, posterior, T, Transsection. Color code indicates the intensity.

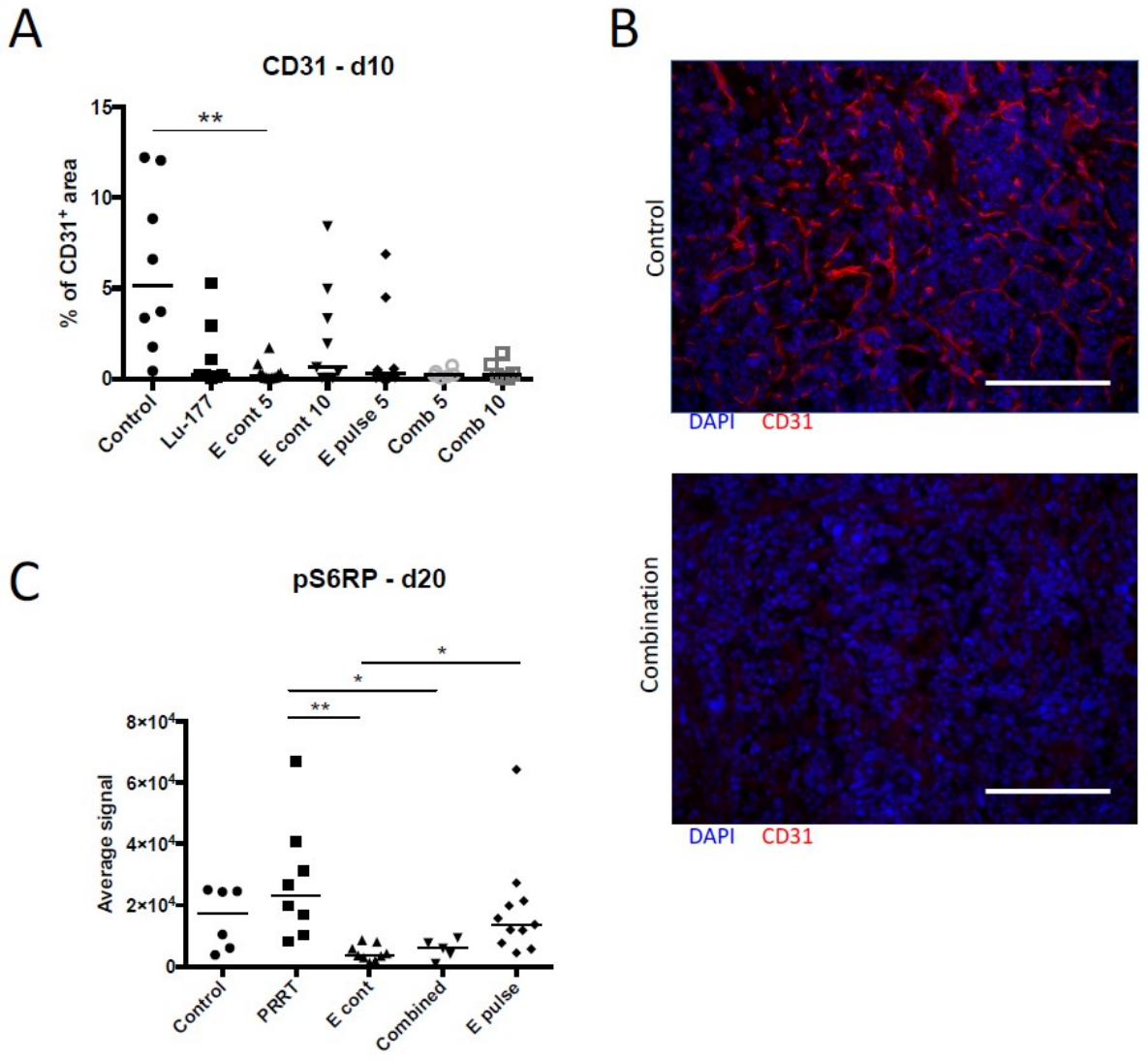


Figure VIII-3 : Reduced microvessel density and decreased mTOR pathway activation upon treatment. **A**, Median percentage of the $CD31^+$ area per view field for mice after 10 days of therapy. Statistical analysis by Mann–Whitney *U* test. **, $P < 0.01$. Right upper picture: immunofluorescence of CD31 in red and DAPI in blue for control mice and for combination mice in lower picture. **B**, Median phosphorylation of the downstream kinase phospho-S6 after 20 days of therapy. Statistical analysis by Mann–Whitney *U* test. **, $P < 0.01$.

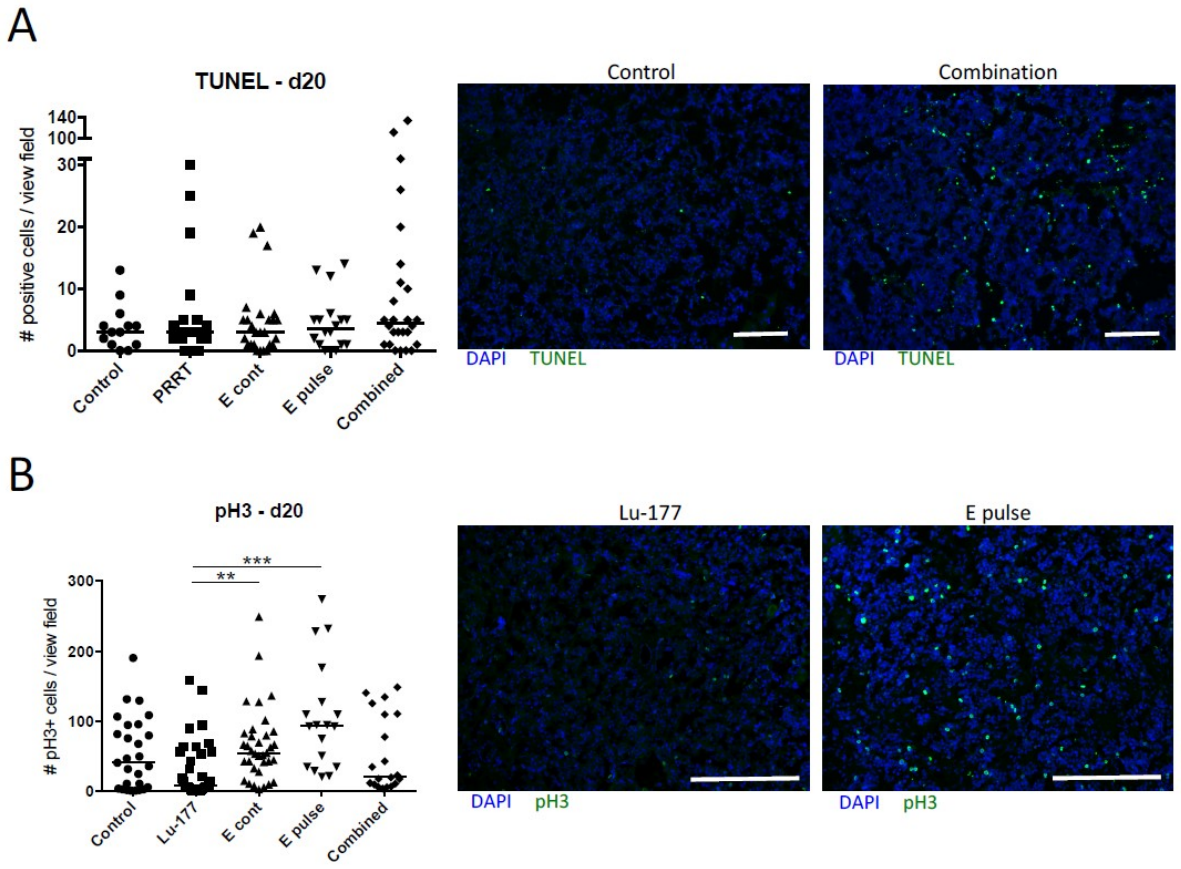


Figure VIII-4 : Apoptosis and proliferation.

**A**, Median percentage of the TUNEL$^{+}$ cells per view field for mice after 20 days of therapy. Statistical analysis by Mann–Whitney *U* test. Left picture: immunofluorescence of TUNEL in green and DAPI in blue for control mice and for combination mice in left picture. Scale bar = xx µm. **B**, Median percentage of the phospho-Histone3$^{+}$ cells per view field for mice after 20 days of therapy. Statistical analysis by Mann–Whitney *U* test. Left picture: immunofluorescence of pH3 in green and DAPI in blue for control mice and for combination mice in left picture. Scale bar = xx µm.

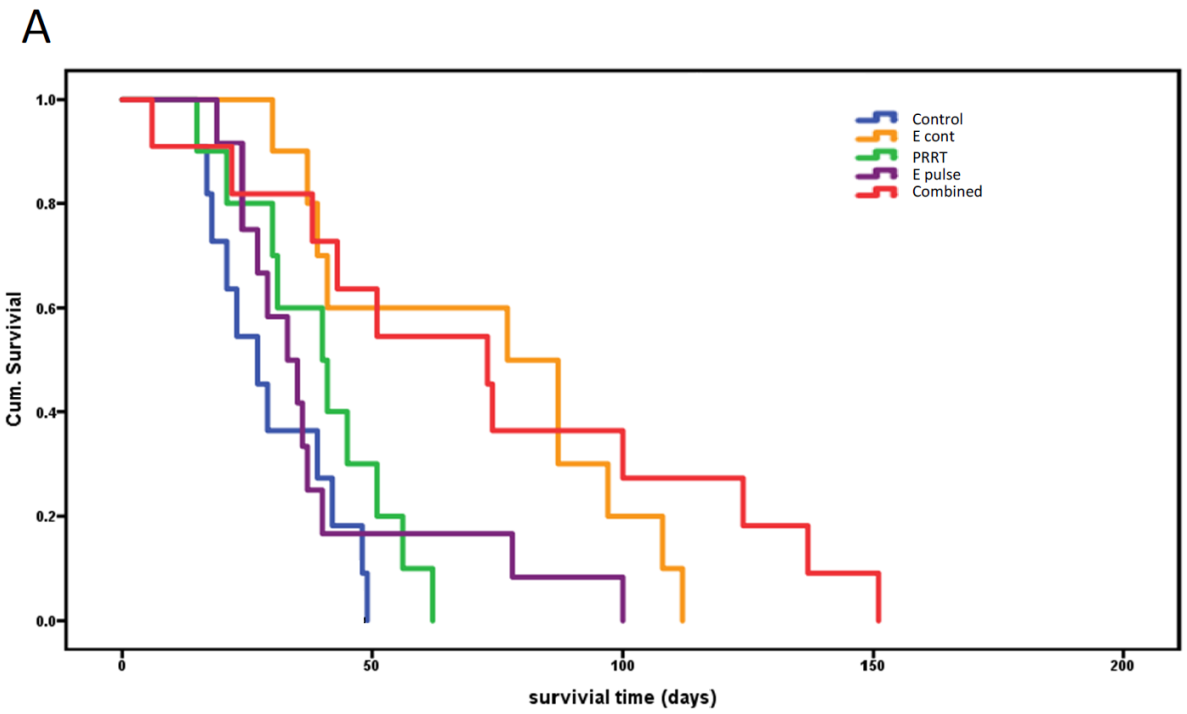


Figure VIII-5 : Increased survival in treated mice.

Kaplan-meier curve with overall survival on the Y-axis and the consecutive days on the X-axis.

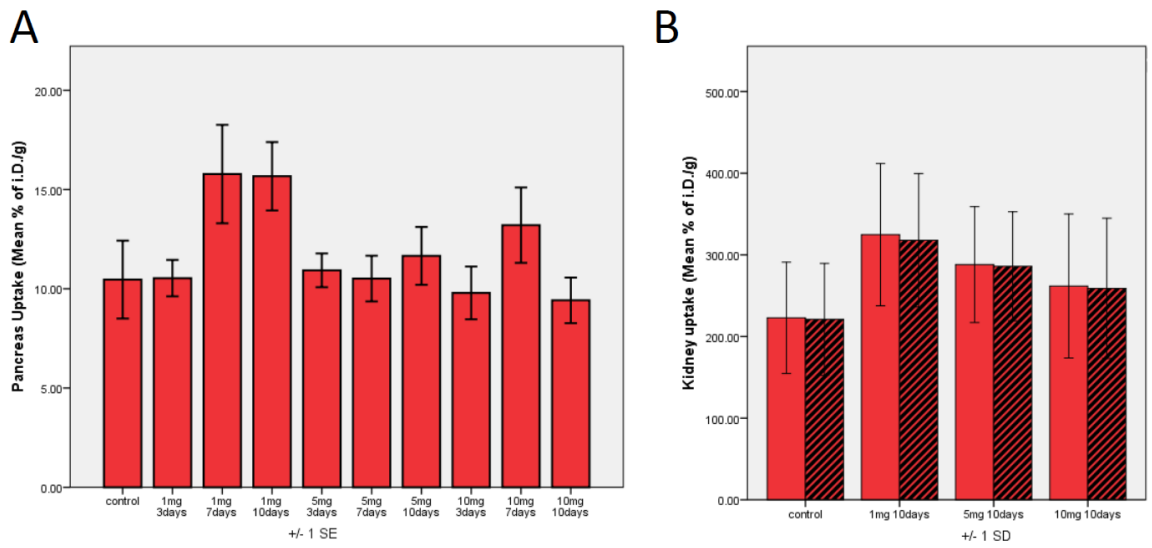


Suppl. Figure VIII-1

Pancreas and kidney uptake. **A**, Mean tumor uptake for the normal pancreas +/- 95% confidence interval for 3, 7 and resp. 10 day of pre-treatmin with 1, 5 and 10 mg/kg bodyweight Everolimus. **B**, Mean tumor uptake for the left kidney (left bar on each pair) and right kidney (right bar on each pair) +/- 95% confidence interval for 3, 7 and resp. 10 day of pre-treatment with 1, 5 and 10 mg/kg bodyweight Everolimus.

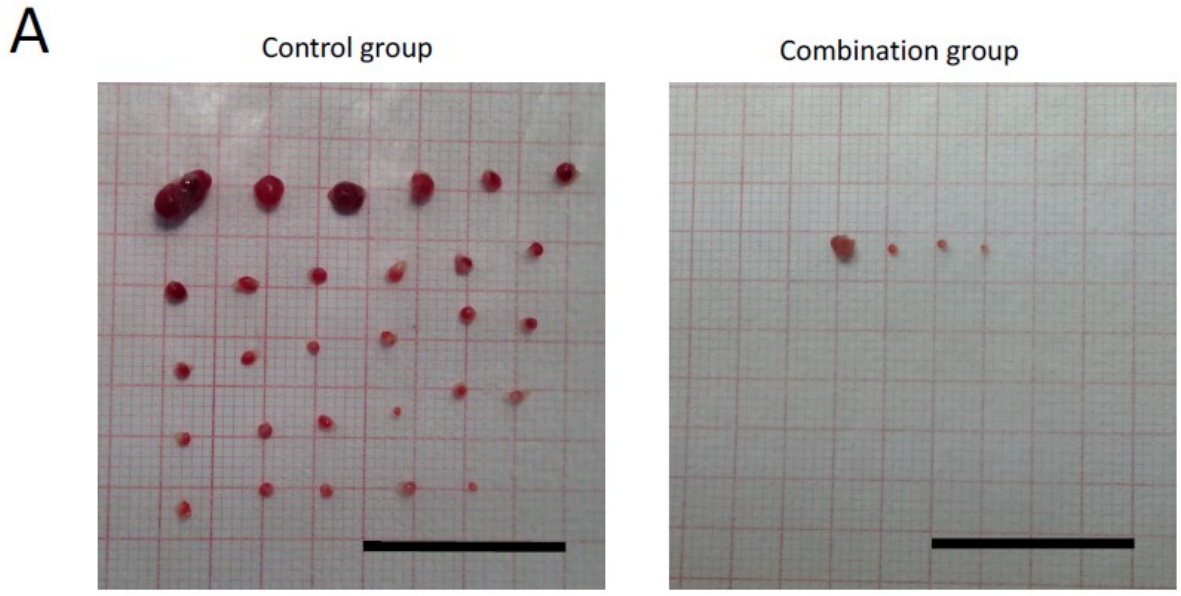


Suppl. Figure VIII-2

Number of tumors is decreased and the color of the tumors altered under combined treatment. Macroscopic comparison of the size and color of all the tumors isolated from one whole pancreas. Left is control group, right is combination group. Scale bars = 4 cm, 1 square = 1 mm.

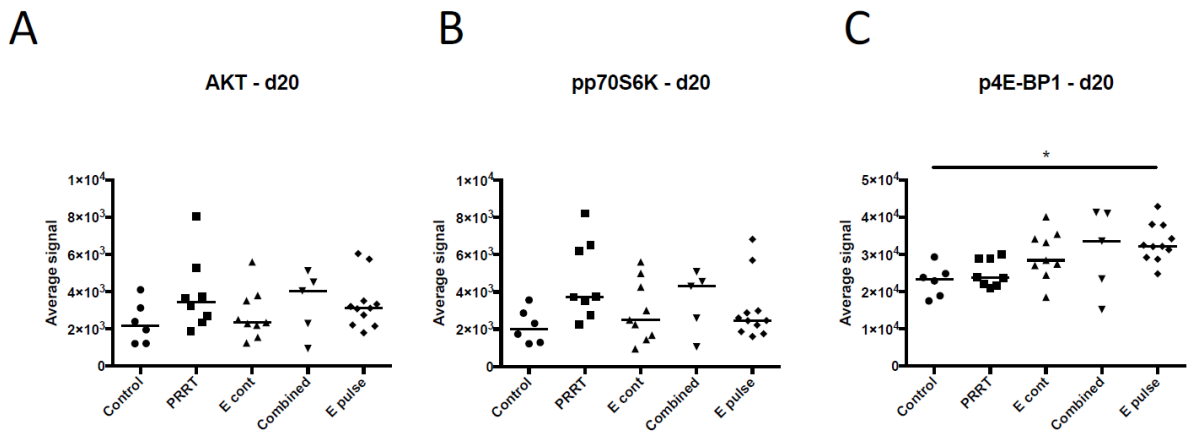


Suppl. Figure VIII-3

Other key target downstream of the mTOR pathway. Median phosphorylation of the downstream AKT (**A**), S6K (**B**) and p-4EBP1 (**C**) after 20 days of therapy. Statistical analysis by Mann–Whitney *U* test. **, $P < 0.01$.

# IX. First in Human, Phase I, Dose Escalation Pharmacokinetic and Pharmacodynamic Study of the Oral Dual PI3K and mTOR Inhibitor PQR309 in Patients with Advanced Solid Tumors.

This paper was published in European Journal of Cancer in June 2018 (Wicki et al. 2018).

European Journal of Cancer 96 (2018) 6–16

Available online at www.sciencedirect.com

ScienceDirect

journal homepage: www.ejcancer.com

Clinical Trial

## First-in human, phase 1, dose-escalation pharmacokinetic and pharmacodynamic study of the oral dual PI3K and mTORC1/2 inhibitor PQR309 in patients with advanced solid tumors (SAKK 67/13)

Andreas Wicki [a,*,1], Nicholas Brown [b,1], Alexandros Xyrafas [c], Vincent Bize [c], Hanne Hawle [c], Simona Berardi [c], Nataša Cmiljanović [d], Vladimir Cmiljanović [d], Michael Stumm [d], Saša Dimitrijević [d], Richard Herrmann [d], Vincent Prêtre [e], Reto Ritschard [e], Alexandar Tzankov [f], Viviane Hess [a], Alexa Childs [b], Cinta Hierro [g], Jordi Rodon [g], Dagmar Hess [h], Markus Joerger [h], Roger von Moos [i], Cristiana Sessa [j], Rebecca Kristeleit [b]

[a] *University Hospital Basel, Division of Oncology, Dept. of Biomedicine, Petersgraben 4, 4031 Basel, Switzerland*
[b] *University College London Hospitals NHS Trust, Gynecological Oncology Team, 235 Euston Road, London NW1 2BU, United Kingdom*
[c] *SAKK Coordinating Center, Effingerstrasse 33, 3008 Bern, Switzerland*
[d] *Piqur Therapeutics AG, Hochbergstrasse 60C, 4057 Basel, Switzerland*
[e] *University Hospital Basel, Dept. of Biomedicine, Petersgraben 4, 4031 Basel, Switzerland*
[f] *University Hospital Basel, Dept. of Pathology, Schönbeinstrasse 40, 4056 Basel, Switzerland*
[g] *Vall d'Hebron Institut d'Oncologia, Universitat Autonoma of Barcelona, Passeig Vall d'Hebron 119-129, 08035 Barcelona, Spain*
[h] *Cantonal Hospital St. Gallen, Dept. of Oncology and Hematology, Rorschacherstrasse 95, 9007 St. Gallen, Switzerland*
[i] *Cantonal Hospital Graubünden, Dept. of Oncology and Hematology, Loestrasse 170, 7000 Chur, Switzerland*
[j] *Istituto Oncologico della Svizzera Italiana, Ospedale San Giovanni, 6500 Bellinzona, Switzerland*

Received 8 December 2017; received in revised form 9 March 2018; accepted 13 March 2018
Available online 13 April 2018

## Abstract

### Background

PQR309 is an orally bioavailable, balanced pan–phosphatidylinositol-3-kinase (PI3K), mammalian target of rapamycin (mTOR) C1 and mTORC2 inhibitor.

### Patients and methods

This is an accelerated titration, 3 + 3 dose-escalation, open-label phase I trial of continuous once-daily (OD) PQR309 administration to evaluate the safety, pharmacokinetics (PK) and pharmacodynamics in patients with advanced solid tumours. Primary objectives were to determine the maximum tolerated dose (MTD) and recommended phase 2 dose (RP2D).

### Results

Twenty-eight patients were included in six dosing cohorts and treated at a daily PQR309 dose ranging from 10 to 150 mg. Common adverse events (AEs; ≥30% patients) included fatigue, hyperglycaemia, nausea, diarrhoea, constipation, rash, anorexia and vomiting. Grade (G) 3 or 4 drug-related AEs were seen in 13 (46%) and three (11%) patients, respectively. Dose-limiting toxicity (DLT) was observed in two patients at 100 mg OD (>14-d interruption in PQR309 due to G3 rash, G2 hyperbilirubinaemia, G4 suicide attempt; dose reduction due to G3 fatigue, G2 diarrhoea, G4 transaminitis) and one patient at 80 mg (G3 hyperglycaemia >7 d). PK shows fast absorption (Tmax 1–2 h) and dose proportionality for Cmax and area under the curve. A partial response in a patient with metastatic thymus cancer, 24% disease volume reduction in a patient with sinonasal cancer and stable disease for more than 16 weeks in a patient with clear cell Bartholin's gland cancer were observed.

### Conclusion

The MTD and RP2D of PQR309 is 80 mg of orally OD. PK is dose-proportional. PD shows PI3K pathway phosphoprotein downregulation in paired tumour biopsies. Clinical activity was observed in patients with and without PI3K pathway dysregulation.

### Clinical trial registration

ClinicalTrials.gov # NCT01940133.

## Highlights

- The maximum tolerated dose and recommended phase 2 dose of PQR309 is 80 mg orally OD.
- Pharmacodynamics shows phosphatidylinositol-3-kinase (PI3K)–mammalian target of rapamycin (mTOR)–S6 pathway inhibition in paired tumour biopsies.
- Pathway inhibition is more pronounced in patients with tumour shrinkage.
- Activity was observed in patients with and without PI3K pathway dysregulation.
- Tumour-associated immune infiltrates were not affected by PI3K/mTOR inhibition.

## Introduction

The phosphatidylinositol-3-kinase (PI3K) and mammalian target of rapamycin (mTOR) signaling cascade serves physiological and pathophysiological cell functions and is of major importance in cancer and inflammatory disease. As a key downstream effector of receptor tyrosine kinases (RTKs) and G protein coupled receptors (GPCRs), PI3K activation initiates a signal transduction pathway that stimulates glucose metabolism, cell proliferation, growth, and survival (Yuan & Cantley 2008; Courtney et al. 2010; Banham-Hall 2012; So & Fruman 2012; So et al. 2013; Engelman 2009; Brana & Siu 2012; Rodon et al. 2013; Liu et al. 2009). One of the principal downstream effectors of PI3K is mTOR. mTOR also integrates growth signals that are independent of PI3K activation (Engelman 2009). Dysregulation of the PI3K/mTOR pathway is associated with many cancers. Inappropriate activation of the pathway may occur through a variety of mechanisms including (i) activating mutations, amplifications, or overexpression of the p110α subunit (PI3KCA); (ii) constitutively active mutants or overexpression of upstream receptor tyrosine kinases (e.g. epidermal growth factor receptor, insulin-like growth factor receptor, Erb-B2, Erb-B3); (iii) constitutive recruitment and activation by Ras oncogene mutants; (iv) loss or inactivating mutations of Phosphatase and tensin homolog (PTEN), an endogenous negative regulator of the pathway; or (v) overexpression and activating mutations of downstream kinases (e.g., Akt) (Courtney et al. 2010; Engelman 2009). In addition, dysregulation of the PI3K/mTOR pathway has been implicated in chemotherapy resistance (Courtney et al. 2010; Engelman 2009; Liu et al. 2009; Samuels et al. 2004; Koti et al. 2013; Saura et al. 2014).

To date, PI3K and PI3K/mTOR inhibitors have demonstrated clinical efficacy in patients with cancers harboring PIK3CA (Baselga J, Im S-A, Iwata H 2015) or PTEN aberrations and also in some patients without detected mutations in these pathways. Idelalisib, a selective inhibitor of PI3Kδ is licensed for use in chronic lymphocytic leukaemia and follicular lymphoma (Janku et al. 2014; EMA 2016; FDA 2016). Similar clinical outcomes have been reported for duvelisib (a PI3K γ/δ inhibitor) and TGR-1202 (another PI3Kδ-selective inhibitor) (Patel et al., 2015 ; O'Connor et al., 2015). Everolimus, a selective inhibitor of mTORC1, is licensed for use in advanced breast cancer, neuroendocrine tumors, and renal cell carcinoma. Although these clinical data are encouraging, clinical resistance to kinase inhibitors has

been shown to occur either due to novel mutations within the targeted kinase, or to other compensatory mechanisms (Van Der Kuip et al. 2005; Barouch-Bentov & Sauer 2011; Daub et al. 2004). In particular, it has been shown that idelalisib resistance is due to increased expression of PI3Kα (Meadows et al. 2015). Alternatively, inhibiting all PI3K isoforms results in upregulation of the mTOR pathway or inactivation of PTEN, accompanied by resistance to these agents (Elkabets et al. 2013). Persistent mTOR activation has been detected in patients with PIK3CA-inhibitor resistant tumors. Thus, targeting two nodal points within a pathway may reduce the probability of resistance or increase the latency period prior to the development of resistance (Elkabets et al. 2013). Dual inhibition of PI3K and mTOR is therefore a promising strategy for anticancer therapy.

PQR309 (Piqur Therapeutics AG, Basel, Switzerland) is an oral pan-class I PI3K inhibitor that selectively targets all four isoforms of class I PI3K (α, β, γ, δ), with a balanced activity against mTOR. It is equipotent against $p110\alpha^{H1047R/E542K/E545K}$ somatic mutations often observed in human cancers (Beaufils et al. 2017). PQR309 demonstrates anti-proliferative activity in a variety of cell lines with and without inappropriate PI3K pathway activation (Cmiljanovic et al. 2015; Tarantelli et al. 2018; Tarantelli C, Gaudio E, Kwee I, Rinaldi A, Bernasconi E, Cascione L 2015; Bohnacker et al. 2017).

The primary objectives of this first-in-human, phase 1, dose-escalation study were to assess the safety and tolerability and determine the MTD and RP2D of oral PQR309 with once-daily continuous dosing in patients with advanced solid tumors. Secondary objectives included characterization of the pharmacokinetics (PK) and pharmacodynamics (PD), and preliminary assessment of anti-tumor activity of PQR309.

## Patient & Methods

*Ethics*

This study was conducted in accordance with the Declaration of Helsinki and the guidelines of Good Clinical Practice (GCP) issued by the International Conference on Harmonization of Technical Requirements for Registration of Pharmaceuticals for Human Use (ICH), the European Union (EU), and the Swiss Confederation. The study protocol was approved by ethics committees and regulatory authorities for all participating institutions. All participants provided written informed consent prior to participation in the study.

*Study design*

This was a multicenter, international, open-label first-in-human trial. Based on the No-Observed-Adverse-Effect-Level (NOAEL) in dogs of 4mg/kg, the starting dose in humans was 10mg. An accelerated modified "3+3" dose-escalation design was used. Dose level 1 and 2 enrolled a single patient (pre-determined), with evaluation of a single cycle with no toxicity ≥ G2 prior to enrolment at the next dose level. If a drug-related toxicity ≥ grade 2 occurred, two additional patients were to be enrolled at the same dose level and then the trial would continue as a classical 3+3. From dose level 3 and thereafter, the classical 3+3 design was used. Doses were increased by 100% between dose-levels until dose level 4. After dose level 4 or the first toxicity ≥ grade 2, subsequent dose levels could increase between 30-100%, according to the type and grade of toxicity after discussion with the independent data safety monitoring board (IDSMB). In dose levels 2 to 4, the administered dose was adjusted according to weight (75% dose if < 60kg, 125% dose if > 80kg). Eligible patients received once daily oral PQR309 capsules continuously on a 21 day cycle until progression, unacceptable toxicity, investigator judgement, or withdrawal of consent.

*Patients*

The study enrolled adult patients (age ≥ 18 years) with a histological or cytologically confirmed diagnosis of advanced solid tumor and evidence of tumor progression with measurable or evaluable disease for which no therapy of proven efficacy was available. The inclusion criteria were updated after recruitment of the four initial cohorts to require tumors accessible to biopsy (initially optional). Patients were required to have an Eastern Cooperative Oncology Group (ECOG) performance status of ≤ 1, and adequate hematological [absolute neutrophil count (ANC) ≥ 1.5 x 109/L, platelets ≥ 100 x 109/L, hemoglobin ≥ 90 g/L], liver [total bilirubin ≤ 1.5 times the upper limit of normal (ULN), alanine aminotransferase (ALT) and aspartate aminotransferase (AST) ≤ 2.5 ULN or ALT/AST ≤ 5 times ULN in patients with liver metastasis] and renal [creatinine ≤ 1.5 times ULN] parameters. Steroids [> 20mg

per day of prednisolone or equivalent] were prohibited. Patients were required to be able to swallow and retain oral medication and be willing and able to comply with trial procedures.

Exclusion criteria included medical conditions that could significantly interfere with study drug metabolism, pre-existing diabetes, a fasting glucose > 7 mmol/L or HbA1c > 6.4% (6% in initial cohorts), patients with symptomatic or progressing central nervous system metastases, persisting toxicity ≥ grade 2 secondary to prior anticancer therapy, ischemic heart disease, heart failure (New York Heart Association Class 3 or 4), uncontrolled hypertension, known HIV, serious infection or medical condition which would jeopardize compliance with the protocol. Patients who were pregnant, breast-feeding, or unwilling to use appropriate contraceptive measures were excluded.

*Dose limiting toxicity, maximum tolerated dose, and management of toxicity*

DLTs were defined as any of the following: grade 4 neutropenia for > 7 days, febrile neutropenia, grade 4 thrombocytopenia, grade 4 non-hematological toxicity (e.g. hyperglycemia > 27.8 mmol/L) or grade 3 lasting > 7 days (unless controlled with supportive care), treatment delay > 14 days due to unresolved toxicity, or non-hematological toxicity ≥ grade 2 deemed dose limiting by the IDSMB. DLTs were based on adverse events observed during the first cycle (21 days). The MTD was defined as the highest dose level at which ≤ 1 out of 6 patients experience a DLT.

Management algorithms for the treatment expected toxicities of hyperglycemia, maculopapular rash, acneiform rash, pruritus, and dry skin were defined in the protocol.

*Safety & efficacy assessments*

Monitoring for adverse events, concomitant medications, vital signs, physical examination, weight, performance status, hematology, blood chemistry including glucose, HbA1c, hemostasis, and urinalysis were performed at baseline, weekly in the first two cycles, and once a cycle thereafter. In addition, screening and baseline assessment included medical history, tumor history, and a pregnancy test. ECG was checked at baseline and every two cycles. Adverse events were graded using the National Cancer Institute (NCI) Common Toxicity Criteria for Adverse Events (CTCAE) version 4.03. Serious adverse events were defined as any event that was fatal, life-threatening, required inpatient hospitalization > 24 hours, prolonged hospitalization, was disabling, any new secondary malignancy, a congenital anomaly, or any medically significant condition that occurred between registration and up to 28 days after the last dose of PQR309.

Efficacy parameters were defined using the Response Evaluation Criteria in Solid Tumors (RECIST version 1.1). Tumor assessment by CT or MRI of the tumor area, thorax, and abdomen occurred at baseline, every 6 weeks for the first 4 cycles, every 9 weeks thereafter, and at the end of treatment if no

imaging had been performed in the previous 14 days. Tumor markers were assessed at baseline and every 3 weeks.

*Pharmacokinetics*

Blood samples were collected for PK analysis immediately prior to the first dose; 1, 2, 6, and 24 hours following the first dose of PQR309, 24 hours after the last dose of cycle 1 and prior to the first dose of cycle 2. PQR309 concentrations were determined by high-performance liquid chromatography tandem mass spectrometry (assay range: 1.00-1000ng/ml).

*Pharmacodynamics*

Where feasible, patients underwent tumor biopsy (initially optional, compulsory following protocol amendment June 2014) prior to treatment initiation and at the end of cycle 1. Samples underwent next generation DNA sequencing (Ion AmpliSeq™ Cancer Hotspot Panel v2 panel, analysis of expression of 88 PI3K- and mTOR related mRNAs (RT2 Profiler PCR Array) (Suppl. Figure 1), analysis of phosphorylation of 16 PI3K/mTOR associated phosphorylation sites (PathScan® Akt Signaling Antibody Array Kit, Pierce™ BCA Protein Assay Kit), and stained for CD3, CD4, CD8, and FoxP3 positive T cells immune infiltrate. If samples were insufficient for all intended translational analyses, analysis was prioritized as follows: assessment of phosphoproteins, next generation sequencing, analysis of immune infiltrates and RNA array.
Blood samples for fasting glucose and insulin were collected immediately prior to the first dose of PQR309, 1 and 24 hours following the first dose, and at day 21 of cycle 1 following a protocol amendment (June 2014).

*Biopsy handling*

Upon reception at the University Hospital Basel, the two biopsies were taken out of the cryotube, and placed on a pre-cooled aluminum block on dry ice. At the time when the isopentan was evaporated, the biopsies were measured with a caliper, photographed, and the macroscopic properties were assessed and documented. One of the two biopsy cores was dedicated for RNA analysis, and was embedded in a horizontal position. The other biopsy, usually the thicker one, was dedicated to phospho-protein applications and was embedded vertically. The sample was then placed in a plastic cryomold on dry ice and a drop of slightly pre-cooled optimal cutting temperature (OCT) embedding medium was added. The frozen biopsy was taken with a pre-cooled forceps, put on the bottom of the cryomold and the mold was filled with OCT. After 10 minutes, the cryomold was put in a labeled, sealed minigrip and stored in a -80°C freezer in a dedicated box.

*Histology*

Freshly frozen biopsies embedded in OCT and stored at -80°C were cutted in a cryotome in serial sections. One serial section cycle was composed of three 7µm thick sections followed by ten 40µm thick sections stored in pre-cooled Eppendorf on dry ice. The excess of OCT was carefully removed with a pre-cooled scalpel before being transferred in the Eppendorf. The first 3 sections of each cycle were then stained for H&E and evaluated by a pathologist. The sections were then evaluated for the tumor content in percentage of the positive cross-sectional area and the tissue quality was designated with a scoring system from 1 (poor quality) to 3 (high quality) as assessed by the pathologist. The selection of slides for further use was based on the evaluation of the pathologist: the cut-off for the tumor content was 30%, and 2 for the scoring system. In case of biopsies with a smaller cross-sectional area than average, two cycles of the same tumor biopsy were lysed in the same Eppendorf.

*Phosphoprotein analysis*

The PathScan® Akt Signaling Antibody Array Kit (Fluorescent Readout, #9700, Cell Signaling Technology, Denvers MA, USA) and Protease Inhibitor Cocktail 100x were purchased at BioConcept AG (Allschwil, Switzerland), and the Pierce™ BCA Protein Assay Kit (Thermo Fischer Scientific, USA) were purchased at LuBio Science GmbH (Switzerland). The Laboratory of Tumor Immunology and Biology and the Department of Biomedicine of the University of Basel provide the laboratory equipment.

For lysate preparation, the centrifuge was pre-cooled at +4°C and the aluminum blocks were put on ice. The lysis buffer (LB) was prepared by adding the Proteinase Inhibitor Cocktail, diluted 1:100 and used within 1 hour. 110µl of LB are needed for 1 serial section cycle, 200µl for 2 cycles pooled together. The Eppendorf containing the biopsy slice was taken out from the -80°C freezer to let them equilibrate in an aluminum block for 2-3 minutes. Then, 110µl or 200µl, respectively, of LB was added, pipetted up and down 10-15 times without creating bubbles and incubated for 5 min. The Eppendorf's were centrifuged for 10 min at minimally 13'000 rpm in a pre-cooled centrifuge (+4°C). The supernatant was then transferred to a new pre-cooled and labeled Eppendorf.

For determination of the protein concentration, the dilutions of the standard albumin and the assay were prepared accordingly to manufacturer's instructions. The plate was read at 562nm in an ELISA reader. The values were copied in the *BCA_excel* layout and the linear regression curve equation was calculated to determine the amount of total proteins.

To perform the assay, PathScan® Akt Signaling Antibody Array Kit protocol was followed according to the manufacturer's instructions. The protein lysate was incubated 2 hours at room temperature and 20µg of total protein were assessed in 75µl, which means 0.26mg/ml (recommended range [0.2-1.0mg/ml]). The first four blocks of each plate were used for the standard lysate. It was made of MCF7 induced 1 hour with 20ng/µl IGF-1 after an overnight starvation and lysed with lysis buffer. The first

concentration corresponds to 10 times the sample concentration, the second 1 time, the third 0.1 time and the fourth 0.01 time.

The image was captured and analyzed by LiCOR Image Studio (Ver4.0 or later). The scanning properties were set to high quality, 21µm/px, 0.0mm interval and intensity 2.0. After rotating from the right to the left, the image was analyzed with a grid array composed of 8x2 arrays, each consisting of 6 rows and 6 columns. The size of each case is 1005 pixels and the background was adjusted by selecting the spot at the right bottom.

All data were exported in an excel file and then analyzed with GraphPad Prism (Ver6.0f or later). The Wilcoxon signed-rank test, a nonparametric test that compares the median of a column of numbers against a hypothetical median (median=100) was chosen to test the significance. The comparison between samples from patients with growing or shrinking tumors was analyzed through the Mann-Whitney test, a non-parametric test that compares the distributions of two independent groups.

*RNA analysis*

Zymo Research Direct-zol RNA MiniPrep and Tri-zol Extraction Buffer (#T9424, Sigma Aldrich) were purchased at Lucerna Chem AG (Switzerland). PI3K-AKT specific RT$^2$ PreAMP cDNA Synthesis (#PBH-058Z, Sabioscience, Qiagen) and RT$^2$ Profiler PCR Array (#PAHS-058Z, Sabioscience, Qiagen) were purchased at Qiagen AG (Switzerland) (Suppl. Figure IX-1). The Laboratory of Tumor Immunology and Biology and the Department of Biomedicine of the University of Basel provided the laboratory equipment and the Applied Biosystems ViiA7 PCR cycler.

For RNA extraction, the Eppendorf containing the biopsy slice was taken out from the -80°C freezer to let them equilibrate in an aluminum block for 2-3 minutes in the chemical hood, sprayed with RNAlater. 500µl of Trizol were added to each sample, and the sample was vortexed at least 3 times. 500µl of absolute ethanol was added and vortexed again 3 times. RNA was extracted with the Direct-zol RNA MiniPrep kit according to the manufacturer's instructions. The optional genomic DNA digestion step was added. The elution buffer was 25µl and was run through the column two times with centrifugation. The eluate was put directly on ice. RNA purity and concentration were assessed by Nanodrop. The sample was released only if it matched the 4 following criteria: (i) $A_{260}$:$A_{230}$ ratio > 1.7, (ii) $A_{260}$:$A_{280}$ ratio = [1.8; 2.0], (iii) Concentration by $A_{260}$ > 6ng/µl, and (iv) biopsy A and biopsy B from the same patient were available.

For specific pre-amplification, between 60 and 100ng of RNA (recommended range [10-100ng] in 8µl were preamplified by PI3K-AKT RT$^2$ PreAMP cDNA Synthesis according to the manufacturer's instructions.

For quantitative PCR, the PI3K-AKT specific RT$^2$ Profiler PCR Array protocol for 384-well plate (type E) was run according to the manufacturer's instructions on an ABI ViiA7 PCR cycler.

*DNA sequencing*

Libraries preparation using the Ion AmpliSeq™ Cancer Hotspot Panel v2 panel (Thermo Fisher Scientific) were performed following the manufacturer's instructions and as previously described (Dacheva et al. 2015; Simen et al. 2015). The Ion AmpliSeq™ Cancer Hotspot Panel v2 panel was designed to allow amplification-based capture and sequencing of coding regions of 50 cancer-related genes (http://tools.thermofisher.com/content/sfs/brochures/Ion-AmpliSeq-CancerHotspot-Panel Flyer.pdf). This panel includes 207 primer pairs and requires a minimum initial amount of 10 ng of DNA as input. After DNA extraction and quantification, multiplex PCR for targets enrichment was performed using genomic DNA mixed with primer pools and the Ion AmpliSeq™ HiFi master mix (Ion AmpliSeq™ Library Kit 2.0, Thermo Fisher Scientific) for 2 min at 99°C, followed by 22 cycles of 99°C for 15 sec and 60°C for 4 min and holding at 10°C. The obtained PCR products were sub sequentially treated with 2 $\mu$L of FuPa reagent (Ion AmpliSeq™ Library Kit 2.0, Thermo Fisher Scientific) to partially digest the primer sequences and then phosphorylated at 50°C for 10 min, followed by 55°C for 10 min, and finally at 60°C for 20 min. The generated amplicons were ligated to Ion beads adapters (Ion AmpliSeq™ Library Kit 2.0, Thermo Fisher Scientific) and sample-specific barcodes from the Ion Xpress™ Barcode Adapters kit (Thermo Fisher Scientific) for 30 min at 22°C and then at 72°C for 20 min. Afterwards, the generated barcoded libraries were purified using Agencourt® AMPure® XP reagents (Beckman Coulter). The library concentration was determined using an Ion Univesal Library Quantitation Kit (Thermo Fisher Scientific) and the amplicons size controlled with the Bioanalyzer 2100 (Agilent). 30 pM for each library were loaded into the IonChef System using the IC Hi-Q sequencing Kit for fully automated emulsion polymerase chain reaction (PCR) and chip loading (6 samples were multiplexed on one 318v2 chip). Finally, loaded chips were sequenced using the Ion PGM Hi-Q Sequencing Kit using the IonPGM (500 flows).

Raw data (BAM files) for each sample were processed for the alignment of sequencing reads with the human genome reference (hg19) using the Torrent Suite software v5.0 (Thermo Fisher Scientific). The alignment pipeline also included signaling processing, base calling, quality score assignment, adapter trimming, PCR duplicate removal and control of mapping quality. Local re-alignment, duplicate removal and quality base score recalibration were as well carried out using the Genome Analysis Toolkit (GATK) (McKenna et al. 2010). Coverage metrics for each amplicon (minimal acceptable coverage threshold was set at 300x) was obtained by running the Coverage Analysis Plugin software v5.0.1 (Thermo Fisher Scientific). Base calling was performed using the IonReporter v5.0 (Thermo Fisher Scientific). In additions, also MuTect (Cibulskis et al. 2013) and Varscan2 (Koboldt et al. 2012) algorithms were used to call somatic single nucleotide variants (SNVs) and Varscan2 (Koboldt et al. 2012), Strelka (Saunders et al. 2012) and Scalpel (Narzisi et al. 2014) for insertions and deletions (indels). We have chosen these specific mutations caller strategy as it allows identifying somatic mutations down to 1-2% mutant allele fraction (MAF) (i.e. 1-2% of the reads harboring a given

mutation). Finally, all candidate mutations were manually reviewed using the Integrative Genomics Viewer (Robinson et al. 2011; Thorvaldsdóttir et al. 2013).

*Staining for CD3, CD4, CD8 and FoxP3 positive cells in tumor biopsies*

Immunohistochemistry was performed on an automated immunostainer (Benchmark, Ventana/Roche). The primary antibody for CD3 was purchased from Ventana/Roche (ab790-4341, Tucson, Arizona). Antigen retrieval pre-treatment was achieved by mild cell conditioning with CC1 for 32 minutes. The antibody was incubated 12 minutes and detected applying OptiView and diaminobenzidine as chromogen. Finally, slides were counterstained with hematoxylin and bluing reagent (all from Ventana/Roche).
The primary antibody for CD8 was purchased from Ventana/Roche (ab790-4460, Tucson, Arizona). Pretreatment with CC1 was for 24 minutes, the antibody incubation time 16 minutes.
The primary antibody for was purchased from Ventana/Roche (ab790-4423, Tucson, Arizona). Pre-treatment was for 16 minutes with CC1, the antibody incubation time 12 minutes.
The primary antibody for FoxP3 was purchased from Abcam (ab22510, Cambridge, UK). Pre-treatment was for 64 minutes with CC1, the antibody dilution was 1:400, the antibody incubation at 37°C for 60 minutes.

*Statistical analysis*

Patient demographics, adverse events, PK and efficacy data were presented using descriptive statistics. Patients evaluable for safety analysis were defined as all patients who received at least 1 dose of PQR309. The DLT evaluable population was defined as all patients who missed no more than 1/3 of doses during the first cycle including any patient who experienced a DLT during cycle 1 regardless of the number of doses received. Patients who did not complete 1 cycle of treatment for reasons other than study related toxicity were replaced.
Analysis was performed using SAS version 9.2. GraphPad Prism 6 (GraphPad Prism Software Inc.) was used for additional analysis of the data and generation of graphs.

## Results

*Patient characteristics*

Twenty-eight patients (20 female, 8 male) were treated between January 2014 and February 2015 at six centers (Switzerland, the United Kingdom and Spain) (Table IX-1). Patients were enrolled into six dosing cohorts (10mg n=1; 20mg n=1; 40mg n=4; 80mg n=9; 100mg n=7; 120mg n=6), with dose adjusted for body weight in the first four cohorts (Table IX-2). The median age of patients was 58 years (range 21-75). The most frequent primary tumor types were colorectal cancer (n=7) and ovarian cancer (n=6). The study population was heavily pre-treated: the median number of lines of prior treatment was 4 (range 0-9; Table IX-1). Fourteen patients (50%) discontinued trial treatment due to progressive disease. Five patients discontinued due to adverse events (18%), six due to withdrawal of consent (21%; toxicity and intolerance of supportive therapies were given as reason), one due to death secondary to cancer, and one was withdrawn by the investigator. One patient left the trial after 21 cycles and continued PQR309 treatment within the framework of a compassionate use program.

*Adverse events*

Fatigue was the most common adverse event in this trial (Table IX-3). 26 of 28 patients (93%) experienced at least one episode of fatigue. Of those, 3 (11%) had fatigue grade 3-4.
Hyperglycemia was observed in 25 (89%) patients, 7 (25%) had G3-4 hyperglycemia. Blood glucose levels, PQR309 dosage and anti-hyperglycemic therapy are presented graphically (Suppl. Figure 2). Hyperglycemia onset was 7-14 days after commencing PQR309. The median time to normalization of blood glucose levels after stopping PQR309 was 7 days. Hyperglycaemia was managed with metformin, sulfonylureas, SGLT-2 inhibitors, and insulin. Insulin was required in 5 of the 7 patients with G3-4 hyperglycemia.
Anorexia occurred in 15 patients (54%) and weight loss >5% in 13 (46%) participants. Weight loss was reversible after stopping PQR309.
8 (29%) patients developed a maculopapular rash which was G3-4 severity in 5 patients. Corticosteroids were effective and induced rapid remission of the rash.
Depression was observed in 6 (21%) patients. In 1 patient (4%) a psychotic episode with suicide attempt was witnessed a few days after stopping the trial drug. No Grade 5 toxicities were observed.

*Dose-limiting toxicities*

Dose-escalation continued to 120mg once daily. No DLT was observed in the initial four dose-escalation cohorts up to 80mg daily (Table IX-2). Although no formal DLT was declared in the 120mg cohort, the investigators judged this dose to be above the maximum tolerated dose due to the frequency of Grade 3 AEs including hyperglycemia in 4 out of 6 patients; rash in 2 patients; and fatigue, anemia, nausea,

vomiting, diarrhea, broncho-pulmonary infection, hypoxia, ALT increase, AST increase, ALP increase, headache, and hypertension in 1 patient. Based on this assessment, an additional cohort was accrued at the 80mg flat dose level. No DLT occurred. As specified by the protocol an intermittent dose level of 100mg daily was opened. In this cohort, a G3 rash and G4 suicide attempt in a patient with colorectal cancer was considered a DLT. A second DLT in the 100mg cohort occurred in a patient with ovarian cancer at the same dose level who experienced G3 fatigue, G3 diarrhea and G3 elevation of liver enzymes. Given 2 DLTs in the 100mg cohort, three additional patients were enrolled in the 80mg cohort, of whom one patient experienced a DLT (G3 hyperglycemia for more than 7 days). Given a single DLT in a cohort of nine patients, 80mg was declared the maximum tolerated dose and the recommended phase 2 dose (RP2D) for continuous daily dosing of PQR309.

*Response*

Twenty-four patients were evaluable for response by radiological assessment of target lesions using RECIST v1.1 (Table IX-2). A partial response was observed in one patient. Best response of stable disease or progressive disease was observed in nine and fourteen patients respectively. The median duration of treatment was 41.5 days (range 12-446). Two patients were on treatment for over 100 days; a patient with thymic carcinoma with a known RICTOR1 amplification with a partial response on imaging (ongoing on day 705 ); and a patient with Bartholin's gland carcinoma with a SMARCB1 mutation and stable disease (152 days).

*Pharmacokinetics*

Absorption was moderately fast to fast. The peak plasma concentration, Cmax, was generally reached between 1 to 2 hours after oral administration of PQR309, except for some patients at 50, 80 and 120 mg PQR309 where Cmax was reached at 6 to 24 hours after oral administration of PQR309. The average peak concentration (Cmax) and exposure (AUClast) increased with increasing dose levels of PQR309 in a roughly dose proportional manner; with a minimum of 49.9 ng/mL and 273 h*ng/mL (15 mg) and a maximum of 998 ng/mL (150 mg) and 12600 h*ng/mL (120 mg), for Cmax and AUC respectively. The variability per group in the PK parameters Cmax and AUC, evaluated by %CV, varied from 13 to 80%. After repeated administration of PQR309 most patients showed higher plasma values after 21 days of treatment of PQR309 as compared to the pre-dose levels on Day 2 (=24-hour post first dose on Day 1), independent of dose level. Average accumulation ratios when comparing pre-dose Day 22 (Cycle 2 Day 1) to pre-dose Day 2 (=24 hours post first dose on Day 1, Cycle 1) varied from 1.0 to 9.7, and were not dose-related. T1/2 of PQR309 is estimated to be around 40 hours from the 0-24 hour profile carried out in this study.

*Pharmacodynamics*

17 patients had at least one tumor biopsy taken for pharmacodynamic analysis, although not all samples were sufficient for all planned translational assays.

Sequencing of tumor samples revealed a variety of sequence variations and amplifications (Table IX-2). Two patients had variations detected in their tumors that may have influenced the observed response to PQR309. A patient with thymic carcinoma treated at 100mg daily had an amplification of RICTOR, a component of mTORC2. This patient experienced a partial response (-42%) which lasted for more than 700 days. A patient with sinunasal cancer, also at 100mg daily, had an activating PIK3CA mutation; a minor response occurred in this patient.

The analysis of 88 PI3K-related mRNAs (Suppl. Figure IX-1) in PTB of 6 patients showed a non-significant threefold upregulation of PDGFRA (Suppl. Figure IX-3). No consistent up- or downregulation of the remaining 87 mRNAs was detected. Thus, there is no indication of transcriptional feedback regulation after 21 days of therapy with PQR309. No association of the analysed mRNAs and response was observed.

Samples from 13 patients were eligible for the analysis of phospho-proteins. Table 4 summarizes key characteristics of the 13 eligible paired biopsies. Changes in the level of phosphorylation are demonstrated in Figure IX-1 and supplementary Figure IX-4. Akt phosphorylation sites (Thr308 and Ser473), p-mTOR, p-S6-RiboProtein, p-AMPKa, p-PRAS40, p-GSK3b, p-Bad, p-RSK1, p-PTEN and p-Erk1/2 were significantly downregulated in comparison to baseline ($p<0.05$, Wilcoxon signed-rank test). p-4E-BP1, p-GSK3a and p-PDK1 showed a trend to reduced phosphorylation, but this was not statistically significant. Patients with tumor reduction by radiological assessment had stronger p-Akt Thr308, p-mTOR Ser2481 and phospho-S6-RiboProtein Ser235/236 (figure IX-1, suppl. figure IX-4) suppression than those with tumor increase ($p<0.05$, Mann-Whitney test). Importantly, MAPK activity (Erk1/2 phosphorylation) was the same in patients with tumor shrinkage as compared to those with tumor growth. Due to the small sample size per dose level, the trial lacked power to show a dose-dependent downreguation of PI3K-mTOR associated phospho-proteins.

The results of the analysis of immune infiltrates in tumor biopsies are shown in Figure 2. No significant change was observed in any of the T cell subpopulations assessed.

## Discussion

This first-in-human trial investigated the tolerability and RP2D of PQR309, an oral dual inhibitor of pan-PI3K and mTORC1/2. The main adverse events were fatigue, hyperglycemia, loss of appetite and rash. Six patients (21%) had depression, and amnesia was recorded in one patient (4%). The profile of AEs was broadly similar to that of other pan-PI3K inhibitors such as Buparlisib (NVP-BKM120) or dual inhibitors such as NVP-BEZ235 (Di Leo et al. 2016). The MTD and RP2D of PQR309 was defined as 80mg continuous once daily in advanced solid cancers. Clinical activity including a partial response was observed in patients with and without known PI3K pathway dysregulation. The pharmacokinetic profile suggests dose proportionality and a half-life of 40 hours. Based on the observed toxicity profile and the PK data, alternating dose schedules of PQR309 or 2 days on / 5 days off regimens should be evaluated.

NGS of tumor tissue identified a range of mutations that reflect the known heterogeneity of advanced cancers. Although it is rational to hypothesize that tumors harbouring activating PI3K or mTOR mutations respond better to PI3K-mTOR inhibitors than tumors without, only the BELLE-2 trial has been able to assign a predictive value to such mutations (Baselga J, Im S-A, Iwata H, 2015). In the present trial, one patient with *RICTOR* amplification (Cheng et al. 2015) and one with an activating *PI3K* mutation (*PIK3CA* p.Glu545Lys) derived benefit from the trial medication. The overall predictive value of PI3K pathway mutations remains unconfirmed. The analysis of PI3K related mRNAs showed a threefold upregulation of PDGFRA during PQR309 therapy. However, the result did not cross the pre-defined boundary for statistical significance and no predictive value could be assigned to mRNAs associated with PI3K signaling. Despite this, upregulation of PDGFRA may represent a mechanism of resistance and should be further evaluated in future trials with PQR309.

Exposure to PQR309 significantly downregulates the signaling activity of several PI3K-mTOR associated phospho-proteins, indicating that PQR309 effectively inhibits the intended targets in patients. Consistent with previous preclinical data, PQR309 can also inhibit Erk1/2 signalling in patients. The sample size (1-6 patients per dose level) is too small to show dose-dependent downregulation of PI3K/Akt/mTOR signaling. However, a more pronounced downregulation of p-Akt Thr308, p-mTOR Ser2481 and p-S6-RiboProtein Ser235/236 was observed in those patients whose tumors reduced while on therapy. Whether this correlates with a higher baseline activation of PI3K/mTOR or is due to a stronger inhibitory effect of the drug in responding patients cannot be determined with any certainty from the experimental data. From the perspective of predicting response to PI3K/Akt/mTOR pathway inhibition, it seems that the concomitant downregulation of p-Akt Thr308 and mTORC1 activity in patients treated with PQR309 may be indicative of tumors that respond. On examination of all the phosphorylation data, phosphorylation sites closely associated with activation of p-Akt Thr308 and mTORC1 show concordant directional change. For example, S6-Riboprotein phosphorylation is

downregulated because S6K depends on p-Akt Thr308 activation. In contrast, S6K phosphorylation does not need p-Akt Ser4738. Furthermore, p-mTOR Ser2481, which is auto-phosphorylated by TSC1/2 and then p-Akt Thr308, is also downregulated. In addition, there is evidence that TSC1/2 phosphorylation can be triggered by isolated p-Akt Thr308 phosphorylation and p-mTOR S2481 is also reported to associate with mTORC2 (Copp et al. 2009).

The exceptions in this dataset are GSK3a and b, which are thought to rely on p-Akt Thr308. However, they are also reported to be targeted by PKC, which may account for the observed discordance. The decrease of PDK1 is not significant.

PI3K signalling is involved in the activation of T-cells. There was no evidence that therapy with a dual PI3K-mTOR inhibitor induced immunosuppression in this trial. The analysis of immune infiltrates showed no downregulation of CD8-positive cytotoxic T cells or upregulation of regulatory T cells.
This trial supports further clinical investigation of PQR309 which continues in phase I andII trials including solid tumors with activating *PI3K* mutations (alternative dose scheduling and more intensive PK testing (NCT02850744), lymphoma (NCT02249429), glioblastoma multiforme (NCT02850744), and CNS lymphoma (NCT02669511). The cytostatic nature of PI3K/mTOR inhibitors supports combination therapy approaches and a Phase I/II clinical trial of PQR309 in combination with eribulin is underway in patients with metastatic HER2 negative and triple negative breast cancer (NCT02723877).

*Conflict of interest statement*

N.C., V.C., M.S., S.D. and R.H. are employees of PIQUR. The other authors declare that they have no conflict of interest to disclose.

*Source of funding*

This clinical trial was fully funded by PIQUR Therapeutics.

*Role of the funding source*

PIQUR Therapeutics provided financial support for the study and participated in the design, study conduct and data analysis. PIQUR Therapeutics was involved in review and approval of the manuscript.

*Acknowledgements*

This trial was carried out and supported by the Swiss Group for Clinical Cancer Research (SAKK), Bern, the National Institute for Health Research (NIHR) UCLH Clinical Research Facility and the Cancer Research UK Experimental Cancer Medicine Centre (ECMC). Rebecca Kristeleit is supported by the UCL/UCLH Biomedical Research Centre. A.W., R.K. and C.S. were involved in trial design, patient accrual, data acquisition, data interpretation and writing of the manuscript. N.B., V.H., A.C., C.H., J.R., D.H., M.J. and R.v.M. were involved in patient accrual, data acquisition, data interpretation and writing of the manuscript. A.X., V.B., H.H. and S.B. took part in data acquisition and data interpretation. N.C., V.C., M.S., S.D. and R.H. contributed to the trial design. A.W., V.P., R.R., and A.T. performed the translational research.

## Tables

Table 1. Baseline demographics and clinical characteristics

| | **Patients (n=28)** |
|---|---|
| Sex | |
| Male | 8 |
| Female | 20 |
| Age (years) | 58 (21-75) |
| ECOG performance status | |
| 0 | 12 |
| 1 | 16 |
| Tumor type | |
| Colorectal cancer | 7 |
| Ovarian cancer | 6 |
| Endomentrial carcinosarcoma | 2 |
| Lung cancer | 2 |
| Breast cancer | 2 |
| Other | 9 |
| Previous lines of systemic treatment | 4 (0-9) |
| 0 | 1 |
| 1 | 2 |
| 2 | 5 |
| ≥3 | 20 |

Table IX-1 : Baseline demographics and clinical characteristics.

Table 2. **Dose level, primary tumor, treatment duration, response, and genotype.**

| Patient Number | Dose PQR309 | Tumor type | Treatment duration (days) | DLT | Best response | Gene mutation | AA Change |
|---|---|---|---|---|---|---|---|
| 6713_001 | 10 mg | Ewing-sarcoma | 26 | None | PD | | |
| 6713_002 | 15 mg | Colorectal carcinoma | 25 | None | PD | | |
| 6713_003 | 50 mg | Breast carcinoma | 40 | None | PD | TP53 | p.Glu198Ter |
| 6713_005 | 40 mg | Ovarian carcinoma | 84 | None | SD | | |
| 6713_006 | 40 mg | Ovarian carcinoma | 7 | NE | NE | | |
| 6713_007 | 30 mg | Colorectal carcinoma | 41 | None | PD | | |
| 6713_008 | 80 mg | Bartholin's gland carcinoma | 152 | None | SD | SMARCB1 | p.Thr72Lys |
| 6713_010 | 60 mg | Breast carcinoma | 42 | None | PD | | |
| 6713_011 | 60 mg | Ovarian carcinoma | 42 | None | SD | | |
| 6713_012 | 120 mg | Ovarian carcinoma | 31 | None | SD | PIK3CA<br>JAK3 | p.Ile391Met<br>p.Pro132Thr |
| 6713_013 | 120 mg | Cholangio carcinoma | 8 | NE | NE | | |
| 6713_014 | 120 mg | Colorectal carcinoma | 42 | None | PD | | |
| 6713_015 | 90 mg | Lung carcinoma | 12 | None | NE | | |
| 6713_018 | 150 mg | Lung carcinoma | 31 | None | SD | | |
| 6713_019 | 90 mg | Ovarian carcinoma | 36 | None | PD | | |
| 6713_021 | 80 mg | Mesothelioma | 37 | None | PD | MET | p.Arg988Cys |
| 6713_022 | 80 mg | Colorectal carcinoma | 40 | None | PD | KRAS | p.Gly12Ser |
| 6713_023 | 80 mg | Endometrial carcinoma | 46 | None | SD | | |
| 6713_024 | 100 mg | Squamous cell cancer of the tongue | 44 | None | PD | NOTCH1<br>ATM | p.Pro2465Leu<br>p.Ser1691Arg |
| 6713_026 | 100 mg | Colorectal carcinoma | 83 | None | SD | KRAS<br>APC<br>TP53<br>TP53 | p.Gln61His<br>p.Ser1315*<br>p.Ser240Cys<br>p. Gly244Ser |
| 6713_028 | 100 mg | Endometrial carcinoma | 42 | None | PD | | |
| 6713_029 | 100 mg | Thymic carcinoma | 446 | None | PR | RICTOR1 amplification | |
| 6713_031 | 100 mg | Colorectal carcinoma | 20 | G3 Rash<br>G4 Suicide attempt | PD | TP53<br>PTEN | p.Ile255Thr<br>p.Gln110Ter |
| 6713_032 | 100 mg | Sinonasal carcinoma | 55 | None | SD | PIK3CA | p.Glu545Lys |
| 6713_033 | 100 mg | Ovarian carcinoma | 50 | G3 Fatigue<br>G3 Diarrhea<br>G3 Transaminitis | SD | | |
| 6713_034 | 80 mg | Colorectal carcinoma | 18 | G3 Hyperglycemia | NE | | |
| 6713_035 | 80 mg | Endometrial carcinoma | 21 | None | PD | | |
| 6713_036 | 80 mg | Cervical carcinoma | 63 | None | PD | KIT | p.Met541Leu |

DLT=dose limiting toxicity. PD=progressive disease. SD=stable disease. PR=partial response. CR=complete response. NE=not evaluable. Tumor assessment: clinically every 3 weeks, by CT or MRI every 6 weeks for the first 4 cycles. Thereafter every 9 weeks.
* = non-sense substitution.

Table IX-2 : Dose level, primary tumor, treatment duration, response, and genotype.

Table 3. **Adverse Events of Grade 1-2 and Grade 3 or worse**

| | NCI CTC severity grade | | Total |
|---|---|---|---|
| | 1-2 | 3-4 | |
| Patients with at least one AE | 28 (100%) | 21 (75.0%) | 28 (100%) |
| Fatigue | 23 (82.1%) | 3 (10.7%) | 26 (92.9%) |
| Hyperglycaemia | 17 (60.7%) | 7 (25.0%) | 24 (85.7%) |
| Decreased appetite | 15 (53.6%) | 0 | 15 (53.6%) |
| Diarrhoea | 12 (42.9%) | 3 (10.7%) | 15 (53.6%) |
| Nausea | 14 (50.0%) | 1 ( 3.6%) | 15 (53.6%) |
| Rash maculo-papular | 8 (28.6%) | 5 (17.9%) | 13 (46.4%) |
| Weight decreased | 13 (46.4%) | 0 | 13 (46.4%) |
| Vomiting | 11 (39.3%) | 1 ( 3.6%) | 12 (42.9%) |
| Abdominal pain | 10 (35.7%) | 0 | 10 (35.7%) |
| Constipation | 9 (32.1%) | 0 | 9 (32.1%) |
| Hypertension | 5 (17.9%) | 4 (14.3%) | 9 (32.1%) |
| Pruritus | 8 (28.6%) | 0 | 8 (28.6%) |
| Depression | 6 (21.4%) | 0 | 6 (21.4%) |
| Dyspnoea | 6 (21.4%) | 0 | 6 (21.4%) |
| Dry skin | 5 (17.9%) | 0 | 5 (17.9%) |
| Alanine aminotransferase increased | 2 ( 7.1%) | 2 ( 7.1%) | 4 (14.3%) |
| Cough | 4 (14.3%) | 0 | 4 (14.3%) |
| Oedema peripheral | 4 (14.3%) | 0 | 4 (14.3%) |
| Urinary tract infection | 4 (14.3%) | 0 | 4 (14.3%) |
| Agitation | 3 (10.7%) | 0 | 3 (10.7%) |
| Aspartate aminotransferase increased | 1 ( 3.6%) | 2 ( 7.1%) | 3 (10.7%) |
| Back pain | 2 ( 7.1%) | 1 ( 3.6%) | 3 (10.7%) |
| Disease progression | 0 | 3 (10.7%) | 3 (10.7%) |
| Insomnia | 3 (10.7%) | 0 | 3 (10.7%) |
| Pollakiuria | 3 (10.7%) | 0 | 3 (10.7%) |
| Stomatitis | 3 (10.7%) | 0 | 3 (10.7%) |
| Abdominal pain upper | 2 ( 7.1%) | 0 | 2 ( 7.1%) |
| Alopecia | 2 ( 7.1%) | 0 | 2 ( 7.1%) |
| Ascites | 1 ( 3.6%) | 1 ( 3.6%) | 2 ( 7.1%) |
| Cognitive disorder | 2 ( 7.1%) | 0 | 2 ( 7.1%) |
| Dizziness | 2 ( 7.1%) | 0 | 2 ( 7.1%) |
| Embolism | 2 ( 7.1%) | 0 | 2 ( 7.1%) |
| Gamma-glutamyltransferase increased | 1 ( 3.6%) | 1 ( 3.6%) | 2 ( 7.1%) |
| Haematuria | 2 ( 7.1%) | 0 | 2 ( 7.1%) |
| Headache | 1 ( 3.6%) | 1 ( 3.6%) | 2 ( 7.1%) |
| Hyponatraemia | 0 | 2 ( 7.1%) | 2 ( 7.1%) |
| Insulin C-peptide increased | 2 ( 7.1%) | 0 | 2 ( 7.1%) |

Table 3. **Adverse Events of Grade 1-2 and Grade 3 or worse**

| | NCI CTC severity grade | | Total |
|---|---|---|---|
| | 1-2 | 3-4 | |
| Muscular weakness | 2 ( 7.1%) | 0 | 2 ( 7.1%) |
| Pain | 2 ( 7.1%) | 0 | 2 ( 7.1%) |
| Palmar-plantar erythrodysaesthesia syndrome | 2 ( 7.1%) | 0 | 2 ( 7.1%) |
| Polydipsia | 2 ( 7.1%) | 0 | 2 ( 7.1%) |
| Pyrexia | 2 ( 7.1%) | 0 | 2 ( 7.1%) |
| Rash | 2 ( 7.1%) | 0 | 2 ( 7.1%) |
| Seizure | 2 ( 7.1%) | 0 | 2 ( 7.1%) |
| Abdominal discomfort | 1 ( 3.6%) | 0 | 1 ( 3.6%) |
| Abdominal distension | 1 ( 3.6%) | 0 | 1 ( 3.6%) |
| Amnesia | 1 ( 3.6%) | 0 | 1 ( 3.6%) |
| Anxiety | 1 ( 3.6%) | 0 | 1 ( 3.6%) |
| Asthenia | 1 ( 3.6%) | 0 | 1 ( 3.6%) |
| Blood alkaline phosphatase increased | 1 ( 3.6%) | 0 | 1 ( 3.6%) |
| Blood bilirubin increased | 1 ( 3.6%) | 0 | 1 ( 3.6%) |
| Blood cholesterol increased | 1 ( 3.6%) | 0 | 1 ( 3.6%) |
| Blood creatine phosphokinase increased | 1 ( 3.6%) | 0 | 1 ( 3.6%) |
| Bone pain | 1 ( 3.6%) | 0 | 1 ( 3.6%) |
| Bronchitis | 1 ( 3.6%) | 0 | 1 ( 3.6%) |
| Bronchopneumonia | 0 | 1 ( 3.6%) | 1 ( 3.6%) |
| Confusional state | 1 ( 3.6%) | 0 | 1 ( 3.6%) |
| Deafness | 1 ( 3.6%) | 0 | 1 ( 3.6%) |
| Dermatitis acneiform | 1 ( 3.6%) | 0 | 1 ( 3.6%) |
| Disturbance in attention | 1 ( 3.6%) | 0 | 1 ( 3.6%) |
| Dry eye | 1 ( 3.6%) | 0 | 1 ( 3.6%) |
| Dry mouth | 1 ( 3.6%) | 0 | 1 ( 3.6%) |
| Dysgeusia | 1 ( 3.6%) | 0 | 1 ( 3.6%) |
| Dyspepsia | 1 ( 3.6%) | 0 | 1 ( 3.6%) |
| Dysphagia | 1 ( 3.6%) | 0 | 1 ( 3.6%) |
| Dysphonia | 1 ( 3.6%) | 0 | 1 ( 3.6%) |
| Enteritis | 1 ( 3.6%) | 0 | 1 ( 3.6%) |
| Flank pain | 1 ( 3.6%) | 0 | 1 ( 3.6%) |
| Gastritis | 1 ( 3.6%) | 0 | 1 ( 3.6%) |
| Gastrooesophageal reflux disease | 1 ( 3.6%) | 0 | 1 ( 3.6%) |
| Glossitis | 1 ( 3.6%) | 0 | 1 ( 3.6%) |
| Hepatic pain | 1 ( 3.6%) | 0 | 1 ( 3.6%) |
| Hypersensitivity | 1 ( 3.6%) | 0 | 1 ( 3.6%) |
| Hypokalaemia | 1 ( 3.6%) | 0 | 1 ( 3.6%) |
| Hypomagnesaemia | 1 ( 3.6%) | 0 | 1 ( 3.6%) |
| Hypotension | 1 ( 3.6%) | 0 | 1 ( 3.6%) |

Table 3. **Adverse Events of Grade 1-2 and Grade 3 or worse**

| | NCI CTC severity grade | | Total |
|---|---|---|---|
| | 1-2 | 3-4 | |
| Hypothermia | 1 ( 3.6%) | 0 | 1 ( 3.6%) |
| Hypoxia | 0 | 1 ( 3.6%) | 1 ( 3.6%) |
| Insulin C-peptide | 1 ( 3.6%) | 0 | 1 ( 3.6%) |
| Irritability | 1 ( 3.6%) | 0 | 1 ( 3.6%) |
| Lethargy | 1 ( 3.6%) | 0 | 1 ( 3.6%) |
| Lower respiratory tract infection | 0 | 1 ( 3.6%) | 1 ( 3.6%) |
| Lung infection | 0 | 1 ( 3.6%) | 1 ( 3.6%) |
| Lymph node pain | 1 ( 3.6%) | 0 | 1 ( 3.6%) |
| Mucosal infection | 1 ( 3.6%) | 0 | 1 ( 3.6%) |
| Muscle spasms | 1 ( 3.6%) | 0 | 1 ( 3.6%) |
| Neck injury | 1 ( 3.6%) | 0 | 1 ( 3.6%) |
| Non-cardiac chest pain | 1 ( 3.6%) | 0 | 1 ( 3.6%) |
| Oesophageal pain | 1 ( 3.6%) | 0 | 1 ( 3.6%) |
| Pain in extremity | 1 ( 3.6%) | 0 | 1 ( 3.6%) |
| Photopsia | 1 ( 3.6%) | 0 | 1 ( 3.6%) |
| Pleural effusion | 1 ( 3.6%) | 0 | 1 ( 3.6%) |
| Polyuria | 1 ( 3.6%) | 0 | 1 ( 3.6%) |
| Post procedural haematuria | 0 | 1 ( 3.6%) | 1 ( 3.6%) |
| Proctalgia | 1 ( 3.6%) | 0 | 1 ( 3.6%) |
| Psychotic disorder | 0 | 1 ( 3.6%) | 1 ( 3.6%) |
| Suicide attempt | 0 | 1 ( 3.6%) | 1 ( 3.6%) |
| Toothache | 1 ( 3.6%) | 0 | 1 ( 3.6%) |
| Tremor | 1 ( 3.6%) | 0 | 1 ( 3.6%) |
| Tumour pain | 0 | 1 ( 3.6%) | 1 ( 3.6%) |
| Upper respiratory tract infection | 1 ( 3.6%) | 0 | 1 ( 3.6%) |
| Urinary tract pain | 1 ( 3.6%) | 0 | 1 ( 3.6%) |
| Vaginal infection | 1 ( 3.6%) | 0 | 1 ( 3.6%) |
| Vertigo | 1 ( 3.6%) | 0 | 1 ( 3.6%) |
| Visual acuity reduced | 1 ( 3.6%) | 0 | 1 ( 3.6%) |
| Vulvovaginal dryness | 1 ( 3.6%) | 0 | 1 ( 3.6%) |
| Vulvovaginal pain | 1 ( 3.6%) | 0 | 1 ( 3.6%) |

A patient with multiple occurrences of an AE is counted only once (with the worst grade) in the AE category.

Table IX-3 : Adverse events of grade 1-2 and grade 3 or worse.

Table 4
Analysis of paired tumour biopsies in 13 patients.

| # | UPN | Cycle day | Hours after last PQR309 intake | Dose-normalised AUC ([h*ng/mL]/mg) | Overall response | Target lesion sum—change from baseline (%) | Symbol |
|---|---|---|---|---|---|---|---|
| 1 | 003 | C2D5 | 2 | 58.2 | PD | −8.7% | |
| 2 | 008 | C1D16 | 23 | 6.95 | SD | −15.0% | |
| 3 | 012 | C2D1 | 24 | 80.7 | SD | −7.3% | |
| 4 | 014 | C2D1 | 22 | 126 | PD | **18.8%** | |
| 5 | 021 | C2D7 | 3 | 93.4 | PD | −61.3% | |
| 6 | 022 | C1D19 | 22 | 15.5 | PD | **17.5%** | |
| 7 | 026 | C2D5 | 5 | 80.9 | SD | −9.2% | |
| 8 | 028 | C1D18 | 29 | 65.3 | PD | **2.1%** | |
| 9 | 031 | C2D1 | 27 | 65.2 | PD | **8.6%** | |
| 10 | 032 | C2D7 | 26 | 67.6 | SD | −25.0% | |
| 11 | 033 | C2D4 | 4 | 45.7 | SD | **2.7%** | |
| 12 | 035 | C1D21 | 2 | 64.2 | PD | −11.9% | |
| 13 | 036 | C2D1 | 25 | 120 | PD | **22.0%** | |

UPN = unique patient number; PD, progressive disease; SD, stable disease. Bold = tumor growth.

Table IX-4 : Analysis of PTB in 13 patients.

The table indicates the exact day of the drug administration cycle the biopsy was taken, the delay after the last dose of oral PQR309, the 1mg dose-normalized Area Under the Curve from the beginning and until 24 hours ($AUC_{0\text{-}24}$), and the tumor content on the analyzed tumor slices.

## Figures

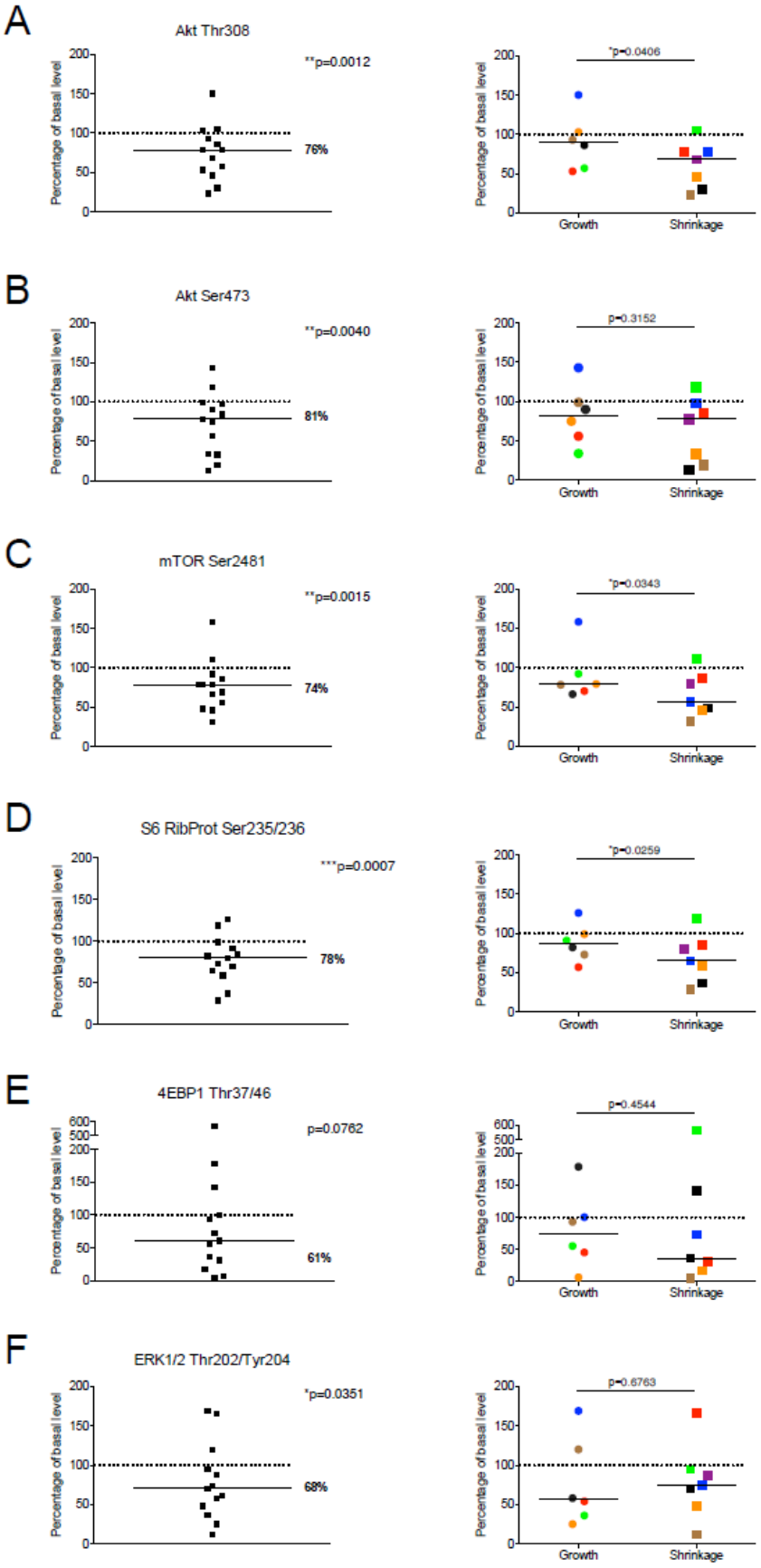
A
Akt Thr308
**p=0.0012
76%
*p=0.0406
Growth
Shrinkage
B
Akt Ser473
**p=0.0040
81%
p=0.3152
C
mTOR Ser2481
**p=0.0015
74%
*p=0.0343
D
S6 RibProt Ser235/236
***p=0.0007
78%
*p=0.0259
E
4EBP1 Thr37/46
p=0.0762
61%
p=0.4544
F
ERK1/2 Thr202/Tyr204
*p=0.0351
68%
p=0.6763
Percentage of basal level

Figure IX-1 : Activation of phosphorylation sites in the PI3K-mTOR signaling axis after 21 days of treatment with PQR309.

The graphs on the left hand side show the change of the level of phosphorylation of a specific phosphorylation site while the patient is on therapy, in comparison to the baseline (first biopsy, equivalent to 100%). One data point represents 1 patient. The colour-code is explained in Tab. 4. The data-point corresponds to the mean of two independent measurements of the respective phospho-protein per biopsy and time-point. On the right hand side, patients were divided into one group, whose tumors grew despite therapy (round symbols), and a second group, whose tumors shrank (square symbols). Growth or shrinkage was defined by the best response of each patient. We considered all lesions that were also considered target lesions for the assessment according to RECIST 1.1.

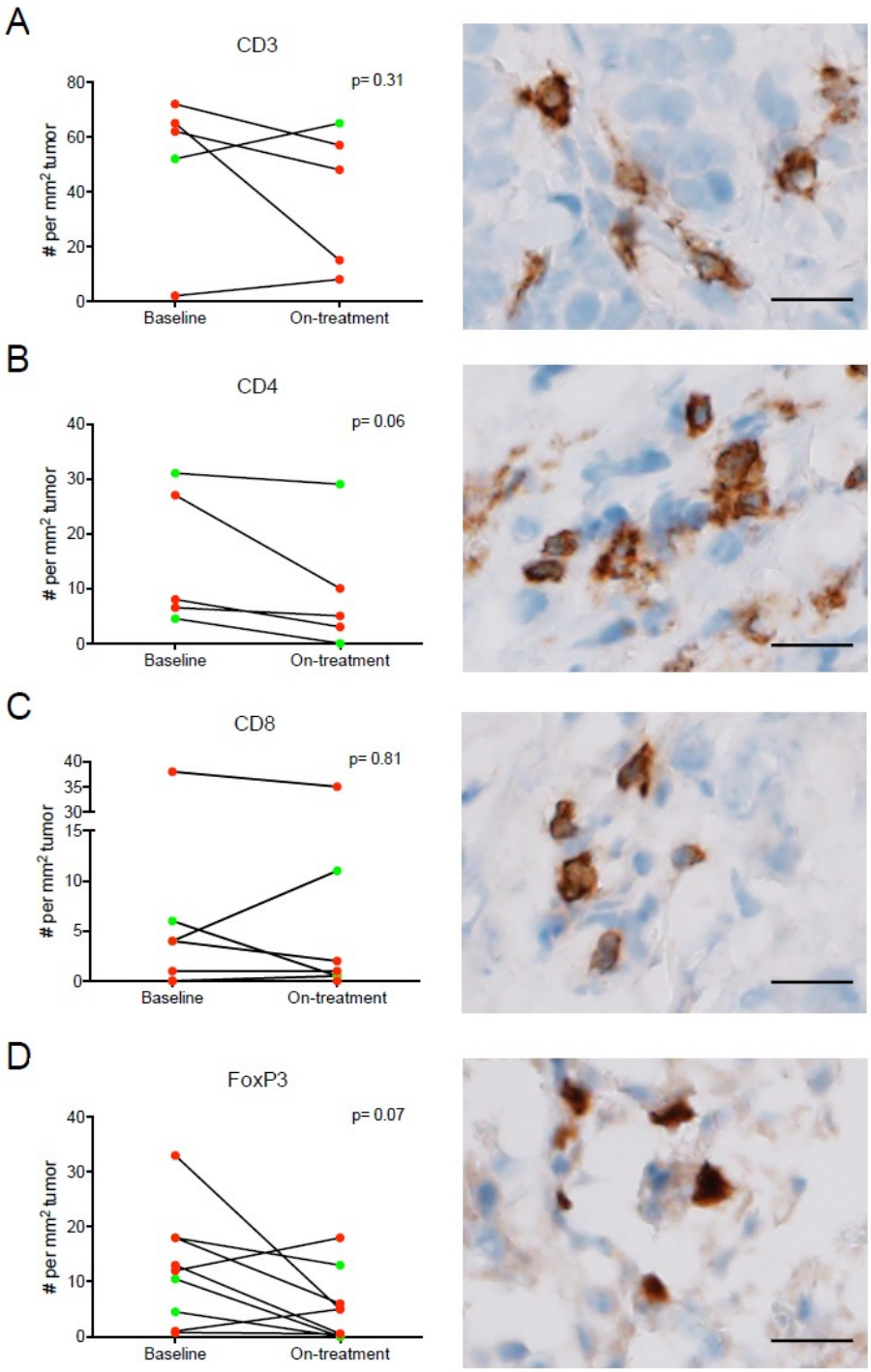


Figure IX-2 : Infiltration of the tumor with CD3, CD4, CD8 and FoxP3 positive immune cells (panels A-D, as indicated).

Red dots = immune infiltrates in patients with tumor growth. Green dots = immune infiltrates in patients with tumor shrinkage. Left-hand column: Quantification of immune infiltrates. Right-hand column: Exemplary image of IHC staining. Bar = 10 µm.

| # | Symbol | GeneBank | # | Symbol | GeneBank |
|---|---|---|---|---|---|
| 1 | ADAR | NM_001111 | 43 | MAPK3 | NM_002746 |
| 2 | AKT1 | NM_005163 | 44 | MAPK8 | NM_002750 |
| 3 | AKT2 | NM_001626 | 45 | MTCP1 | NM_001018025 |
| 4 | AKT3 | NM_005465 | 46 | MTOR | NM_004958 |
| 5 | APC | NM_000038 | 47 | MYD88 | NM_002468 |
| 6 | BAD | NM_004322 | 48 | NFKB1 | NM_003998 |
| 7 | BTK | NM_000061 | 49 | NFKBIA | NM_020529 |
| 8 | CASP9 | NM_001229 | 50 | PABPC1 | NM_002568 |
| 9 | CCND1 | NM_053056 | 51 | PAK1 | NM_002576 |
| 10 | CD14 | NM_000591 | 52 | PDGFRA | NM_006206 |
| 11 | CDC42 | NM_001791 | 53 | PDK1 | NM_002610 |
| 12 | CDKN1B | NM_004064 | 54 | PDK2 | NM_002611 |
| 13 | CHUK | NM_001278 | 55 | PDPK1 | NM_002613 |
| 14 | CSNK2A1 | NM_001895 | 56 | PIK3CA | NM_006218 |
| 15 | CTNNB1 | NM_001904 | 57 | PIK3CG | NM_002649 |
| 16 | EIF2AK2 | NM_002759 | 58 | PIK3R1 | NM_181504 |
| 17 | EIF4B | NM_001417 | 59 | PIK3R2 | NM_005027 |
| 18 | EIF4E | NM_001968 | 60 | PRKCA | NM_002737 |
| 19 | EIF4EBP1 | NM_004095 | 61 | PRKCB | NM_002738 |
| 20 | EIF4G1 | NM_182917 | 62 | PRKCZ | NM_002744 |
| 21 | ELK1 | NM_005229 | 63 | PTEN | NM_000314 |
| 22 | FASLG | NM_000639 | 64 | PTK2 | NM_005607 |
| 23 | FKBP1A | NM_000801 | 65 | PTPN11 | NM_002834 |
| 24 | FOS | NM_005252 | 66 | RAC1 | NM_006908 |
| 25 | FOXO1 | NM_002015 | 67 | RAF1 | NM_002880 |
| 26 | FOXO3 | NM_001455 | 68 | RASA1 | NM_002890 |
| 27 | GJA1 | NM_000165 | 69 | RBL2 | NM_005611 |
| 28 | GRB10 | NM_005311 | 70 | RHEB | NM_005614 |
| 29 | GRB2 | NM_002086 | 71 | RHOA | NM_001664 |
| 30 | GSK3B | NM_002093 | 72 | RPS6KA1 | NM_002953 |
| 31 | HRAS | NM_005343 | 73 | RPS6KB1 | NM_003161 |
| 32 | HSPB1 | NM_001540 | 74 | SHC1 | NM_003029 |
| 33 | IGF1 | NM_000618 | 75 | SOS1 | NM_005633 |
| 34 | IGF1R | NM_000875 | 76 | SRF | NM_003131 |
| 35 | ILK | NM_004517 | 77 | TCL1A | NM_021966 |
| 36 | IRAK1 | NM_001569 | 78 | TIRAP | NM_001039661 |
| 37 | IRS1 | NM_005544 | 79 | TLR4 | NM_138554 |
| 38 | ITGB1 | NM_002211 | 80 | TOLLIP | NM_019009 |
| 39 | JUN | NM_002228 | 81 | TSC1 | NM_000368 |
| 40 | MAP2K1 | NM_002755 | 82 | TSC2 | NM_000548 |
| 41 | MAPK1 | NM_002745 | 83 | WASL | NM_003941 |
| 42 | MAPK14 | NM_001315 | 84 | YWHAH | NM_003405 |

Suppl. Figure IX-1

List of 88 PI3K-mTOR associated mRNAs analyzed in PTB.

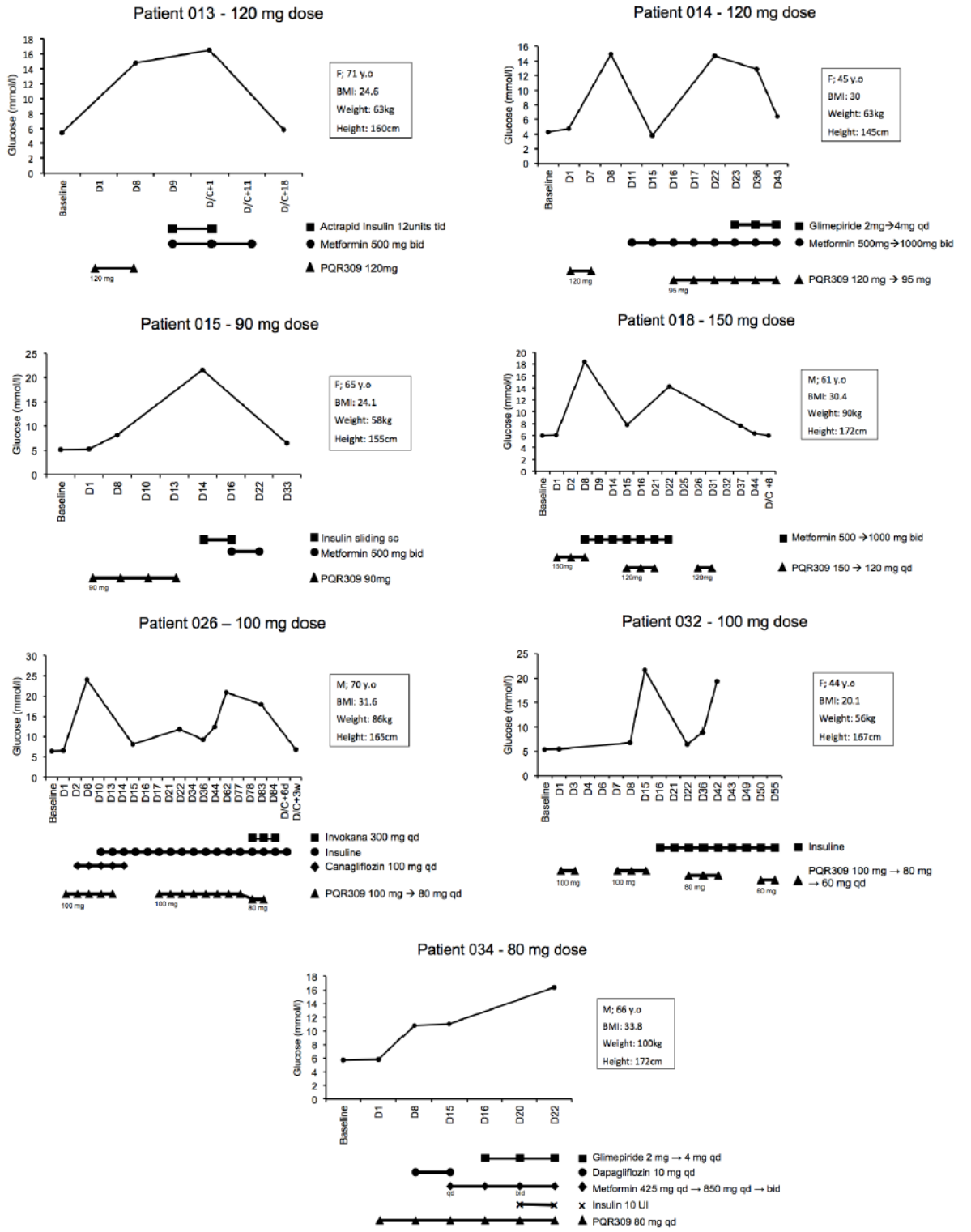


Suppl. Figure IX-2

Glucose levels and treatment of hyperglycemia in patients with hyperglycemia grade 3-4. Individual data are presented for all 7 patients with hyperglycemia grade ≥3.

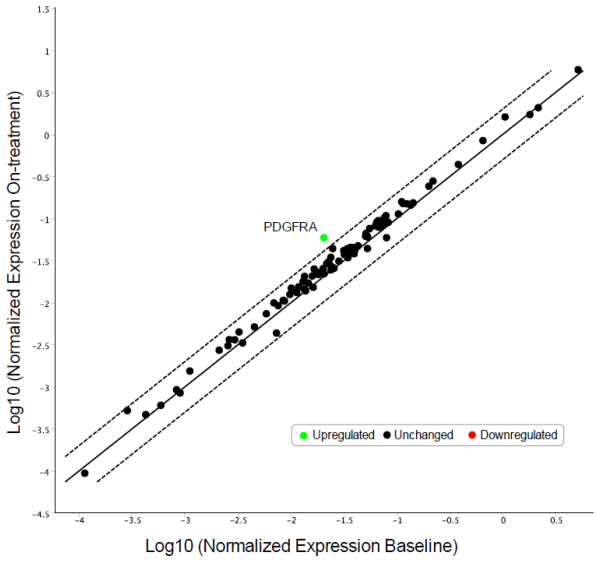


Suppl. Figure IX-3

Changes of the expression level of 88 mRNAs associated with PI3K-mTOR signaling after 21 days of treatment with PQR309. PDGFRA is the only mRNA showing a trend towards upregulation. No statistically significant up- or down-regulation was observed.

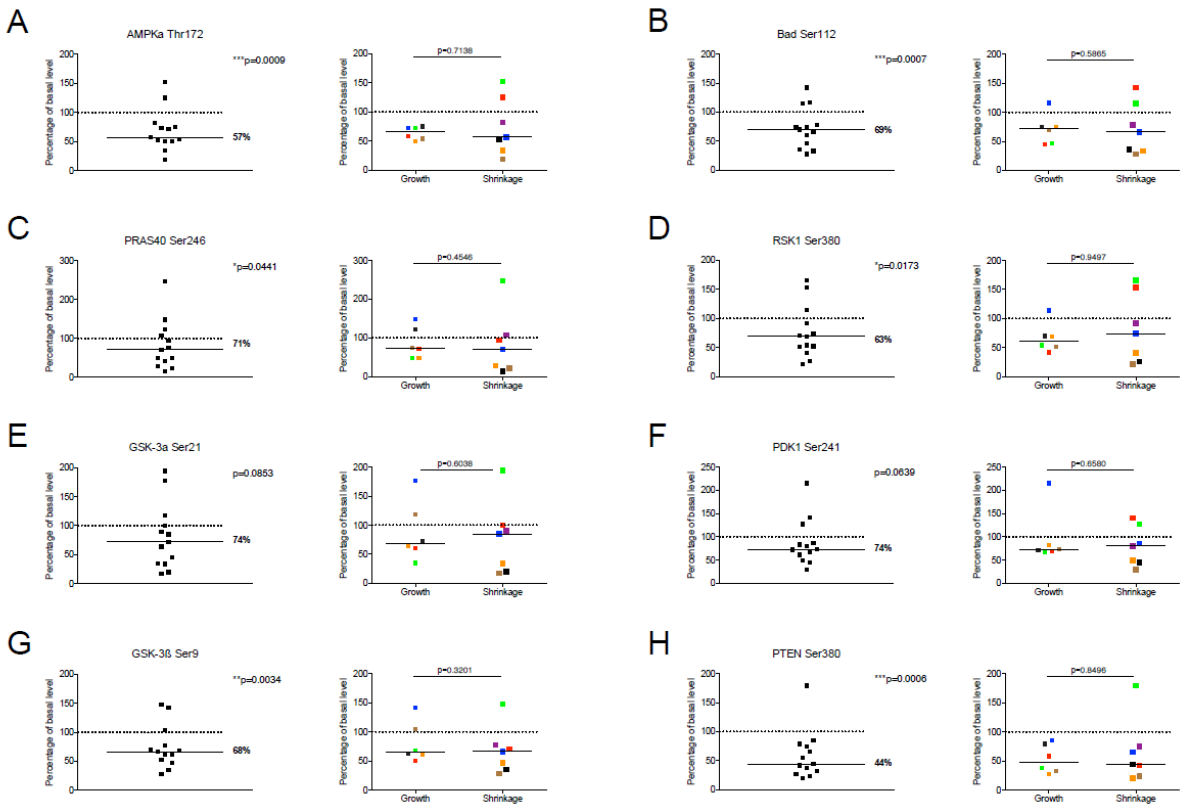


Suppl. Figure IX-4

Full panel of phospho-sites analysed in addition to those presented in Fig. 1. The colour-code is explained in Tab. 4.

# X. Global Discussion and Perspective

These three diverse projects provide novel insights on the impact of PDPN and other treatments on the mTOR/PI3K/Akt pathway. We showed that podoplanin was responsible for the Akt-driven activation of the EGFR pathway and a mechanism of resistance for the squamous cell carcinomas upon treatments. Then we treated mice harboring pNET malignancy with a combination of radionuclide and Everolimus, where the mTOR inhibit in a critical dose-dependent manner. These results contradict previous studies in a non-appropriate rat model that stopped all the clinical trials for this potential combination treatment. Finally, we analyzed paired human biopsies confirming the efficacy of the investigational dual mTOR/PI3K inhibitor and the inhibition of the phospho-proteins in the metastasis as a surrogate of the primary tumor. The inhibition could eventually predict the response to this compound that received this year an orphan drug designation from the FDA for primary central nervous system lymphoma (PCNSL) and an EMA orphan drug designation for Diffuse Large B-cell Lymphoma. A more general perspective on this central pathway for cancer can be considered along several points based on the recent research, preclinical and clinical data :

Firstly, while the inhibitors concentrated their studies on solid tumors, hematological cancers should be targeted as well. [I didn't really understand how the following sentences support your first sentence here about hematological cancers. Is it obvious to everyone else? Otherwise maybe spell out the link more clearly] Given the critical functions of mTOR in most human tissues, complete catalytic inhibition causes severe dose-limiting toxicities, while rapalogs also suffer from the drawbacks associated with lack of tissue specificity and unwanted disruption of mTORC2 (Saxton & Sabatini 2017). Rapalogues do not fully suppress mTOR activity or translation but ATP-competitive mTOR inhibitors could overcome these problems (Hsieh et al. 2012; Turner et al. 2017b). The lack of predictive biomarkers is a major challenge and opportunity of targeted therapies. A new generation of compounds is now being tested and developed according to our understanding of the resistance mechanisms to TKI.

Secondly, isoform-selective PI3K inhibitors have seen promising success in early- and late-stage clinical trials for solid and hematological malignancies, highlighting the potential for isoform-selective PI3K therapeutics (Thorpe et al. 2015). In order to reduce toxicities while stabilizing or increasing the effect, a pulsatile as opposed to continuous treatment should be tested in early phase clinical trials.

We should decipher the effect of these inhibitors on the immune system and the tumor microenvironment. The effect of an inhibition of this pathway can either enhance or inhibit diverse subsets of innate and adaptive immune cells. Many xenograft-based preclinical studies do not address this aspect of the side effects of the drug and possibly bias the results towards combinations with

checkpoint inhibitors or potential vaccines cancer. For these reasons, for our preclinical combination treatment with Everolimus, we used an engineered mouse model with a fully competent immune system. Isoform selective PI3K inhibitors should also prevent this type of interactions with the immune system.

AGC inhibitors have demonstrated preclinical and preliminary clinical efficacy against cancer. Although the toxicity profile is usually manageable, as single agents, the efficacy is limited. Therefore, current trials tend to combine AGC inhibitors with other compounds, and many trials try to enrich the study population with patients with activated AGC-kinase dependent signaling, e.g., an activated PI3K-Akt-mTOR axis (Temple 2010). The adequate way to demonstrate pathway activation in a clinical setting is still a matter of debate. One potential strategy is to break the growth dynamic with an AGC kinase inhibitor, and then use combination partners to either target mechanisms of resistance (such as PI3K or ROCK inhibitors) or address alternative targets (e.g., the immune-environment). To our knowledge, it remains to be demonstrated whether AGC inhibitors influence antigen expression or modifying immunogenicity, two major prerequisites for efficacy in immunotherapies.

Finally, after our phase 1 study, matching patients with the relevant combination of drugs is the pinnacle of personalized medicine / precision medicine. Because treating patients with single RTK inhibitors results within some weeks or months in acquired resistance, preclinical data support the testing of combinations with approved TKI, especially in breast cancer (Turner et al. 2017a). However, with more combinations than cancer patients and knowing that only 3% of cancer patients are involved in clinical trials, we should re-think our approach to approving new drugs based on a phase III trial comparing vs the gold standard of treatment. New or forgotten approaches like basket trials and umbrella trials could accelerate this process.

# XI. References


Algazi, A.P. et al., 2015. Phase II trial of trametinib in combination with the AKT inhibitor GSK 2141795 in BRAF wild-type melanoma. *ASCO Meeting Abstracts*, 33(15_suppl), p.9068.

Almhanna, K. et al., 2013. MK-2206, an Akt inhibitor, enhances carboplatinum/paclitaxel efficacy in gastric cancer cell lines. *Cancer Biology & Therapy*, 14(10), pp.932–936.

Argiris, A. et al., 2013. Phase III randomized, placebo-controlled trial of docetaxel with or without gefitinib in recurrent or metastatic head and neck cancer: An eastern cooperative oncology group trial. *Journal of Clinical Oncology*, 31(11), pp.1405–1414.

Ariizumi, T. et al., 2010. Expression of podoplanin in human bone and bone tumors: New marker of osteogenic and chondrogenic bone tumors. *Pathology International*, 60(3), pp.193–202.

Arowolo, O.A. et al., 2011. Evaluation of tension-free mesh inguinal hernia repair in Nigeria: a preliminary report. *West African journal of medicine*, 30(2), pp.110–113.

Baldwin, A. et al., 2010. Kinase requirements in human cells: V. Synthetic lethal interactions between p53 and the protein kinases SGK2 and PAK3. *Proceedings of the National Academy of Sciences of the United States of America*, 107(28), pp.12463–8.

Banham-Hall, E., 2012. The Therapeutic Potential for PI3K Inhibitors in Autoimmune Rheumatic Diseases. *The Open Rheumatology Journal*, 6(1), pp.245–258.

Barouch-Bentov, R. & Sauer, K., 2011. Mechanisms of drug resistance in kinases. *Expert Opinion on Investigational Drugs*, 20(2), pp.153–208.

Baselga J, Im S-A, Iwata H, et al., 2015. PIK3CA status in circulating tumor DNA (ctDNA) predicts efficacy of buparlisib (BUP) plus fulvestrant (FULV) in postmenopausal women with endocrine-resistant HR+/HER2–advanced breast cancer (BC): first results from the randomized, phase III BELLE-2 trial. *Presented at: San Antonio Breast Cancer Symposium; Dec 8–12, 2015; San Antonio, TX, USA. Abstr S6-01.*

Beaufils, F. et al., 2017. 5-(4,6-Dimorpholino-1,3,5-triazin-2-yl)-4-(trifluoromethyl)pyridin-2-amine (PQR309), a Potent, Brain-Penetrant, Orally Bioavailable, Pan-Class i PI3K/mTOR Inhibitor as Clinical Candidate in Oncology. *Journal of Medicinal Chemistry*, 60(17), pp.7524–7538.

Bendell, J.C., 2012. Results of the X-PECT study: A phase III randomized double-blind, placebo-controlled study of perifosine plus capecitabine (P-CAP) versus placebo plus capecitabine (CAP) in patients (pts) with refractory metastatic colorectal cancer (mCRC). *J Clin Oncol 30, 2012 (suppl; abstr LBA3501)*.

Bill, R. & Christofori, G., 2016. The Rip1Tag2 transgenic mouse model. In *Methods in Molecular Biology*. pp. 151–161.

Bison, S.M. et al., 2014. Peptide receptor radionuclide therapy (PRRT) with [177Lu-DOTA0,Tyr3]octreotate in combination with RAD001 treatment: further investigations on tumor metastasis and response in the rat pancreatic CA20948 tumor model. *EJNMMI Research*, 4(1), pp.1–10.

van Blitterswijk, W.J. & Verheij, M., 2013. Anticancer mechanisms and clinical application of alkylphospholipids. *Biochimica et Biophysica Acta (BBA) - Molecular and Cell Biology of Lipids*, 1831(3), pp.663–674.

Bohnacker, T. et al., 2017. Deconvolution of Buparlisib's mechanism of action defines specific PI3K and tubulin inhibitors for therapeutic intervention. *Nature Communications*, 8, p.14683.

Brana, I. & Siu, L.L., 2012. Clinical development of phosphatidylinositol 3-kinase inhibitors for cancer treatment. *BMC Medicine*, 10, p.161.

Breiteneder-Geleff, S. et al., 1999. Angiosarcomas express mixed endothelial phenotypes of blood and lymphatic capillaries: Podoplanin as a specific marker for lymphatic endothelium. *American Journal of Pathology*, 154(2), pp.385–394.

Breiteneder-Geleff, S. et al., 1997. Podoplanin, novel 43-kd membrane protein of glomerular epithelial cells, is down-regulated in puromycin nephrosis. *The American journal of pathology*, 151(4), pp.1141–52.

Britschgi, A. et al., 2012. JAK2/STAT5 Inhibition Circumvents Resistance to PI3K/mTOR Blockade: A Rationale for Cotargeting These Pathways in Metastatic Breast Cancer. *Cancer Cell*, 22(6), pp.796–811.

Cancer Genome Atlas Research Network, J. et al., 2017. Integrated genomic characterization of oesophageal carcinoma. *Nature*, 541(7636), pp.169–175.

Carita, G. et al., 2016. Dual inhibition of protein kinase C and p53-MDM2 or PKC and mTORC1 are novel efficient therapeutic approaches for uveal melanoma. *Oncotarget*, 7(23), pp.33542–56.

Carvajal, R.D. et al., 2016. Metastatic disease from uveal melanoma: treatment options and future prospects. *British Journal of Ophthalmology*, p.bjophthalmol-2016-309034.

Cheng, H. et al., 2015. RICTOR amplification defines a novel subset of patients with lung cancer who may benefit from treatment with mTORC1/2 inhibitors. *Cancer Discovery*, 5(12), pp.1262–1270.

Cheraghchi-Bashi, A. et al., 2015. A putative biomarker signature for clinically effective AKT inhibition: correlation of in vitro, in vivo and clinical data identifies the importance of modulation of the mTORC1 pathway. *Oncotarget*, 6(39).

Chiarini, F. et al., 2008. The novel Akt inhibitor, perifosine, induces caspase-dependent apoptosis and downregulates P-glycoprotein expression in multidrug-resistant human T-acute leukemia cells by a JNK-dependent mechanism. *Leukemia*, 22(6), pp.1106–1116.

Cibulskis, K. et al., 2013. Sensitive detection of somatic point mutations in impure and heterogeneous cancer samples. *Nature Biotechnology*, 31(3), pp.213–219.

Claringbold, P.G. & Turner, J.H., 2016. Pancreatic neuroendocrine tumor control: Durable objective response to combination177Lu-octreotate-capecitabine-temozolomide radiopeptide chemotherapy. *Neuroendocrinology*, 103(5), pp.432–439.

Clive, S., Gardiner, J. & Leonard, R.C., 1999. Miltefosine as a topical treatment for cutaneous metastases in breast carcinoma. *Cancer chemotherapy and pharmacology*, 44 Suppl, pp.S29-30.

Cmiljanovic, V. et al., 2015. Abstract 4514: PQR309: A potent, brain-penetrant, dual pan-PI3K/mTOR inhibitor with excellent oral bioavailability and tolerability. *Cancer research. 2015;75:4514.*

Coleman, R.L. et al., 2011. Phase II multi-institutional study of docetaxel plus aflibercept (AVE0005, NSC# 724770) in patients with recurrent ovarian, primary peritoneal, and fallopian tube cancer. *J Clin Oncol 29: 2011 (suppl; abstr 5017)*.

Copp, J., Manning, G. & Hunter, T., 2009. TORC-Specific phosphorylation of mammalian target of rapamycin (mTOR): phospho-Ser 2481 is a marker for intact mTOR signaling complex 2. *Cancer Research*, 69(5), pp.1821–1827.

Courtney, K.D., Corcoran, R.B. & Engelman, J.A., 2010. The PI3K pathway as drug target in human cancer. *Journal of Clinical Oncology*, 28(6), pp.1075–1083.

Crump, M. et al., 2016. Randomized, Double-Blind, Phase III Trial of Enzastaurin Versus Placebo in Patients Achieving Remission After First-Line Therapy for High-Risk Diffuse Large B-Cell Lymphoma. *Journal of Clinical Oncology*, 34(21), pp.2484–2492.

Cueni, L.N. & Detmar, M., 2009. Galectin-8 interacts with podoplanin and modulates lymphatic endothelial cell functions. *Experimental Cell Research*, 315(10), pp.1715–1723.

da Cunha Santos, G., Shepherd, F.A. & Tsao, M.S., 2005. EGFR mutations and lung cancer. *PLoS*

*Medicine*, 2(11), p.1053.

Dacheva, D. et al., 2015. Validation of an NGS Approach for Diagnostic BRCA1/BRCA2 Mutation Testing. *Molecular Diagnosis and Therapy*, 19(2), pp.119–130.

Daub, H., Specht, K. & Ullrich, A., 2004. Strategies to overcome resistance to targeted protein kinase inhibitors. *Nature Reviews Drug Discovery*, 3(12), pp.1001–1010.

Davidson, N.E. et al., 2016. AACR Cancer Progress Report 2016. *Clinical cancer research : an official journal of the American Association for Cancer Research*, 22, pp.S1–S137.

Do, K. et al., 2015. Biomarker-driven phase 2 study of MK-2206 and selumetinib (AZD6244, ARRY-142886) in patients with colorectal cancer. *Investigational New Drugs*, 33(3), pp.720–728.

Dumble, M. et al., 2014. Discovery of Novel AKT Inhibitors with Enhanced Anti-Tumor Effects in Combination with the MEK Inhibitor I. U. Agoulnik, ed. *PLoS ONE*, 9(6), p.e100880.

Dumstorf, C.A. et al., 2010. Modulation of 4E-BP1 Function as a Critical Determinant of Enzastaurin-Induced Apoptosis. *Molecular Cancer Therapeutics*, 9(12).

Eder, A.M. et al., 2005. Atypical PKC  contributes to poor prognosis through loss of apical-basal polarity and Cyclin E overexpression in ovarian cancer. *Proceedings of the National Academy of Sciences*, 102(35), pp.12519–12524.

Elkabets, M. et al., 2013. mTORC1 inhibition is required for sensitivity to PI3K p110α inhibitors in PIK3CA-mutant breast cancer. *Science translational medicine*, 5(196), p.196ra99.

Elvin, P. et al., 2014. No Pharmacodynamic activity of the AKT inhibitor AZD5363 in patients with advanced solid tumors. *J Clin Oncol 32:5s, 2014 (suppl; abstr 2541)*.

EMA, 2016. European Medicines Agency - Find Medicine - Zydelig. Available at: http://www.ema.europa.eu/ema/index.jsp?curl=pages/medicines/human/medicines/003843/human_med_001803.jsp&mid=WC0b01ac058001d124 [Accessed March 10, 2016].

Engelman, J.A., 2009. Targeting PI3K signalling in cancer: Opportunities, challenges and limitations. *Nature Reviews Cancer*, 9(8), pp.550–562.

Erlanson, D.A. et al., 2016. Twenty years on: the impact of fragments on drug discovery. *Nature Reviews Drug Discovery*, 15(9), pp.605–619.

Erpenbeck, L. & Schön, M.P., 2010. Deadly allies: The fatal interplay between platelets and metastasizing cancer cells. *Blood*, 115(17), pp.3427–3436.

Evenou, J.-P. et al., 2009. The Potent Protein Kinase C-Selective Inhibitor AEB071 (Sotrastaurin) Represents a New Class of Immunosuppressive Agents Affecting Early T-Cell Activation. *Journal of Pharmacology and Experimental Therapeutics*, 330(3), pp.792–801.

FDA, 2016. Approved Drugs > Idelalisib. 2015.

Ferlay, J. et al., 2010. Estimates of worldwide burden of cancer in 2008: GLOBOCAN 2008. *International Journal of Cancer*, 127(12), pp.2893–2917.

Fleuren, E.D.G. et al., 2016. The kinome “at large” in cancer. *Nature Reviews Cancer*, 16(2), pp.83–98.

Forte, V.A. et al., 2016. The potential for liquid biopsies in the precision medical treatment of breast cancer. *Cancer Biology and Medecine*.

Fouladi, M. et al., 2014. A phase I trial of MK-2206 in children with refractory malignancies: a Children’s Oncology Group study. *Pediatric blood & cancer*, 61(7), pp.1246–51.

Fritsch, R. et al., 2013. XRAS and RHO families of GTPases directly regulate distinct phosphoinositide 3-kinase isoforms. *Cell*, 153(5), pp.1050–1063.

Fruman, D.A. & Rommel, C., 2014. PI3K and cancer: lessons, challenges and opportunities. *Nature reviews. Drug discovery*, 13(2), pp.140–56.

Fu, L. et al., 2010. c-Jun NH2-terminal kinase-dependent upregulation of DR5 mediates cooperative induction of apoptosis by perifosine and TRAIL. *Molecular Cancer*, 9(1), p.315.

Galvez-Peralta, M. et al., 2014. Context-Dependent Antagonism between Akt Inhibitors and Topoisomerase Poisons. *Molecular Pharmacology*, 85(5), pp.723–734.

Gao, Y. et al., 2011. The alkylphospholipid, perifosine, radiosensitizes prostate cancer cells both in vitro and in vivo. *Radiation Oncology*, 6(1), p.39.

Ghobrial, I.M. et al., 2012. A Multicenter Phase II Study of Single-Agent Enzastaurin in Previously Treated Waldenstrom Macroglobulinemia. *Clinical Cancer Research*, 18(18), pp.5043–5050.

Giraudo, E., Inoue, M. & Hanahan, D., 2004. An amino-bisphosphonate targets MMP-9 - Expressing macrophages and angiogenesis to impair cervical carcinogenesis. *Journal of Clinical Investigation*, 114(5), pp.623–633.

Graff, J.R. et al., 2005. The protein kinase Cbeta-selective inhibitor, Enzastaurin (LY317615.HCl), suppresses signaling through the AKT pathway, induces apoptosis, and suppresses growth of human colon cancer and glioblastoma xenografts. *Cancer research*, 65(16), pp.7462–9.

Guidetti, A. et al., 2014. Phase II Study of Perifosine and Sorafenib Dual-Targeted Therapy in Patients with Relapsed or Refractory Lymphoproliferative Diseases. *Clinical Cancer Research*, 20(22), pp.5641–5651.

Gungor, H. et al., 2011. Pharmacokinetic (PK)/pharmacodynamic (PD) analysis of escalating repeat doses of the AKT inhibitor GSK2141795 (GSK795) in patients (pts) with ovarian cancer. *J Clin Oncol 29: 2011 (suppl; abstr 5064)*.

Guri, Y. & Hall, M.N., 2016. mTOR Signaling Confers Resistance to Targeted Cancer Drugs. *Trends in Cancer*, 2(11), pp.688–697.

Hainsworth, J.D. et al., 2016. A randomized, phase 2 study of R-CHOP plus enzastaurin vs R-CHOP in patients with intermediate- or high-risk diffuse large B-cell lymphoma. *Leukemia & Lymphoma*, 57(1), pp.216–218.

Hall, M.N., 2016. TOR and paradigm change: cell growth is controlled. *Molecular Biology of the Cell*, 27(18), pp.2804–2806.

Hammerman, P.S. et al., 2012. Comprehensive genomic characterization of squamous cell lung cancers. *Nature*, 489(7417), pp.519–525.

Hanahan, D., 1985. Heritable formation of pancreatic β-cell tumours in transgenic mice expressing recombinant insulin/simian virus 40 oncogenes. *Nature*, 315(6015), pp.115–122.

Hanks, S.K. & Hunter, T., 1995. Protein kinases 6. The eukaryotic protein kinase superfamily: kinase (catalytic) domain structure and classification. *FASEB journal : official publication of the Federation of American Societies for Experimental Biology*, 9(8), pp.576–96.

Hedberg, M.L. et al., 2016. Genetic landscape of metastatic and recurrent head and neck squamous cell carcinoma. *Journal of Clinical Investigation*, 126(1), pp.169–180.

Heigwer, F., Kerr, G. & Boutros, M., 2014. E-CRISP: fast CRISPR target site identification. *Nature Methods*, 11(2), pp.122–123.

Herzog, B.H. et al., 2013. Podoplanin maintains high endothelial venule integrity by interacting with platelet CLEC-2. *Nature*, 502(7469), pp.105–109.

Hideshima, T., 2006. Perifosine, an oral bioactive novel alkylphospholipid, inhibits Akt and induces in vitro and in vivo cytotoxicity in human multiple myeloma cells. *Blood*, 107(10), pp.4053–4062.

Hilgard, P. et al., 1997. D-21266, a new heterocyclic alkylphospholipid with antitumour activity. *European journal of cancer (Oxford, England : 1990)*, 33(3), pp.442–6.

Hirai, H. et al., 2010. MK-2206, an Allosteric Akt Inhibitor, Enhances Antitumor Efficacy by Standard Chemotherapeutic Agents or Molecular Targeted Drugs In vitro and In vivo. *Molecular Cancer*

*Therapeutics*, 9(7).

Hollebecque, A. et al., 2014. A phase Ib trial of LY2584702 tosylate, a p70 S6 inhibitor, in combination with erlotinib or everolimus in patients with solid tumours. *European Journal of Cancer*, 50(5), pp.876–884.

Hou, S., Han, X. & Ji, H., 2016. Squamous Transition of Lung Adenocarcinoma and Drug Resistance. *Trends in Cancer*, 2(9), pp.463–466.

Hsieh, A.C. et al., 2012. The translational landscape of mTOR signalling steers cancer initiation and metastasis. *Nature*, 485(7396), pp.55–61.

Imhof, A. et al., 2011. Response, survival, and long-term toxicity after therapy with the radiolabeled somatostatin analogue [90Y-DOTA]-TOC in metastasized neuroendocrine cancers. *Journal of Clinical Oncology*, 29(17), pp.2416–2423.

Jacinto, E. et al., 2006. SIN1/MIP1 Maintains rictor-mTOR Complex Integrity and Regulates Akt Phosphorylation and Substrate Specificity. *Cell*, 127(1), pp.125–137.

Janku, F. et al., 2014. Assessing PIK3CA and PTEN in early-phase trials with PI3K/AKT/mTOR inhibitors. *Cell Reports*, 6(2), pp.377–387.

Jansen, V.M., Mayer, I.A. & Arteaga, C.L., 2016. Is There a Future for AKT Inhibitors in the Treatment of Cancer? *Clinical cancer research : an official journal of the American Association for Cancer Research*, 22(11), pp.2599–601.

Johannessen, C.M. et al., 2005. The NF1 tumor suppressor critically regulates TSC2 and mTOR. *Proceedings of the National Academy of Sciences of the United States of America*, 102(24), pp.8573–8.

Kato, Y. et al., 2003. Molecular Identification of Aggrus/T1α as a Platelet Aggregation-inducing Factor Expressed in Colorectal Tumors. *Journal of Biological Chemistry*, 278(51), pp.51599–51605.

Kimura, N. & Kimura, I., 2005. Podoplanin as a marker for mesothelioma. *Pathology International*, 55(2), pp.83–86.

Kobayashi, S. et al., 2005. EGFR Mutation and Resistance of Non–Small-Cell Lung Cancer to Gefitinib. *New England Journal of Medicine*, 352(8), pp.786–792.

Koboldt, D.C. et al., 2012. VarScan 2: Somatic mutation and copy number alteration discovery in cancer by exome sequencing. *Genome Research*, 22(3), pp.568–576.

Kojima, Y. et al., 2008. The overexpression and altered localization of the atypical protein kinase C lambda/iota in breast cancer correlates with the pathologic type of these tumors. *Human pathology*, 39(6), pp.824–31.

Koti, M. et al., 2013. Identification of the IGF1/PI3K/NF κB/ERK gene signalling networks associated with chemotherapy resistance and treatment response in high-grade serous epithelial ovarian cancer. *BMC Cancer*, 13, p.549.

Van Der Kuip, H. et al., 2005. Mechanisms of clinical resistance to small molecule tyrosine kinase inhibitors targeting oncogenic tyrosine kinases. *American Journal of PharmacoGenomics*, 5(2), pp.101–112.

Kumar, R. et al., 2014. First-in-human, first-in-class phase 1 study of a novel oral multi-AGC kinase inhibitor AT13148 in patients (pts) with advanced solid tumors. *ASCO Meeting Abstracts*, 32(15_suppl), p.2554.

Kunita, A. et al., 2018. Inflammatory Cytokines Induce Podoplanin Expression at the Tumor Invasive Front. *The American Journal of Pathology*, 188(5), pp.1276–1288.

Kwekkeboom, D.J. et al., 2008. Treatment with the radiolabeled somatostatin analog [177Lu-DOTA0,Tyr3]octreotate: Toxicity, efficacy, and survival. *Journal of Clinical Oncology*, 26(13), pp.2124–2130.

Lane, H.A. et al., 2009. mTOR inhibitor RAD001 (Everolimus) has antiangiogenic/vascular properties distinct from a VEGFR tyrosine kinase inhibitor. *Clinical Cancer Research*, 15(5), pp.1612–1622.

Laplante, M. et al., 2012. mTOR signaling in growth control and disease. *Cell*, 149(2), pp.274–93.

Laurent-Puig, P. et al., 2015. Clinical relevance of KRAS-mutated subclones detected with picodroplet digital PCR in advanced colorectal cancer treated with Anti-EGFR therapy. *Clinical Cancer Research*, 21(5), pp.1087–1097.

Lee, H.J. et al., 2014. Drug resistance via feedback activation of stat3 in oncogene-addicted cancer cells. *Cancer Cell*, 26(2), pp.207–221.

Leemans, C.R., Braakhuis, B.J.M. & Brakenhoff, R.H., 2011. The molecular biology of head and neck cancer. *Nature Reviews Cancer*, 11(1), pp.9–22.

Di Leo, A. et al., 2016. BELLE-3: A Phase III study of buparlisib + fulvestrant in postmenopausal women with HR+, HER2-, aromatase inhibitor-treated, locally advanced or metastatic breast cancer, who progressed on or after mTOR inhibitor-based treatment. *San Antonio Breast Cancer Symposium (SABCS)*, Abstract S(Presented December 8, 2016.).

Leonard, R. et al., 2001. Randomized, double-blind, placebo-controlled, multicenter trial of 6% miltefosine solution, a topical chemotherapy in cutaneous metastases from breast cancer. *Journal of Clinical Oncology*, 19(21), pp.4150–4159.

Li, B., Wang, L. & Chi, B., 2013. Upregulation of periostin prevents P53-mediated apoptosis in SGC-7901 gastric cancer cells. *Molecular Biology Reports*, 40(2), pp.1677–1683.

Lin, J. et al., 2013. Targeting activated Akt with GDC-0068, a novel selective Akt inhibitor that is efficacious in multiple tumor models. *Clinical Cancer Research*, 19(7), pp.1760–1772.

Lin Kui, 2011. GDC-0068: A novel, selective, ATP-competitive inhibitor of Akt. *Cancer Res, 2011, 71(8 Supplement), abstract DDT02-01.*

Liu, P. et al., 2009. Targeting the phosphoinositide 3-kinase pathway in cancer. *Nature reviews. Drug discovery*, 8(8), pp.627–44.

Locatelli, S.L. et al., 2013. Perifosine and sorafenib combination induces mitochondrial cell death and antitumor effects in NOD/SCID mice with Hodgkin lymphoma cell line xenografts. *Leukemia*, 27(8), pp.1677–1687.

Machiels, J.P.H. et al., 2015. Afatinib versus methotrexate as second-line treatment in patients with recurrent or metastatic squamous-cell carcinoma of the head and neck progressing on or after platinum-based therapy (LUX-Head & Neck 1): An open-label, randomised phase 3 trial. *The Lancet Oncology*, 16(5), pp.583–594.

Machl, A. et al., 2016. M2698 is a potent dual-inhibitor of p70S6K and Akt that affects tumor growth in mouse models of cancer and crosses the blood-brain barrier. *American journal of cancer research*, 6(4), pp.806–18.

Maehama, T. & Dixon, J.E., 1998. The tumor suppressor, PTEN/MMAC1, dephosphorylates the lipid second messenger, phosphatidylinositol 3,4,5-trisphosphate. *Journal of Biological Chemistry*, 273(22), pp.13375–13378.

Manegold, P.C. et al., 2008. Antiangiogenic therapy with mammalian target of rapamycin inhibitor RAD001 (Everolimus) increases radiosensitivity in solid cancer. *Clinical Cancer Research*, 14(3), pp.892–900.

Manish R. Patel, Susan Mary O'Brien, Kerrie Faia, Kerry White, Mark Douglas, Kerstin Allen, Jeffrey Lorne Kutok, Jennifer Sweeney, Virginia Kelly, Ian Flinn, John C. Byrd, H.S.S.C., 2015. Early clinical activity and pharmacodynamic effects of duvelisib, a PI3K-{delta},{gamma} inhibitor, in patients with treatment-naive CLL. *J Clin Oncol 33, 2015 (suppl; abstr 7074)*.

Manning, G. et al., 2002. The protein kinase complement of the human genome. *Science (New York, N.Y.)*, 298(5600), pp.1912–34.

Mansfield, A.S. et al., 2013. Phase I dose escalation study of the PKCι inhibitor aurothiomalate for advanced non-small-cell lung cancer, ovarian cancer, and pancreatic cancer. *Anti-cancer drugs*, pp.1–5.

Martin-Villar, E. et al., 2010. Podoplanin Associates with CD44 to Promote Directional Cell Migration. *Molecular Biology of the Cell*, 21(24), pp.4387–4399.

Martin-Villar, E. et al., 2006. Podoplanin binds ERM proteins to activate RhoA and promote epithelial-mesenchymal transition. *Journal of Cell Science*, 119(21), pp.4541–4553.

Mauceri, H.J. et al., 2012. Everolimus exhibits efficacy as a radiosensitizer in a model of non-small cell lung cancer. *Oncology Reports*, 27(5), pp.1625–1629.

Mayer, I.A. & Arteaga, C.L., 2016. The PI3K/AKT Pathway as a Target for Cancer Treatment. *Annual Review of Medicine*, 67(1), pp.11–28.

McKenna, A. et al., 2010. The genome analysis toolkit: A MapReduce framework for analyzing next-generation DNA sequencing data. *Genome Research*, 20(9), pp.1297–1303.

Meadows, S. et al., 2015. Up-Regulation of the PI3K Signaling Pathway Mediates Resistance to Idelalisib. *Blood. 2015;126:3707-*.

Modlin, I.M., Lye, K.D. & Kidd, M., 2003. A 5-decade analysis of 13,715 carcinoid tumors. *Cancer*, 97(4), pp.934–959.

Moreau, A.-S. et al., 2007. Protein kinase C inhibitor enzastaurin induces in vitro and in vivo antitumor activity in Waldenstrom macroglobulinemia. *Blood*, 109(11), pp.4964–4972.

Morschhauser, F. et al., 2008. A phase II study of enzastaurin, a protein kinase C beta inhibitor, in patients with relapsed or refractory mantle cell lymphoma. *Annals of Oncology*, 19(2), pp.247–253.

Muranen, T. et al., 2012. Inhibition of PI3K/mTOR Leads to Adaptive Resistance in Matrix-Attached Cancer Cells. *Cancer Cell*, 21(2), pp.227–239.

Nagae, M. et al., 2014. A Platform of C-type Lectin-like Receptor CLEC-2 for Binding O-Glycosylated Podoplanin and Nonglycosylated Rhodocytin. *Structure*, 22(12), pp.1711–1721.

Nakazawa, Y. et al., 2008. Tetraspanin family member CD9 inhibits Aggrus/podoplanin-induced platelet aggregation and suppresses pulmonary metastasis. *Blood*, 112(5), pp.1730–1739.

Naqvi, J. et al., 2008. Epithelioid hemangioendothelioma of the head and neck: Role of podoplanin in the differential diagnosis. *Head and Neck Pathology*, 2(1), pp.25–30.

Narzisi, G. et al., 2014. Accurate de novo and transmitted indel detection in exome-capture data using microassembly. *Nature Methods*, 11(10), pp.1033–1036.

Naylor, T.L. et al., 2011. Protein Kinase C Inhibitor Sotrastaurin Selectively Inhibits the Growth of CD79 Mutant Diffuse Large B-Cell Lymphomas. *Cancer Research*, 71(7), pp.2643–2653.

O'Brien, N.A. et al., 2014. Targeting PI3K/mTOR Overcomes Resistance to HER2-Targeted Therapy Independent of Feedback Activation of AKT. *Clinical Cancer Research*, 20(13), pp.3507–3520.

O'Connor OA, Flinn IW, Patel MR, Fenske TS, Deng C, Brander DM, et al., 2015. GR-1202, a Novel Once Daily PI3K-Delta Inhibitor, Demonstrates Clinical Activity with a Favorable Safety Profile in Patients with CLL and B-Cell Lymphoma. *Blood. 2015;126:4154-*.

O'Donnell, A. et al., 2008. Phase I pharmacokinetic and pharmacodynamic study of the oral mammalian target of rapamycin inhibitor everolimus in patients with advanced solid tumors. *Journal of Clinical Oncology*, 26(10), pp.1588–1595.

Okuzumi, T. et al., 2009. Inhibitor hijacking of Akt activation. *Nature Chemical Biology*, 5(7), pp.484–493.

Pachl, F. et al., 2013. Characterization of a Chemical Affinity Probe Targeting Akt Kinases. *Journal of*

*Proteome Research*, 12(8), pp.3792–3800.

Pao, W. et al., 2005. Acquired resistance of lung adenocarcinomas to gefitinib or erlotinib is associated with a second mutation in the EGFR kinase domain E. T. Liu, ed. *PLoS Medicine*, 2(3), pp.0225–0235.

Papagiannaros, A. et al., 2006. A liposomal formulation of doxorubicin, composed of hexadecylphosphocholine (HePC): physicochemical characterization and cytotoxic activity against human cancer cell lines. *Biomedicine & Pharmacotherapy*, 60(1), pp.36–42.

Pavel, M. et al., 2016. ENETS consensus guidelines update for the management of distant metastatic disease of intestinal, pancreatic, bronchial neuroendocrine neoplasms (NEN) and NEN of unknown primary site. In *Neuroendocrinology*. Karger Publishers, pp. 172–185.

Pavel, M.E. et al., 2011. Everolimus plus octreotide long-acting repeatable for the treatment of advanced neuroendocrine tumours associated with carcinoid syndrome (RADIANT-2): A randomised, placebo-controlled, phase 3 study. *The Lancet*, 378(9808), pp.2005–2012.

Pearce, L.R. et al., 2007. Identification of Protor as a novel Rictor-binding component of mTOR complex-2. *Biochemical Journal*, 405(3), pp.513–522.

Peterson, T.R. et al., 2009. DEPTOR Is an mTOR Inhibitor Frequently Overexpressed in Multiple Myeloma Cells and Required for Their Survival. *Cell*, 137(5), pp.873–886.

Phin, S., Moore, M.W. & Cotter, P.D., 2013. Genomic Rearrangements of PTEN in Prostate Cancer. *Frontiers in oncology*, 3(September), p.240.

Planting, A.S., Stoter, G. & Verweij, J., 1993. Phase II study of daily oral miltefosine (hexadecylphosphocholine) in advanced colorectal cancer. *European journal of cancer (Oxford, England : 1990)*, 29A(4), pp.518–9.

Pool, S.E. et al., 2013. mTOR Inhibitor RAD001 Promotes Metastasis in a Rat Model of Pancreatic Neuroendocrine Cancer. *Cancer Research* , 73(1), pp.12–18.

Prêtre, V. & Wicki, A., 2018. Inhibition of Akt and other AGC kinases: A target for clinical cancer therapy? *Seminars in Cancer Biology*, 48, pp.70–77.

Prevo, R. et al., 2008. Class I PI3 kinase inhibition by the pyridinylfuranopyrimidine inhibitor PI-103 enhances tumor radiosensitivity. *Cancer Research*, 68(14), pp.5915–5923.

Principe, P. et al., 1992. Evaluation of combinations of antineoplastic ether phospholipids and chemotherapeutic drugs. *Anti-cancer drugs*, 3(6), pp.577–87.

Querfeld, C. et al., 2011. Multicenter phase II trial of enzastaurin in patients with relapsed or refractory advanced cutaneous T-cell lymphoma. *Leukemia & Lymphoma*, 52(8), pp.1474–1480.

Rebecca, V.W. et al., 2014. Inhibition of autophagy enhances the effects of the AKT inhibitor MK-2206 when combined with paclitaxel and carboplatin in BRAF wild-type melanoma. *Pigment cell & melanoma research*, 27(3), pp.465–78.

Regala, R.P. et al., 2005. Atypical protein kinase C iota is an oncogene in human non-small cell lung cancer. *Cancer research*, 65(19), pp.8905–11.

Regala, R.P., Thompson, E.A. & Fields, A.P., 2008. Atypical Protein Kinase C Expression and Aurothiomalate Sensitivity in Human Lung Cancer Cells. *Cancer Research*, 68(14), pp.5888–5895.

Reubi, J.C. et al., 2010. Glucagon-like peptide-1 (GLP-1) receptors are not overexpressed in pancreatic islets from patients with severe hyperinsulinaemic hypoglycaemia following gastric bypass. *Diabetologia*, 53(12), pp.2641–2645.

Reubi, J.C. & Waser, B., 2003. Concomitant expression of several peptide receptors in neuroendocrine tumours: Molecular basis for in vivo multireceptor tumour targeting. *European Journal of Nuclear Medicine and Molecular Imaging*, 30(5), pp.781–793.

Robertson, M.J. et al., 2007. Phase II Study of Enzastaurin, a Protein Kinase C Beta Inhibitor, in Patients With Relapsed or Refractory Diffuse Large B-Cell Lymphoma. *Journal of Clinical Oncology*, 25(13), pp.1741–1746.

Robinson, J.T. et al., 2011. Integrative genomics viewer. *Nature Biotechnology*, 29(1), pp.24–26.

Rodon, J. et al., 2013. Development of PI3K inhibitors: Lessons learned from early clinical trials. *Nature Reviews Clinical Oncology*, 10(3), pp.143–153.

Rodrik-Outmezguine, V.S. et al., 2011. mTOR Kinase Inhibition Causes Feedback-Dependent Biphasic Regulation of AKT Signaling. *Cancer Discovery*, 1(3), pp.248–259.

Rübel, A. et al., 2006. The membrane targeted apoptosis modulators erucylphosphocholine and erucylphosphohomocholine increase the radiation response of human glioblastoma cell lines in vitro. *Radiation oncology (London, England)*, 1, p.6.

Ruiter, G.A. et al., 1999. Alkyl-lysophospholipids activate the SAPK/JNK pathway and enhance radiation-induced apoptosis. *Cancer research*, 59(10), pp.2457–63.

Ruiter, G.A. et al., 2003. Anti-cancer alkyl-lysophospholipids inhibit the phosphatidylinositol 3-kinase-Akt/PKB survival pathway. *Anti-cancer drugs*, 14(2), pp.167–73.

Sacco, A.G. & Cohen, E.E., 2015. Current treatment options for recurrent or metastatic head and neck squamous cell carcinoma. *Journal of Clinical Oncology*, 33(29), pp.3305–3315.

Sadok, A. et al., 2015. Rho Kinase Inhibitors Block Melanoma Cell Migration and Inhibit Metastasis. *Cancer Research*, 75(11), pp.2272–2284.

Samuels, Y. et al., 2004. High frequency of mutations of the PIK3CA gene in human cancers. *Science (New York, N.Y.)*, 304(5670), p.554.

Sangai, T. et al., 2012. Biomarkers of Response to Akt Inhibitor MK-2206 in Breast Cancer. *Clinical Cancer Research*, 18(20), pp.5816–5828.

Saunders, C.T. et al., 2012. Strelka: Accurate somatic small-variant calling from sequenced tumor-normal sample pairs. *Bioinformatics*, 28(14), pp.1811–1817.

Saura, C. et al., 2014. Phase lb study of buparlisib plus trastuzumab in patients with HER2-positive advanced or metastatic breast cancer that has progressed on trastuzumab-based therapy. *Clinical Cancer Research*, 20(7), pp.1935–1945.

Saxton, R.A. & Sabatini, D.M., 2017. mTOR Signaling in Growth, Metabolism, and Disease. *Cell*, 168(6), pp.960–976.

Schwartzberg, L. et al., 2014. Open-label, single-arm, phase II study of enzastaurin in patients with follicular lymphoma. *British Journal of Haematology*, 166(1), pp.91–97.

Shinohara, E.T. et al., 2005. Enhanced radiation damage of tumor vasculature by mTOR inhibitors. *Oncogene*, 24(35), pp.5414–5422.

Simen, B.B. et al., 2015. Validation of a next-generation-sequencing cancer panel for use in the clinical laboratory. *Archives of Pathology and Laboratory Medicine*, 139(4), pp.508–517.

Sindermann, H., Krasovec, M. & Burg, G., 1993. Topical administration of hexadecylphosphocholine in patients with cutaneous lymphomas: Results of a phase I/II study. *Journal of the American Academy of Dermatology*, 29(6), pp.963–970.

So, L. et al., 2013. Selective inhibition of phosphoinositide 3-kinase p110 α preserves lymphocyte function. *Journal of Biological Chemistry*, 288(8), pp.5718–5731.

So, L. & Fruman, D.A., 2012. PI3K signalling in B- and T-lymphocytes: new developments and therapeutic advances. *Biochemical Journal*, 442(3), pp.465–481.

Soares, H.P. et al., 2015. Dual PI3K/mTOR Inhibitors Induce Rapid Overactivation of the MEK/ERK Pathway in Human Pancreatic Cancer Cells through Suppression of mTORC2. *Molecular Cancer*

*Therapeutics*, 14(4), pp.1014–1023.

Song, G., Ouyang, G. & Bao, S., The activation of Akt/PKB signaling pathway and cell survival. *Journal of cellular and molecular medicine*, 9(1), pp.59–71.

Sonne, S.B. et al., 2006. Identity of M2A (D2-40) antigen and gp36 (Aggrus, T1A-2, podoplanin) in human developing testis, testicular carcinoma in situ and germ-cell tumours. *Virchows Archiv*, 449(2), pp.200–206.

Spencer, A. et al., 2015. Novel AKT Inhibitor GSK2110183 Shows Favorable Safety, Pharmacokinetics, and Clinical Activity in Multiple Myeloma. Preliminary Results From a Phase I First-Time-In-Human Study. *Blood*, 118(21).

Stallings-Mann, M. et al., 2006. A Novel Small-Molecule Inhibitor of Protein Kinase Cι Blocks Transformed Growth of Non–Small-Cell Lung Cancer Cells. *Cancer Research*, 66(3).

Tabernero, J. et al., 2011. First-in-human phase I study evaluating the safety, pharmacokinetics (PK), and intratumor pharmacodynamics (PD) of the novel, oral, ATP-competitive Akt inhibitor GDC-0068. *J Clin Oncol 29: 2011 (suppl; abstr 3022)*.

Tao, J.J. et al., 2014. Antagonism of EGFR and HER3 Enhances the Response to Inhibitors of the PI3K-Akt Pathway in Triple-Negative Breast Cancer. *Science Signaling*, 7(318), pp.ra29-ra29.

Tarantelli C, Gaudio E, Kwee I, Rinaldi A, Bernasconi E, Cascione L, et al., 2015. Abstract 2652: Pre-clinical activity and mechanism of action of the novel dual PI3K/mTOR inhibitor PQR309 in B-cell lymphomas. *Cancer research. 2015;75:2652.*

Tarantelli, C. et al., 2018. PQR309 Is a Novel Dual PI3K/mTOR Inhibitor with Preclinical Antitumor Activity in Lymphomas as a Single Agent and in Combination Therapy. *Clinical Cancer Research*, 24(1), pp.120–129.

Tebbutt, N., Pedersen, M.W. & Johns, T.G., 2013. Targeting the ERBB family in cancer: Couples therapy. *Nature Reviews Cancer*, 13(9), pp.663–673.

Temple, R., 2010. Enrichment of clinical study populations. *Clinical pharmacology and therapeutics*, 88(6), pp.774–778.

Teymouri, M. et al., 2015. Investigation of Hexadecylphosphocholine (miltefosine) usage in Pegylated liposomal doxorubicin as a synergistic ingredient: In vitro and in vivo evaluation in mice bearing C26 colon carcinoma and B16F0 melanoma. *European Journal of Pharmaceutical Sciences*, 80, pp.66–73.

Thorpe, L.M., Yuzugullu, H. & Zhao, J.J., 2015. PI3K in cancer: Divergent roles of isoforms, modes of activation and therapeutic targeting. *Nature Reviews Cancer*, 15(1), pp.7–24.

Thorvaldsdóttir, H., Robinson, J.T. & Mesirov, J.P., 2013. Integrative Genomics Viewer (IGV): High-performance genomics data visualization and exploration. *Briefings in Bioinformatics*, 14(2), pp.178–192.

Tolcher, A. et al., 2014. A phase I trial of LY2584702 tosylate, a p70 S6 kinase inhibitor, in patients with advanced solid tumours. *European Journal of Cancer*, 50(5), pp.867–875.

Tougeron, D. et al., 2013. Effect of low-frequency KRAS mutations on the response to anti-EGFR therapy in metastatic colorectal cancer. *Annals of Oncology*, 24(5), pp.1267–1273.

Tsuneki, M. et al., 2013. Extracellular heat shock protein A9 is a novel interaction partner of podoplanin in oral squamous cell carcinoma cells. *Biochemical and Biophysical Research Communications*, 434(1), pp.124–130.

Turner, N.C. et al., 2017a. Advances in the treatment of advanced oestrogen-receptor-positive breast cancer. *The Lancet*, 389(10087), pp.2403–2414.

Turner, N.C. et al., 2017b. Advances in the treatment of advanced oestrogen-receptor-positive breast cancer. *The Lancet*, 389(10087), pp.2403–2414.

Uberall, F. et al., 1991. Hexadecylphosphocholine inhibits inositol phosphate formation and protein kinase C activity. *Cancer research*, 51(3), pp.807–12.

Verweij, J., Krzemieniecki, K., et al., 1993. Phase II study of miltefosine (hexadecylphosphocholine) in advanced soft tissue sarcomas of the adult--an EORTC Soft Tissue and Bone Sarcoma Group Study. *European journal of cancer (Oxford, England : 1990)*, 29A(2), pp.208–9.

Verweij, J., Gandia, D., et al., 1993. Phase II study of oral miltefosine in patients with squamous cell head and neck cancer. *European journal of cancer (Oxford, England : 1990)*, 29A(5), pp.778–9.

Villard, L. et al., 2012. Cohort study of somatostatin-based radiopeptide therapy with [90Y-DOTA]-TOC versus [90Y-DOTA]-TOC plus [177Lu-DOTA]-TOC in neuroendocrine cancers. *Journal of Clinical Oncology*, 30(10), pp.1100–1106.

Vink, S.R. et al., 2006. Radiosensitization of squamous cell carcinoma by the alkylphospholipid perifosine in cell culture and xenografts. *Clinical cancer research : an official journal of the American Association for Cancer Research*, 12(5), pp.1615–22.

Whitman, M. et al., 1988. Type I phosphatidylinositol kinase makes a novel inositol phospholipid, phosphatidylinositol-3-phosphate. *Nature*, 332(6165), pp.644–646.

Wicki, A. et al., 2007. [Lys40(Ahx-DTPA-111In)NH2]-Exendin-4 is a highly efficient radiotherapeutic for glucagon-like peptide-1 receptor-targeted therapy for insulinoma. *Clinical cancer research : an official journal of the American Association for Cancer Research*, 13(12), pp.3696–705.

Wicki, A. et al., 2016. Acquired Resistance to Clinical Cancer Therapy: A Twist in Physiological Signaling. *Physiological Reviews*, 96(3), pp.805–829.

Wicki, A. et al., 2018. First-in human, phase 1, dose-escalation pharmacokinetic and pharmacodynamic study of the oral dual PI3K and mTORC1/2 inhibitor PQR309 in patients with advanced solid tumors (SAKK 67/13). *European Journal of Cancer*, 96, pp.6–16.

Wicki, A. et al., 2014. Synergism of peptide receptor-targeted Auger electron radiation therapy with anti-angiogenic compounds in a mouse model of neuroendocrine tumors. *EJNMMI Research*, 4(1), pp.1–25.

Wicki, A. et al., 2006. Tumor invasion in the absence of epithelial-mesenchymal transition: podoplanin-mediated remodeling of the actin cytoskeleton. *Cancer cell*, 9(4), pp.261–72.

Wicki, A. & Christofori, G., 2007. The potential role of podoplanin in tumour invasion. *British journal of cancer*, 96(1), pp.1–5.

Wild, D., Béhé, M. & Wicki, A., 2006. exendin-4, a very promising ligand for glucagon-like peptide-1 (GLP-1) receptor targeting. *Journal of Nuclear …*, 40, pp.2025–2033.

Xi, Y. et al., 2016. AT13148, a first-in-class multi-AGC kinase inhibitor, potently inhibits gastric cancer cells both in vitro and in vivo. *Biochemical and Biophysical Research Communications*, 478(1), pp.330–336.

Yan, L., 2014. Abstract #DDT01-1: MK-2206: A potent oral allosteric AKT inhibitor. *Cancer Research*, 69(9 Supplement).

Yan, Y. et al., 2013. Evaluation and Clinical Analyses of Downstream Targets of the Akt Inhibitor GDC-0068. *Clinical Cancer Research*, 19(24), pp.6976–6986.

Yang, H. et al., 2013. MTOR kinase structure, mechanism and regulation. *Nature*, 497(7448), pp.217–223.

Yang, Y.-L. et al., 2008. Amplification ofPRKCI, located in 3q26, is associated with lymph node metastasis in esophageal squamous cell carcinoma. *Genes, Chromosomes and Cancer*, 47(2), pp.127–136.

Yao, J.C. et al., 2011. Everolimus for Advanced Pancreatic Neuroendocrine Tumors. *New England Journal of Medicine*, 364(6), pp.514–523.

Yao, J.C. et al., 2008. One hundred years after “carcinoid”: Epidemiology of and prognostic factors for neuroendocrine tumors in 35,825 cases in the United States. *Journal of Clinical Oncology*, 26(18), pp.3063–3072.

Yap, T.A. et al., 2012. AT13148 Is a Novel, Oral Multi-AGC Kinase Inhibitor with Potent Pharmacodynamic and Antitumor Activity. *Clinical Cancer Research*, 18(14), pp.3912–3923.

Yap, T.A. et al., 2011. First-in-man clinical trial of the oral pan-AKT inhibitor MK-206 in patients with advanced solid tumors. *Journal of Clinical Oncology*, 29(35), pp.4688–4695.

Yap, T.A. et al., 2014. Interrogating two schedules of the AKT inhibitor MK-2206 in patients with advanced solid tumors incorporating novel pharmacodynamic and functional imaging biomarkers. *Clinical Cancer Research*, 20(22), pp.5672–5685.

Yonemura, S. et al., 1998. Ezrin/radixin/moesin (ERM) proteins bind to a positively charged amino acid cluster in the juxta-membrane cytoplasmic domain of CD44, CD43, and ICAM-2. *Journal of Cell Biology*, 140(4), pp.885–895.

Yuan, T.L. & Cantley, L.C., 2008. PI3K pathway alterations in cancer: Variations on a theme. *Oncogene*, 27(41), pp.5497–5510.

Zardavas, D., Phillips, W.A. & Loi, S., 2014. PIK3CA mutations in breast cancer: Reconciling findings from preclinical and clinical data. *Breast Cancer Research*, 16(1), p.201.

Zhang, L. et al., 2006. Integrative genomic analysis of protein kinase C (PKC) family identifies PKCiota as a biomarker and potential oncogene in ovarian carcinoma. *Cancer research*, 66(9), pp.4627–35.

# XII. Contributions to the work

I planned, conducted, analyzed, created the figures and wrote the manuscript for all the experiments of these three projects with few exceptions:

Concerning the Podoplanin project, some of the experiments were done by our technician, Reto Ritschard and some in vitro 3D / Matrigel experiments by Dr. Gongda Xue. Dr. Michal Stanczak established for the a lab CRISPR/Cas9 knockout platform and conducted the FACS analysis.

Concerning the combined treatment of PRRT and Everolimus, Dr. Ole Maas did the breeding of the mice and we did together all the mice dissections, i.v. injections and biodistribution experiment. Dr. Melpomeni Fani did the radiolabeling of the compound in the radiochemical pharmacy department.

Concerning the dual inhibitor PQR309, the SAKK and Dr. Andreas Wicki did the clinical part (including the pharmacokinetics and the patient characteristics) and organized the biopsies' protocol. The NGS analysis was done by the Pathology of the University Hospital Basel and the tumor microenvironment analysis was done by Prof. Aleksandar Tzankov.

# XIII. Acknowledgements

First and foremost I would like to thank Andreas. During these almost five years, you allowed me to work in your new lab on such a variety of exotic projects for a PhD. I am very grateful for your confidence in me that brought me a lot of autonomy. I also appreciated your optimism, your pragmatism and your anecdotes during our famous “very-early-7.10am-labmeeting”.

I would like to thank the members of my PhD advisory committee: many thanks to Prof. Gerhard Christofori for allowing me to present my work in your weekly labmeeting and in your labretreat, for giving me precious feedbacks and for being always available when we had an issue. Sincere thanks to Alfred for making the link between all the subunits of this lab and your expertise in immunology. Prof. Michael N. Hall, thank you for kindly accepting to be my representative supervisor for the natural science faculty and to evaluate my work.

A huge thank you to all the present and past member of the lab. First to Reto for the scientific and organizational support, the ideas, our discussions, our intensive productions in the pharmacy hospital and your coming to each dodgeball beach tournament ! Then I would like to thank Gongda for his always valuable scientific inputs, his energy, his realism and experiences of the academia. I enjoyed the scientific exchange with Christoph Rochlitz and our monthly meeting in his office at the beginning of my PhD. Many thanks to our two medical students, Leo and Sereina, for bringing their energy and willingness to learn to the team !

A special thanks to Michal who helped me, advised me, didn’t let me be the only PhD student in the lab and even traveled with me. I won’t forget the pizza pazza and all the discussion concerning the lab after the office hours! Thanks to Yvonne for her encouragements throughout my first year of PhD (“Life is hard.. and then you die”) and together with Kea to convince me to take the job here in this lab. Thank you scientifically but also sportively to Marcel for our ultimate under the rain and swimming sessions. Then all the present and former postdocs of the lab, Sébastien, Matthias, Jens, Daniela, Franziska, Abhi, Heinz, Lucia and Sandra. Finally I enjoyed my time with all the other members of the lab, Béa, Petra, Mélanie as well as the other collegues from the lab 416 and lab 420 during our momentary exile there.

I had nice discussions and collaborations with the clinical team composed of all the doctors during our common Klinikmeeting, Seelenstündchen and department activies, especially Marcus, Frank, Sacha and Catharina. Finally thanks to the secretary on the 8$^{th}$ floor, Carmen, Corinne and Susanne for organizing the activities and Carmen for all my due bills (including the spectacular 8. Mahnung) and the

administrative stuffs. I had a great pleasure to be part of the DBM PhD Committee with all the PhD students involved as well as of the friends at the DBM across all the five buildings (almost, I still don't know the fifth one).

Out of the collaborations I had, no one was as intensive as with the nuclear medicine department. A huge thank to Ole and all these ours to dissect pancreas and organs together, listening to Radio Hamburg and planning for the holidays. Thanks to Damian for showing me how to dissect microscopic tumors and for his scientific interest. I also enjoyed the labelling and the discussions with Melpo. Finally, thanks to Rudi, who made this study possible, and the rest of the team.

I would like to thank the people from PIQUR Therapeutics for sharing with me the life of a (not so small) biotech startup. Especially the CEO, Vladimir, for inviting me twice to the annual AACR meeting, Saša for his precious help and our discussion in Basel and in the U.S, Petra and Debora for the informations and advices, as well as Michael for the database insights.

A big thank to Christoph Mamot as well as the team of the pharmacy hospital for this big adventure that was the upscaling of our compound's production.

Un merci tout spécial à mon ancien labo de la pathologie à Fribourg, à Curzio pour son aide sur le projet SAKK24/09, à Jelena pour m'avoir incité à rester dans la recherche malgré les multiples situations frustrantes et les blots difficiles à interpréter ainsi que Sarah pour m'avoir fait pipeter ma première qPCR !

Merci à ma famille, spécialement ma soeur, ma mère et mon père pour leur support indéfectible, les heures passées à m'encourager et à comprendre ce que j'essayais de faire. Ils m'ont toujours soutenu et cru en moi pour devenir (peut-être) le premier docteur de la famille (restreinte), surtout de mon exode de l'autre côté de la Sarine.

Un tout dernier incommensurable merci à Elizabeth qui aura su me motiver à finir ce travail, qui se dressait telle une montagne au milieu d'un été caniculaire. Tu as su me pousser intellectuellement sur beaucoup de fronts et trouver les mots pour que j'y croie autant que sur les pentes qui mènent au Gempen à vélo !

# XIV. Curriculum vitae

September 13, 1987 | Swiss | single
v.pretre@gmail.com | +41 79 703 78 02
Metzerstrasse 24, 4056 Basel

Experience

2018-present **Novartis** **Basel, Switzerland**

*Scientist* then *Senior Scientist* in Precision Medicine, Oncology Global Drug Development.

- Supported the general strategy and execution of clinical biomarker and CDx plans of one early stage and one late stage programs, transitioning directly from cardiovascular/rare disease into Oncology Unit.
- Supported the creation and reviewed clinical protocols and regulatory documents submitted to Health Authorities.
- Supported cross-divisional workshops to establish strategy and launch for a new class of immune-oncology drug.
- Supported and managed cross-divisional ad hoc projects with Research, Biostats, Legal, Commercial, Medical Affair, and external collaborations.
- Established a new junior position within a global team and matrix environment.

2012-2017 **University Hospital Basel** **Basel, Switzerland**

*Doctoral* then *Postdoctoral Fellow* at the Lab of Medical Oncology with Andreas Wicki, MD/PhD.

Research thesis focused on the mechanisms of cancer collective invasion. Weekly meetings with the Cancer Immunology Group. Selected additional collaborations:

- Evaluated the PD characteristics of a TKI in Phase 1 with PIQUR Therapeutics.
- Analyzed biomarkers of phase 3 studies within a Swiss Oncologist Network (SAKK)
- Validated a pre-clinical new drug combination with the Nuclear Medicine department.
- Manufactured and led in-process control of an IND for an academic Phase 2 trial.

2011-2012 **University of Fribourg** **Fribourg, Switzerland**

*Research Assistant* at the Lab of Experimental and Translational Oncology with Curzio Rüegg, MD.

Education

2017 **University of Basel**

Doctor of Philosophy (PhD) in Medical Oncology, *cum laude*. PhD Steering Committee member.
President of the Thesis: Prof. Michael N. Hall (Lasker Award ’17)

2017 **HBX | Harvard Business School**

CORe - Credential of Readiness: Economics for Managers, Financial Accounting, and Business Analytics. Selective 160+ hours online program, accelerated cohort.

2012 **University of Bern**

Master of Science in Biomedical Sciences, *magna cum laude*.

2010 **University of Fribourg**
Bachelor of Science in Biomedical Sciences, bilingual F/G.

Publications and IP

- *Scientific publications*: complete record available at http://www.pubmed.com/?term=vincent+prêtre
- *Intellectual property*: Patent holder, Europe EP2950097 A1.

Languages French (native speaker), English (fluent), German (fluent).
Miscellaneous Avid road cyclist and wine enthusiast.